Topological defects and phase transitions in dilute Bose gases

Ville Pietilä

Aalto University School of Science and Technology
Faculty of Information and Natural Sciences
Department of Applied Physics
Espoo, Finland

Dissertation for the degree of Doctor of Science in Technology to be presented with due permission of the Faculty of Information and Natural Sciences for public examination and debate in Auditorium F1 at Aalto University School of Science and Technology (Espoo, Finland) on the 9th of April, 2010, at 13 o'clock.

Dissertations of Department of Applied Physics
Aalto University School of Science and Technology
ISSN 1797-9595 (print)
ISSN 1797-9609 (electronic)

Dissertation 160 (2010):
Ville Pietilä: Topological defects and phase transitions in dilute Bose gases

Opponent:
Prof. Klaus Mølmer, Aarhus University, Denmark

Pre-examiners:
Prof. Alexander L. Fetter, Stanford University, USA
Prof. Matthew J. Davis, University of Queensland, Australia

ISBN 978-952-60-3076-0 (print)
ISBN 978-952-60-3077-7 (electronic)

Cover illustration: *Urchins* by Kelly-Ann Lees. Sculpture by the Sea, Bondi 2008.
Printed with a permission form the artist. Photograph by the author.

Multiprint Oy
Espoo, 2010

Aalto University

ABSTRACT OF DOCTORAL DISSERTATION	AALTO UNIVERSITY SCHOOL OF SCIENCE AND TECHNOLOGY P.O. BOX 11000, FI-00076 AALTO http://www.aalto.fi

Author Pietilä, Ville Seppo Olavi

Name of the dissertation

Topological defects and phase transitions in dilute Bose gases

Manuscript submitted 15.12.2009	Manuscript revised 12.3.2010

Date of the defence 9.4.2010

☐ Monograph ☒ Article dissertation (summary + original articles)

Faculty	Faculty of Information and Natural Sciences
Department	Department of Applied Physics
Field of research	Theoretical atomic physics
Opponent(s)	Prof. Klaus Mølmer
Supervisor	Prof. Risto Nieminen
Instructor	Doc. Mikko Möttönen

Abstract

Since the discovery of Bose-Einstein condensation in dilute atomic vapours in 1995, there has been a monumental increase in the research effort in the field of atomic physics due to the unforeseen opportunities and challenges that the degenerate quantum gases present. In particular, quantum gases can emulate complicated models that arise in solid state and high energy physics, allowing realisations of exotic phenomena that have proven to be elusive in their original context. An outstanding example is the existence of various topological defects in degenerate quantum gases with internal degrees of freedom. Topological excitations such as skyrmions and several types of monopoles can be shown to take place in Bose gases with a hyperfine spin degree of freedom as a result of a coupling to an external field or due to thermal fluctuations.

A central question in the context of dilute Bose gases is the relation between superfluidity and Bose-Einstein condensation. The dimensionality of the underlying space as well as the internal degrees of freedom have a direct impact on the existence and the nature of the Bose-Einstein condensate. For example, any uniform Bose gas in two spatial dimensions or an antiferromagnetic spinor Bose gas can give rise to a superfluid state which does not involve a conventional Bose-Einstein condensate corresponding to a single macroscopically occupied quantum state.

In this Thesis, properties of different topological defects and their relation to superfluidity in dilute Bose gases are investigated. Stability and creation of coreless vortices are first studied and a method to cyclically increase the angular momentum of the condensate is introduced. Subsequently, the properties and creation of different types of monopoles are investigated and an experimentally feasible method to create a Dirac monopole is presented. Finally, finite temperature phase transitions in quasi-two-dimensional Bose gases with a spin degree of freedom are analysed and, as a related subject, the stability of vortex clusters formed by vortices and antivortices is studied.

Keywords Bose-Einstein condensation, superfluidity, vortex, phase transitions

ISBN (printed) 978-952-60-3076-0	ISSN (printed) 1797-9595
ISBN (pdf) 978-952-60-3077-7	ISSN (pdf) 1797-9609
Language English	Number of pages 199

Publisher Department of Applied Physics, Aalto University

Print distribution Department of Applied Physics, Aalto University

☒ The dissertation can be read at http://lib.tkk.fi/Diss/2010/isbn9789526030777/

Aalto-yliopisto

VÄITÖSKIRJAN TIIVISTELMÄ	AALTO-YLIOPISTO TEKNILLINEN KORKEAKOULU PL 11000, 00076 AALTO http://www.aalto.fi

Tekijä Pietilä, Ville Seppo Olavi

Väitöskirjan nimi

Topologiset defektit ja faasimuutokset heikosti vuorovaikuttavissa Bose-kaasuissa

Käsikirjoituksen päivämäärä 15.12.2009	Korjatun käsikirjoituksen päivämäärä 12.3.2010

Väitöstilaisuuden ajankohta 9.4.2010

☐ Monografia	☒ Yhdistelmäväitöskirja (yhteenveto + erillisartikkelit)

Tiedekunta	Informaatio- ja luonnontieteiden tiedekunta
Laitos	Teknillisen fysiikan laitos
Tutkimusala	teoreettinen atomifysiikka
Vastaväittäjä(t)	prof. Klaus Mølmer
Työn valvoja	prof. Risto Nieminen
Työn ohjaaja	dos. Mikko Möttönen

Tiivistelmä

Bosen–Einsteinin-kondensaatin aikaansaaminen heikosti vuorovaikuttavissa alkaliatomikaasuissa merkitsi uuden aikakauden alkua atomifysiikassa. Bosen–Einsteinin-kondensaatio on esimerkki kaasun kvanttimekaanisen luonteen aiheuttamasta faasimuutoksesta ja nykyisin nämä kvanttikaasut tarjoavat jatkuvasti uusia mahdollisuuksia tutkia ilmiöitä, jotka muilla fysiikan alueilla kuten kiinteän olomuodon fysiikassa tai hiukkasfysiikassa olisivat kokeellisesti vaikeasti saavutettavissa. Erilaisten topologisten defektien esiintyminen kvanttikaasuissa, joilla on sisäisiä vapausasteita, tarjoaa tästä erinomaisen esimerkin. Kvanttikaasuissa, joilla on atomien hyperhienoon spiniin liittyviä vapausasteita, esiintyy luonteenomaisesti topologisia objekteja kuten skyrmioneita ja monopoleja. Näitä defektejä syntyy termisten fluktuaatioiden seurauksena ja niitä on mahdollista luoda kontrolloidusti esimerkiksi ulkoisten magneettikenttien avulla.

Eräs keskeisimmistä kysymyksistä kvanttikaasujen tutkimuksessa on ollut suprajuoksevuuden ja Bosen–Einsteinin-kondensaation keskinäinen suhde. Systeemin avaruudellisella dimensiolla ja sisäisten vapausasteiden olemassaololla on suora vaikutus Bosen–Einsteinin-kondensaatin esiintymiseen ja luonteeseen. Tästä esimerkkeinä ovat yleisesti kaksidimensioiset homogeeniset Bose-kaasut sekä spin-vapausasteelliset antiferromagneettiset Bose-kaasut, jotka voivat olla supranesteitä ilman, että ne muodostaisivat tavanomaista Bosen–Einsteinin-kondensaattia vastaten yhden kvanttitilan makroskooppista miehitystä.

Tässä väitöskirjassa tarkastellaan erilaisten topologisten defektien ominaisuuksia heikosti vuorovaikuttavissa Bose-kaasuissa. Erityisesti selvitetään ytimettömien vorteksien ominaisuuksia ja stabiiliutta sekä konstruoidaan menetelmä, jolla voidaan syklisesti kasvattaa kondensaatin kulmaliikemäärää. Seuraavaksi tarkastellaan erityyppisten monopolien ominaisuuksia ja esitellään menetelmä, jolla voidaan luoda kokeellisesti niin sanottu Diracin monopoli. Lopuksi tutkitaan termisten fluktuaatioiden aikaansaamia faasimuutoksia Bose-kaasuissa, joilla on spin-vapausaste. Tähän liittyen tarkastellaan vorteksien ja antivorteksien muodostamien klustereiden stabiiliutta spinittömässä Bosen–Einsteinin-kondensaatissa.

Asiasanat Bosen–Einsteinin-kondensaatio, suprajuoksevuus, vorteksi, faasimuutokset

ISBN (painettu) 978-952-60-3076-0	ISSN (painettu) 1797-9595
ISBN (pdf) 978-952-60-3077-7	ISSN (pdf) 1797-9609
Kieli englanti	Sivumäärä 199

Julkaisija Teknillisen fysiikan laitos, Aalto-yliopisto

Painetun väitöskirjan jakelu Teknillisen fysiikan laitos, Aalto-yliopisto

☒ Luettavissa verkossa osoitteessa http://lib.tkk.fi/Diss/2010/isbn9789526030777/

Affiliation

Author
Ville Pietilä
Department of Applied Physics
Aalto University
Espoo, Finland

Supervisor
Prof. Risto Nieminen
Department of Applied Physics
Aalto University
Espoo, Finland

Opponent
Prof. Klaus Mølmer
Department of Physics and Astronomy
Aarhus University
Aarhus, Denmark

Pre-examiner
Prof. Alexander L. Fetter
Department of Physics
Stanford University
Stanford, USA

Pre-examiner
Prof. Matthew J. Davis
School Mathematics and Physics
University of Queensland
Brisbane, Australia

Preface

This Thesis is written as a result of the research carried out in the Laboratory of Physics and at the Department of Applied Physics, Helsinki University of Technology, during the years 2006–2009.

First, I would like to thank Prof. Risto Nieminen for supervising this Thesis and for the excellent working environment provided by COMP. I am particularly indebted to my instructors Dr. Sami Virtanen and Dr. Mikko Möttönen not only for all the physics I have learnt in the course of my studies, but also for making the everyday research such a cheerful experience. Dr. Ari Harju is acknowledged for the support provided by his group at the initial stages of this Thesis. In spring 2008, I had the privilege to visit Prof. Kazushige Machida's group at the Okayama University in Japan and I would like to thank him for arranging my visit. During the academic year 2008-2009, I had the pleasure to visit the Centre for Quantum Computer Technology at the University of New South Wales, Australia, and I would like to thank Prof. Robert Clark, Prof. Andrew Dzurak, and Dr. Andrea Morello for arranging my stay in Sydney. I would also like to acknowledge my co-authors Dr. Tomoya Isoshima, Dr. Jukka Huhtamäki, Dr. Masahiro Takahashi, Dr. Takeshi Mizushima, Dr. Tapio Simula, and Prof. Mikio Nakahara for the fruitful collaboration.

The financial support from the Jenny and Antti Wihuri Foundation, the Emil Aaltonen Foundation, and the Vilho, Yrjö, and Kalle Väisälä Foundation is gratefully acknowledged. I would also like to thank the Finnish IT Center for Science, CSC, for the computing resources.

Finally, I would like to thank my family for the support and the encouragement that I have enjoyed during my studies, and my friends for reminding me that there is also life outside the university.

Otaniemi, March 2010

Ville Pietilä

Contents

List of Publications

This Thesis consists of an overview of the author's work in the field of ultracold Bose gases and of the following publications which are referred to by their Roman numerals in this overview.

I M. Takahashi, V. Pietilä, M. Möttönen, T. Mizushima, and K. Machida, *Vortex-splitting and phase-separating instabilities of coreless vortices in $F = 1$ spinor Bose-Einstein condensates*, Phys. Rev. A **79**, 023618 (2009).

II V. Pietilä, M. Möttönen, and M. Nakahara, *Topological vortex creation in spinor Bose-Einstein condensates*, in Electromagnetic, Magnetostatic, and Exchange-Interaction Vortices in Confined Magnetic Structures, Ed. E. O. Kamenetskii, pp. 297–329 (2008), ISBN: 978-81-7895-373-1.

III M. Möttönen, V. Pietilä, and S. M. M. Virtanen, *Vortex Pump for Dilute Bose-Einstein Condensates*, Phys. Rev. Lett. **99**, 250406 (2007).

IV V. Pietilä, M. Möttönen, and S. M. M. Virtanen, *Stability of coreless vortices in ferromagnetic spinor Bose-Einstein condensates*, Phys. Rev. A **76**, 023610 (2007).

V J. A. M. Huhtamäki, M. Möttönen, T. Isoshima, V. Pietilä, and S. M. M. Virtanen, *Splitting Times of Doubly Quantized Vortices in Dilute Bose-Einstein Condensates*, Phys. Rev. Lett. **97**, 110406 (2006).

VI V. Pietilä and M. Möttönen, *Creation of Dirac Monopoles in Spinor Bose-Einstein Condensates*, Phys. Rev. Lett. **103**, 030401 (2009).

VII V. Pietilä and M. Möttönen, *Non-Abelian Magnetic Monopole in a Bose-Einstein Condensate*, Phys. Rev. Lett. **102**, 080403 (2009).

VIII V. Pietilä, M. Möttönen, T. Isoshima, J. A. M. Huhtamäki, and S. M. M. Virtanen, *Stability and dynamics of vortex clusters in nonrotated Bose-Einstein condensates*, Phys. Rev. A **74**, 023603 (2006).

IX V. Pietilä, T. P. Simula, and M. Möttönen, *Finite-temperature phase transitions in quasi-two-dimensional spin-1 Bose gases* (2010, accepted to Phys. Rev. A), eprint: arXiv:0909.1898.

Author's contribution

The research presented in this Thesis has been carried out at the Helsinki University of Technology in the Laboratory of Physics during the years 2006–2008 and at the Department of Applied Physics during the years 2008–2009.

In Publication I, the author participated actively in developing the main ideas and contributed to the preparation of the manuscript at all stages. Publication II was mainly written by the author. In Publication III, the author contributed to the formulation of the main ideas, developed the computer program used in the simulation, performed the numerical calculations, and contributed to the preparation of the manuscript. In Publications IV, VI, VII, and IX, the author formulated the central ideas, performed all analytical and numerical calculations, and wrote the manuscripts. The author participated in finalising the manuscript of Publication V. In Publication VIII, the author wrote the manuscript, performed all numerical calculations and developed part of the computer program used in the numerical calculations. The author has also presented the research in several domestic and international conferences.

List of Abbreviations

The following abbreviations are used in this overview

1D	one-dimensional
2D	two-dimensional
3D	three-dimensional
AT	Anderson-Toulouse
BEC	Bose-Einstein condensate
BdG	Bogoliubov-de Gennes
BG	Bogoliubov
BKT	Berezinskii-Kosterlitz-Thouless
GP	Gross-Pitaevskii
HFB	Hartree-Fock-Bogoliubov
HFP	Hartree-Fock-Popov
IP	Ioffe-Pritchard
MH	Mermin-Ho
MOT	magneto-optical trap
ODLRO	off-diagonal long-range order
PGPE	projected Gross-Pitaevskii equation
RWA	rotating wave approximation
VAP	vortex-antivortex pair
VD	vortex dipole
VQ	vortex quadrupole
VT	vortex tripole

List of Symbols

$\alpha = +, 0, -$	index corresponding to the basis consisting of the eigenstates of $\mathcal{F}_z$
$\hat{a}_q$	annihilation operator for a bosonic quasiparticle
$\hat{a}_q^\dagger$	creation operator for a bosonic quasiparticle
A_μ	vector potential
$\mathcal{A}_{\alpha\beta}$	matrix element of the operator $\mathcal{D}_{\alpha\beta}$
$\mathcal{B}_{\alpha\beta}$	matrix element of the operator $\mathcal{D}_{\alpha\beta}$
$\boldsymbol{B}$	magnetic field
$\hat{\boldsymbol{b}} = \boldsymbol{B}/\lvert\boldsymbol{B}\rvert$	unit vector corresponding to the magentic field $\boldsymbol{B}$
$\Delta_{\alpha\beta}$	self-energy matrix
$D_\mu = \partial_\mu - iA_\mu$	covariant derivative
$\mathcal{D}$, $\mathcal{D}_P$, $\mathcal{D}_Q$	derivative operators in the calculation of thermodynamical quantities
$\mathcal{D}_{\alpha\beta} = \begin{pmatrix} \mathcal{A}_{\alpha\beta} & -\mathcal{B}_{\alpha\beta} \\ \mathcal{B}^*_{\alpha\beta} & -\mathcal{A}^*_{\alpha\beta} \end{pmatrix}$	differential operator in the Bogoliubov equation
ε_α	HFP single-particle energies
$\mathcal{F}_x = \frac{1}{\sqrt{2}} \begin{pmatrix} 0 & 1 & 0 \\ 1 & 0 & 1 \\ 0 & 1 & 0 \end{pmatrix}$	spin-1 matrix
$\mathcal{F}_y = \frac{i}{\sqrt{2}} \begin{pmatrix} 0 & -1 & 0 \\ 1 & 0 & -1 \\ 0 & 1 & 0 \end{pmatrix}$	spin-1 matrix
$\mathcal{F}_z = \begin{pmatrix} 1 & 0 & 0 \\ 0 & 0 & 0 \\ 0 & 0 & -1 \end{pmatrix}$	spin-1 matrix
$\boldsymbol{\mathcal{F}} = (\mathcal{F}_x, \mathcal{F}_y, \mathcal{F}_z)$	vector of the spin-1 matrices
g_{F}	Landé g-factor
$\tilde{g} = 4\sqrt{2\pi}Na/a_z$	effective coupling constant for the pancake-shaped condensates
$\bar{g} = 2\sqrt{2\pi}a/a_z$	dimensionless quasi-2D coupling constant

$\mathcal{G}^{-1}_{\alpha\beta}$	inverse Green's function
$\mathcal{G}_P$	polar order parameter space
$\mathcal{G}_F$	ferromagnetic order parameter space
$\hbar = \frac{h}{2\pi}$	Planck constant divided by 2π
$\hbar\omega_q$	quasiparticle energy
$\hat{h}_0 = -\frac{\hbar^2}{2m}\nabla^2 + V_{\rm tr}(\boldsymbol{r})$	single-particle operator in the PGPE equation
$\hat{h}_{\alpha\beta} = [-\frac{\hbar}{2m}\nabla^2 + V_{\rm tr}(\boldsymbol{r})]\delta_{\alpha\beta} + g_{\rm F}\mu_{\rm B}\boldsymbol{B}(\boldsymbol{r})\cdot\boldsymbol{\mathcal{F}}_{\alpha\beta}$	single-particle operator in the spin-1 Hamiltonian
$\hat{H}_0$	mean-field Hamiltonian
$\mathcal{H}_C$	c-field Hamiltonian
$\boldsymbol{\mathcal{J}} = (\mathcal{J}_x, \mathcal{J}_y, \mathcal{J}_z)$	vector of dimensionless spin-F operators
$k_{\rm B}$	Boltzmann constant
$\lambda = \sqrt{2\pi\hbar^2/mk_{\rm B}T}$	thermal wavelength
$\mathcal{L} = -\frac{\hbar^2}{2m}\nabla^2 + V_{\rm tr}(\boldsymbol{r}) - \mu$	single-particle operator in the HFP equations
μ	chemical potential
$\mu_{\rm B}$	Bohr magneton
M	relative magnetisation
$\hat{\boldsymbol{n}}$	local magnetic axis
n^T_α	density of thermal atoms in the component α
n_α	density of all atoms in the component α
N_0	number of condensate atoms
$N, N_{\rm tot}$	total particle number
$\mathcal{N}_C$	number of c-field atoms
$\omega_a,\ a = x, y, z$	trap frequencies to the three spatial directions
$\boldsymbol{\Omega}_s$	vorticity
$\vec{\Psi} = (\psi_+, \psi_0, \psi_-)$	condensate order parameter
$\vec{\Psi}_{\boldsymbol{C}} = (\psi_{\boldsymbol{C},+}, \psi_{\boldsymbol{C},0}, \psi_{\boldsymbol{C},-})$	three-component c field
Φ	scalar potential
$\mathcal{P}_f$	projection operator of a pair atoms to a state with a total hyperfine spin f
$\mathcal{P}_C$	projection operator in the PGPE equation
$\mathcal{Q}_{2D}$	topological charge in 2D
$\mathcal{Q}_{3D}$	topological charge in 3D

Q_{ab}	magnetic quadrupole moment
$\rho^{(1)}(\boldsymbol{r},\boldsymbol{r}')$	one-body density matrix for scalar particles
$\rho^{(1)}(\alpha\boldsymbol{r},\beta\boldsymbol{r}')$	one-body density matrix for a system with internal degrees of freedom
ϱ	particle density
$\boldsymbol{r}$	spatial vector
$\boldsymbol{r}_\perp$	spatial vector in x-y plane
$\Sigma_{\alpha\beta}$	self-energy matrix
$\sigma_1,\sigma^x=\begin{pmatrix}0&1\\1&0\end{pmatrix}$	spin-1/2 Pauli matrix
$\sigma_2,\sigma^y=\begin{pmatrix}0&-i\\i&0\end{pmatrix}$	spin-1/2 Pauli matrix
$\sigma_3,\sigma^z=\begin{pmatrix}1&0\\0&-1\end{pmatrix}$	spin-1/2 Pauli matrix
$\boldsymbol{\mathcal{S}}$	local spin
$\hat{\boldsymbol{s}}=\boldsymbol{\mathcal{S}}/\lvert\boldsymbol{\mathcal{S}}\rvert$	unit vector corresponding to the local spin $\boldsymbol{\mathcal{S}}$
$\tau_k=\sigma_k\otimes\mathbb{1}_{3\times3},\quad k=1,2,3$	symmetry operators corresponding to the Bogoliubov equation
t	time
$\partial_t=\frac{\partial}{\partial t}$	derivative with respect to time
T	temperature
$\boldsymbol{v}_s$	superfluid velocity
$V_{\mathrm{tr}}(\boldsymbol{r})=\frac{1}{2}m(\omega_x^2x^2+\omega_y^2y^2+\omega_z^2z^2)$	optical potential confining the atoms
$w_q=(u_q,v_q)$	quasiparticle amplitudes

1 Introduction

Phase transitions and existence of long-range order are the core of the contemporary statistical mechanics. These general concepts can be utilised to predict properties of various materials of scientific and technological interest as well as to gain understanding of a myriad of phenomena ranging from the origin of our universe to the behaviour of water at different temperatures. One of the most interesting phase transitions is the formation of a Bose-Einstein condensate (BEC). This phase transition originates from the quantum statistical nature of the constituent particles and refers to a process where a single quantum state becomes macroscopically occupied below the transition temperature. It was originally predicted to occur for noninteracting particles obeying Bose statistics by S. Bose and A. Einstein [1–3], but the discovery of superfluidity in liquid ^{4}He [4, 5] and the subsequent interpretation of the superfluidity as a manifestation of Bose-Einstein condensation [6], suggested that the concept of a BEC is more than an anomaly of the non-interacting Bose gas.

Although the idea of superfluidity arising from Bose-Einstein condensation is supported by experiments and numerical calculations for ^{4}He [7, 8], the interparticle interactions in liquid Helium are strong and the details of the superfluid transition and BEC in ^{4}He remain somewhat unclear due to the lack of exhaustive *ab initio* theory. After decades of intensive research on trapping and cooling neutral atoms [9–12], the breakthrough came in 1995 when the Bose-Einstein condensation was realised in dilute gases of alkali atoms [13–15]. Another major experimental achievement followed soon after when the first quantum degenerate Fermi gases were experimentally realised [16–18]. The development of methods to trap neutral atoms by laser fields [19, 20] has given rise to two important advancements in the field of cold atoms: the realisation of degenerate quantum gases with internal degrees of freedom [21, 22] and the manipulation of the interparticle interaction using the Feshbach resonances [23, 24]. The latter breakthrough has led to the realisation of a crossover from a superfluid formed by loosely-bound Cooper pairs to a Bose-Einstein condensate of tightly-bound paired fermions [25–27], whereas the former has enabled studies of Bose gases with a spin degree of freedom [21, 28, 29].

The onset of Bose-Einstein condensation requires a high enough phase-space density which is defined as the number of particles contained in the volume given by the cube of the thermal de Broglie wavelength λ. At the typical experimental temperatures, the particle density required to reach BEC becomes roughly 10^{13} – 10^{15} cm^{-3} [30], indicating that the condensates in atomic gases are very dilute. This renders the range of the interatomic interactions much shorter than the average distance between particles and usually it is sufficient to consider only the two-body

interactions. To date, Bose-Einstein condensation has been realised with various elements and isotopes including ^{87}Rb [13], ^{7}Li [14], ^{23}Na [15], ^{1}H [31], ^{85}Rb [32], metastable helium ^{4}He* [33, 34], ^{41}K [35], ^{133}Cs [36], ^{174}Yb [37] ^{39}K [38], ^{52}Cr [39], ^{40}Ca [40], ^{84}Sr [41, 42] as well as with ^{6}Li$_2$ [43] and ^{40}K$_2$ [44] molecules. Condensates with a spin degree of freedom have so far been realised using ^{23}Na [19], ^{87}Rb [20], and ^{52}Cr [45].

At low temperatures and energies, the properties of the atomic gas do not depend on the specific details of the two-body interaction and the scattering between two colliding atoms is characterised by a single parameter, the s-wave scattering length a. The strength of the atomic interaction potential is characterised by the gas parameter na^3, where n is the density of the gas. Under realistic experimental conditions, the density and the s-wave scattering length satisfy the condition $na^3 \ll 1$ rendering the gas weakly interacting [46]. The development of the Feshbach resonance techniques [46, 47] to adjust the s-wave scattering length in single-component systems enables full exploration of the different regimes characterised by the strength of the interaction $n|a|^3$ and the thermal wavelength λ [47]. In this Thesis, we mostly assume, implicitly or explicitly, that we are considering the weakly interacting quantum degenerate regime.

A central topic in the context of degenerate quantum gases has been the interplay between superfluidity, long-range order, and coherence of these matter waves. The formation of long-range order in Bose gases implies an onset of Bose-Einstein condensation and phase coherence. Superfluidity is intimately related to the phase coherence of the system but it can also exist in the absence of a coherent BEC. Superfluidity is manifested in the formation of quantised vortices—defects for which the flow about the vortex core is restricted to integer multiples of the angular momentum quantum—as a response to external rotation. On the other hand, proliferation of free vortices due to thermal fluctuations can destroy the superfluidity and the (quasi-) long-range order in low-dimensional Bose gases [48–51]. Hence, vortices in dilute Bose gases have been a subject of intense theoretical and experimental research [52–61].

The existence of internal degrees of freedom has a profound impact on the superfluid properties of atomic gases. In this Thesis, Bose gases with the hyperfine spin degree of freedom are analysed and they are referred to as spinor Bose gases [21, 28, 29, 62]. In a single-component BEC corresponding to a fully spin polarised spinor BEC, the superfluid flow is bound to be irrotational owing to the phase coherence of the system. Irrotationality dictates that the circulation of the superfluid flow about the vortex core is quantised to integer multiples of the angular momentum quantum. The superfluid velocity for a single-component BEC is diver-

gent at the vortex core and the particle density vanishes at the core region. Spinor BECs, however, can feature superfluid flow which satisfies a more general condition leading to the quantisation of vorticity [63–66]. In particular, the superfluid velocity can take a finite value at the vortex core, giving rise to coreless vortices with nonvanishing particle density at the vortex core.

In Publications I and IV, stability of the different types of coreless vortices is studied. As a related subject, creation of vortices utilising the spin degree of freedom is investigated in Publications II and III, resulting in a method to cyclically increase the angular momentum of the condensate. This method generalises the topological phase imprinting method [67–69] which has been used to create two- and four-quantum vortices in single-component condensates [57–59, 70]. Vortices with multiple quanta of angular momentum are usually dynamically unstable and they tend to decay into single-quantum vortices with the same total vorticity. In Publications IV and V, the instabilities of two-quantum vortices are studied in the context of the experiment of Shin *et al.* [59].

Condensates with internal degrees of freedom can also host more complicated topological defects such as monopoles, skyrmions, and knotted textures [71–82]. In particular, ferromagnetic spin-1 condensates can host Dirac monopoles where a monopole defect in the spin texture of the condensate is an end point of a vortex [80]. In Publication VI, we show how the Dirac monopole can be created using external magnetic fields. Another type of monopole has been introduced in the context of light-induced gauge potentials [76] that arise in an effective description of adiabatic states of multilevel atoms in external laser fields. The properties of this non-Abelian monopole are analysed in Publication VII and a gauge invariant charge to classify the possible mean-field states is introduced.

In addition to the coreless vortices, spinor Bose gases can feature fractionalised vortices, for which the circulation in the complex phase is a fractional multiple of 2π [83–85]. Coreless (or continuous) vortices and fractional vortices have also been investigated in the context of superfluid ^{3}He [86–89] which, despite being composed of Cooper pairs, shares many common features with the spinor Bose gases. Existence of non-conventional vortices also changes the phase transitions mediated by vortices, most notably the Berezinskii-Kosterlitz-Thouless (BKT) transition [48–51] in which the superfluid transition in two spatial dimensions is associated with the binding of vortices and antivortices. In the case of the total hyperfine spin $F = 1$, the BKT transition turns out to be mediated by either half-quantum vortices [90] or coreless vortices depending on the character of the spin-dependent interactions. The BKT transition for trapped antiferromagnetic spin-1 Bose gases is considered in Publication IX and the BKT crossover temperature is found to depend on the type

of the antiferromagnetic ordering. As a related subject, stability of vortex clusters composed of vortices and antivortices in single-component condensates is studied in Publication VIII.

The classical criterion for the existence of BEC is the presence of off-diagonal long-range order which is manifested in the one-body density matrix of the system [91–93]. This gives rise to the Penrose-Onsager criterion in which the existence of a Bose-Einstein condensate is tantamount to the appearance of a macroscopic eigenvalue in the one-body density matrix while the other eigenvalues remain negligible compared to the total number of particles [93]. Deviation from this simple picture can take place in low-dimensional systems [94–96] and spinor Bose gases [96–98] where the one-body density matrix can have several large eigenvalues and the condensate is referred to as fragmented [99]. In Publication IX, the existence and the nature of the condensate at finite temperatures are investigated in trapped quasi-two-dimensional spinor Bose gases and a crossover to a coherent condensate is found. Unlike the BKT crossover temperature, the temperature at which the condensate forms does not depend on the type of the antiferromagnetic ordering.

1.1 Organisation of the Thesis

Sections 2, 3, and 4 provide a theoretical background for the topics discussed in Publications I–IX. The mean-field theory of dilute Bose gases is introduced in Section 2 with an extension to finite temperatures. In Section 3, the formalism necessary for studies of the finite-temperature phase transitions is presented. The existence of topological defects and superfluidity in spinor Bose gases is reviewed in Section 4. The main results of Publications I and IV are discussed and topological methods to create vortices are analysed in the light of Publications II–V in Section 5. The existence and the properties of monopoles in spinor BECs are analysed in Section 6 and the results of Publications VI and VII are presented. In Section 7, the finite temperature phase transitions in Bose gases are discussed and the theory of the BKT transition is reviewed. As a related issue, the existence of stable clusters of vortices and antivortices is discussed following Publication VIII. Finally, the results of Publication IX concerning the BKT transition and the formation of a condensate in trapped quasi-two-dimensional spinor Bose gases are presented.

2 Mean-field theory of spinor Bose gases

The atomic gases considered in this Thesis consist typically of a very large number of interacting atoms. This makes the detailed dynamics of the system extremely complicated and one needs to resort to various approximations to render the problem tractable. A good starting point is the mean-field theory in which the complicated interaction terms are taken into account as averaged quantities, leading effectively to a single-particle problem that can be solved.

Due to its simplistic nature, the mean-field theory has its limitations and it typically fails in strongly interacting systems as well as for one- and two-dimensional systems due to the enhanced role of thermal and quantum fluctuations. In the ultracold Bose gases, the mean-field theory is capable of describing a large number of phenomena unless the system is by design such that effects beyond the mean-field treatments are important. This is mostly due to the low temperature and weak interactions which render the effects of the non-condensed component negligible. Furthermore, the zero-temperature mean-field theory provides a good starting point for a systematic treatment of the higher order effects such as the thermal non-condensed component.

In this section, the mean-field theory is formulated for the spinor Bose gases. An extension of the mean-field theory to take into account the quasiparticle excitations at zero temperature is presented and a formulation of the Hartree-Fock theory at finite temperatures is discussed. In this section and for the rest of this Thesis, we assume short-range interactions between particles.

2.1 Bose-Einstein condensation

The onset of Bose-Einstein condensation is associated with a formation of the off-diagonal long-range order (ODLRO) in the system. In single-component systems, ODLRO implies that the one-body density matrix

$$\rho^{(1)}(\boldsymbol{r},\boldsymbol{r}') = \langle \hat{\Phi}^\dagger(\boldsymbol{r}')\hat{\Phi}(\boldsymbol{r})\rangle, \tag{2.1}$$

where $\hat{\Phi}$ is a bosonic field operator in the Schrödinger picture, has the asymptotic property [92, 93]

$$\lim_{|\boldsymbol{r}-\boldsymbol{r}'|\to\infty} \rho^{(1)}(\boldsymbol{r},\boldsymbol{r}') = N_0\psi^*(\boldsymbol{r}')\psi(\boldsymbol{r}). \tag{2.2}$$

The complex-valued function $\psi(\boldsymbol{r})$ is referred to as the condensate order parameter and N_0 is the number of condensate atoms. The behaviour of $\psi(\boldsymbol{r})$ in homogeneous systems depends strongly on the spatial dimension, and only three-dimensional (3D)

systems can exhibit true long-range order such that Eq. (2.2) is satisfied. At finite temperatures, the one-body density matrix in uniform systems decays algebraically in two dimensions and exponentially in one dimension for large $|\boldsymbol{r} - \boldsymbol{r}'|$ [100].

Computationally a more convenient characterisation of the ODLRO and the existence of a condensed component is the Penrose-Onsager criterion [93] where the number of the condensed atoms N_0 and the condensate order parameter $\psi(\boldsymbol{r})$ are defined as the largest eigenvalue and the associated eigenstate of the one-body density matrix. The existence of a true condensate requires that N_0 is not negligible compared to the total number of particles N and all other eigenvalues are much smaller than N_0. The internal degrees of freedom can bring additional features such as the condensate fragmentation [99] where the one-body density matrix

$$\rho^{(1)}(\alpha\boldsymbol{r}, \beta\boldsymbol{r}') = \langle \hat{\Phi}^\dagger_\beta(\boldsymbol{r}')\hat{\Phi}_\alpha(\boldsymbol{r})\rangle, \tag{2.3}$$

has several large eigenvalues. In fact, spinor condensates can have a ground state corresponding to fragmented condensate at zero temperature under certain circumstances [97, 98] but in this Thesis, we either consider situations where the fragmented condensate does not exist or where we explicitly find the condensate to be non-fragmented. We define the condensate order parameter $\psi_\alpha(\boldsymbol{r})$ and the corresponding number of the condensate atoms N_0 from the eigenvalue equation

$$\int \mathrm{d}\boldsymbol{r}'\, \rho^{(1)}(\alpha\boldsymbol{r}, \beta\boldsymbol{r}')\, \psi_\beta(\boldsymbol{r}') = N_0\psi_\alpha(\boldsymbol{r}), \tag{2.4}$$

where N_0 is the largest eigenvalue of $\rho^{(1)}(\alpha\boldsymbol{r}, \beta\boldsymbol{r}')$. We use the convention where a summation over repeated indices is assumed. The definitions (2.3) and (2.4) are used in Publication IX to compute the number of condensate atoms at finite temperatures.

2.2 Gross-Pitaevskii equation and quasiparticle excitations

The physical system considered in this Thesis is a Bose gas with the total hyperfine spin $F = 1$, giving rise to a three-component quantum field describing the gas[1]. The spinor Bose gases have the property that the hyperfine spin states of the atoms can change in the two-body scattering events. The interaction part of the Hamiltonian must be formulated such that the total hyperfine spin f of the two colliding particles is taken into account. For the $F = 1$ case, there are only two possibilities $f = 0$

[1]The total hyperfine spin is the sum of the total electronic angular momentum J and the nuclear spin I. For the alkali atoms such as ^{23}Na or ^{87}Rb, one has $J = 1/2$ and $I = 3/2$. This implies a total hyperfine spin $F = 1$ or $F = 2$. In the case of $F = 1$, the system is fully characterised by the states $|F = 1, m_{\mathrm{F}}\rangle$, where $m_{\mathrm{F}} = -1, 0, 1$ refers to the eigenvalue of the z component of the total hyperfine spin operator.

and $f = 2$. The scattering can be described by the projection operators [29] $\mathcal{P}_f = \sum_{\alpha=-f}^{f} \hat{\mathcal{O}}_{f\alpha}^{\dagger}\hat{\mathcal{O}}_{f\alpha}$, where $\hat{\mathcal{O}}_{f\alpha} = \sum_{\beta,\beta'}\langle f,\alpha|F,\beta;F,\beta'\rangle\,\hat{\Phi}_{\beta}\hat{\Phi}_{\beta'}$ and $\hat{\Phi}_{\beta}$ annihilates a particle from the state $|F,\beta\rangle$ which is an eigenstate of $\hat{F}_z$ corresponding to the total hyperfine spin F. The interaction part of the Hamiltonian is of the form $\hat{H}_{\rm int} = g_0\mathcal{P}_0 + g_2\mathcal{P}_2$, where the coupling constants g_f are given by $g_f = 4\pi\hbar^2 a_f/m$, a_f is the scattering length in the channel corresponding to the total hyperfine spin f, and m is the atomic mass.

In the basis consisting of the Zeeman substates $|F,\beta\rangle$, the total Hamiltonian describing the system can be written as [28, 29]

$$\hat{H} = \int \mathrm{d}\boldsymbol{r}\,\big[\hat{\Phi}_{\alpha}^{\dagger}(\boldsymbol{r})\hat{h}_{\alpha\beta}\hat{\Phi}_{\beta}(\boldsymbol{r}) + \frac{c_0}{2}\hat{\Phi}_{\alpha}^{\dagger}(\boldsymbol{r})\hat{\Phi}_{\beta}^{\dagger}(\boldsymbol{r})\hat{\Phi}_{\beta}(\boldsymbol{r})\hat{\Phi}_{\alpha}(\boldsymbol{r}) + \frac{c_2}{2}\hat{\Phi}_{\alpha}^{\dagger}(\boldsymbol{r})\hat{\Phi}_{\alpha'}^{\dagger}(\boldsymbol{r})\boldsymbol{\mathcal{F}}_{\alpha\beta}\cdot\boldsymbol{\mathcal{F}}_{\alpha'\beta'}\hat{\Phi}_{\beta'}(\boldsymbol{r})\hat{\Phi}_{\beta}(\boldsymbol{r})\big]. \quad (2.5)$$

The single particle operator $\hat{h}_{\alpha\beta}$ is given by

$$\hat{h}_{\alpha\beta} = [-\frac{\hbar}{2m}\nabla^2 + V_{\rm tr}(\boldsymbol{r})]\delta_{\alpha\beta} + g_{\rm F}\mu_{\rm B}\boldsymbol{B}(\boldsymbol{r})\cdot\boldsymbol{\mathcal{F}}_{\alpha\beta}, \quad (2.6)$$

where $\boldsymbol{B}$ is the possible external magnetic field, $V_{\rm tr}(\boldsymbol{r}) = \frac{1}{2}m(\omega_x^2x^2 + \omega_y^2y^2 + \omega_z^2z^2)$ is the optical potential confining the atoms, and $\boldsymbol{\mathcal{F}} = (\mathcal{F}_x, \mathcal{F}_y, \mathcal{F}_z)$ is a vector of the spin-1 matrices

$$\mathcal{F}_x = \frac{1}{\sqrt{2}}\begin{pmatrix}0&1&0\\1&0&1\\0&1&0\end{pmatrix}, \quad \mathcal{F}_y = \frac{i}{\sqrt{2}}\begin{pmatrix}0&-1&0\\1&0&-1\\0&1&0\end{pmatrix}, \quad \mathcal{F}_z = \begin{pmatrix}1&0&0\\0&0&0\\0&0&-1\end{pmatrix}. \quad (2.7)$$

The Landé g-factor is denoted by $g_{\rm F}$ and $\mu_{\rm B}$ is the Bohr magneton. The coupling constants c_0 and c_2 are given by $c_0 = (g_0 + 3g_2)/3$ and $c_2 = (g_2 - g_0)/3$. The gas is referred to as ferromagnetic if $c_2 < 0$ and antiferromagnetic (polar) if $c_2 > 0$. Indices α, α', β, and β' take values $+, 0, -$ corresponding to the eigenstates of $\mathcal{F}_z$.

We develop a mean-field theory for the condensate by separating the condensate part from the field operator [101–104] and denoting the non-condensed atoms by another bosonic field $\hat{\phi}_{\alpha}(\boldsymbol{r})$

$$\hat{\Phi}_{\alpha}(\boldsymbol{r}) = \psi_{\alpha}(\boldsymbol{r})\hat{\zeta}_{\alpha}(\boldsymbol{r}) + \hat{\phi}_{\alpha}(\boldsymbol{r}) \approx \psi_{\alpha}(\boldsymbol{r}) + \hat{\phi}_{\alpha}(\boldsymbol{r}), \quad (2.8)$$

where the last approximation is valid for large 3D systems away from the critical region. The approximation in Eq. (2.8) implicitly invokes the spontaneous symmetry breaking description of BEC [105] and it fails for low-dimensional systems for

which the fluctuations represented by the condensate operator $\hat{\zeta}_\alpha(\boldsymbol{r})$ are significant. For the single-component systems, it is possible to derive the mean-field description and the higher-order terms without resorting to the spontaneous symmetry breaking argument [106–109] and, presumably, this treatment can be generalised to the spinor case. Such methods are referred to as the number conserving approximations since they maintain the number of particles fixed in a contrast to the Bogoliubov approximation that treats a system with a well defined phase.

To describe the dynamics of the condensate part at zero temperature, we use the Heisenberg picture and a decomposition $\hat{\Phi}_\alpha(\boldsymbol{r},t) \approx \psi_\alpha(\boldsymbol{r},t) + \hat{\phi}_\alpha(\boldsymbol{r},t)$. The full Hamiltonian in Eq. (2.5) can be written such that

$$\hat{H} = \hat{H}_0 + \hat{H}_1 + \hat{H}_2 + \text{higher order terms}, \tag{2.9}$$

where the different parts are

$$\hat{H}_0 = \int \mathrm{d}\boldsymbol{r}\, \big[\vec{\Psi}^\dagger \hat{h} \vec{\Psi} + \frac{c_0}{2}|\vec{\Psi}|^4 + \frac{c_2}{2}(\vec{\Psi}^\dagger \boldsymbol{\mathcal{F}} \vec{\Psi})^2\big], \tag{2.10}$$

$$\hat{H}_1 = \int \mathrm{d}\boldsymbol{r}\, \hat{\phi}^\dagger_\alpha \big[\hat{h}_{\alpha\beta} + c_0|\vec{\Psi}|^2\delta_{\alpha\beta} + c_2(\vec{\Psi}^\dagger \boldsymbol{\mathcal{F}} \vec{\Psi})\cdot \boldsymbol{\mathcal{F}}_{\alpha\beta}\big]\psi_\beta \;\; + \;\; \text{h.c.}, \tag{2.11}$$

$$\hat{H}_2 = -\frac{1}{2}\int \mathrm{d}\boldsymbol{r}\, :(\hat{\phi}^\dagger_\alpha \;\; \hat{\phi}_\alpha)\, \mathcal{G}^{-1}_{\alpha\beta} \begin{pmatrix} \hat{\phi}_\beta \\ \hat{\phi}^\dagger_\beta \end{pmatrix} :, \tag{2.12}$$

and we have introduced the spinor $\vec{\Psi} = (\psi_+, \psi_0, \psi_-)$. The matrix $(\hat{h}_{\alpha\beta})$ is denoted by $\hat{h}$ in Eq. (2.10). The normal ordering is indicated by $:\cdot:$ and the zero temperature inverse Green's function is of the form

$$\mathcal{G}^{-1}_{\alpha\beta} = -\begin{pmatrix} \hat{h}_{\alpha\beta} + \Sigma_{\alpha\beta} & \Delta_{\alpha\beta} \\ \Delta^*_{\alpha\beta} & \hat{h}_{\beta\alpha} + \Sigma_{\beta\alpha} \end{pmatrix}. \tag{2.13}$$

The self-energies Σ and Δ are given by

$$\Sigma_{\alpha\beta} = c_0(\delta_{\alpha\beta}|\vec{\Psi}|^2 + \psi_\alpha\psi^*_\beta) + c_2(\boldsymbol{\mathcal{F}}_{\alpha\beta}\cdot\boldsymbol{\mathcal{F}}_{\alpha'\beta'} + \boldsymbol{\mathcal{F}}_{\alpha\beta'}\cdot\boldsymbol{\mathcal{F}}_{\alpha'\beta})\psi^*_{\alpha'}\psi_{\beta'}, \tag{2.14}$$

$$\Delta_{\alpha\beta} = c_0\psi_\alpha\psi_\beta + c_2\boldsymbol{\mathcal{F}}_{\alpha\alpha'}\cdot\boldsymbol{\mathcal{F}}_{\beta\beta'}\psi_{\alpha'}\psi_{\beta'}. \tag{2.15}$$

In the Heisenberg picture, the equation of motion for the field $\hat{\Phi}_\alpha(\boldsymbol{r},t)$ can be expressed approximately as

$$i\hbar\,\partial_t\hat{\Phi}_\alpha = [\hat{\Phi}_\alpha, \hat{H}] \approx [\hat{\Phi}_\alpha, \hat{H}_0 + \hat{H}_1 + \hat{H}_2], \tag{2.16}$$

which using Eqs. (2.10)–(2.12) results in

$$i\hbar\,\partial_t\vec{\Psi} = \hat{h}\vec{\Psi} + c_0|\vec{\Psi}|^2\vec{\Psi} + c_2(\vec{\Psi}^\dagger\boldsymbol{\mathcal{F}}\vec{\Psi})\cdot\boldsymbol{\mathcal{F}}\vec{\Psi}, \tag{2.17}$$

$$i\hbar\,\partial_t\hat{\phi}_\alpha = (\hat{h}_{\alpha\beta} + \Sigma_{\alpha\beta})\hat{\phi}_\beta + \Delta_{\alpha\beta}\,\hat{\phi}^\dagger_\beta, \tag{2.18}$$

where Eq. (2.17) is the Gross-Pitaevskii (GP) equation for the spin-1 Bose gas. The GP equation (2.17) forms the backbone of the mean-field analysis used in Publications I, III, IV, and VI.

Typically we are interested in the stationary solutions of the GP equation which are of the form $\psi_\alpha(\boldsymbol{r},t) = e^{-i\mu t/\hbar}\psi_\alpha(\boldsymbol{r})$, and the quasiparticle excitations corresponding to these mean-field states. In this case, the quasiparticle spectrum can be solved using Eq. (2.18) and a Bogoliubov transformation of the form

$$\hat{\phi}_\alpha(\boldsymbol{r},t) = e^{-i\mu t/\hbar}\sum_q [u_{q,\alpha}e^{-i\omega_q t}\hat{a}_q - v^*_{q,\alpha}e^{i\omega^*_q t}\hat{a}^\dagger_q], \tag{2.19}$$

where $\hat{a}^\dagger_q$ and $\hat{a}_q$ are the creation and annihilation operators for quasiparticles with energy $\hbar\omega_q$. The quasiparticle amplitudes are denoted by $u_{q,\alpha}$ and $v_{q,\alpha}$. Substituting Eq. (2.19) in Eq. (2.18) results in an eigenvalue problem

$$\mathcal{D}_{\alpha\beta}\begin{pmatrix} u_{\beta,q} \\ v_{\beta,q}\end{pmatrix} \equiv \begin{pmatrix} \mathcal{A}_{\alpha\beta} & -\mathcal{B}_{\alpha\beta} \\ \mathcal{B}^*_{\alpha\beta} & -\mathcal{A}^*_{\alpha\beta}\end{pmatrix}\begin{pmatrix} u_{\beta,q} \\ v_{\beta,q}\end{pmatrix} = \hbar\omega_q\begin{pmatrix} u_{\alpha,q} \\ v_{\alpha,q}\end{pmatrix}, \tag{2.20}$$

which is referred to as the Bogoliubov (BG) equation [110,111]. The matrix elements are given by $\mathcal{A}_{\alpha\beta} = \hat{h}_{\alpha\beta} - \mu\delta_{\alpha\beta} + \Sigma_{\alpha\beta}$ and $\mathcal{B}_{\alpha\beta} = \Delta_{\alpha\beta}$. The Bogoliubov transformation (2.19) is not unique but the different transformations yield BG equations that differ only by unitary transformations which leave the spectrum invariant. We also note that the matrix $\mathcal{A} = (\mathcal{A}_{\alpha\beta})$ is hermitian and the matrix $\mathcal{B} = (\mathcal{B}_{\alpha\beta})$ is symmetric. In the Bogoliubov transformation in Eq. (2.19), one may assume without loss of generality that only the quasiparticle amplitudes carry the spin index. In the Appendix A, we show that the Bogoliubov transformation of the form (2.19) is not imperative for resolving the quasiparticle spectrum.

The spectrum of the elementary excitations determines the stability of the corresponding stationary state. If all excitation energies $\hbar\omega_q$ are positive, the stationary state is referred to as energetically stable [30, 112]. This implies that the condensed component cannot lower its energy by exciting quasiparticles. The existence of excitations with negative energy indicates that the corresponding stationary solution of the time-independent GP equation does not correspond to a local minimum of the mean field energy[2]. However, such states can be quite long-lived since the relaxation

[2]If the state is an absolute minimum of the mean-field energy, that is, the ground state of the system, it is referred to as thermodynamically stable [54, 111, 113].

to the ground state necessitates the existence of dissipation which comes mostly in the form of the non-condensed atoms. An example of an energetically unstable state is a vortex in non-rotated condensates [114, 115]. The typical temperatures in the experiments are low enough such that the non-condensed component and, consequently, the dissipation are initially negligibly small, and the thermal component is largely generated during the relaxation processes [54]. In most situations, it is sufficient to use a zero-temperature formalism based on the GP equation.

In the Bogoliubov transformation (2.19), the quasiparticle energies $\hbar\omega_q$ can have a nonzero imaginary part. This is due to the fact that the operator $\mathcal{D}_{\alpha\beta}$ in the BG equation (2.20) is non-hermitian and can therefore have complex eigenvalues. Such eigenvalues correspond to dynamical instabilities which cause an exponential growth of initially small perturbations, driving the system dynamics beyond the scope of the linear approximation which is inherent to the BG equation. Vortices with multiple quanta of angular momentum in non-rotated condensates are an example of dynamically unstable states [116]. Dynamical instability can lead to the decay of a stationary configuration even in the absence of dissipation. Furthermore, the existence of an energetic instability is a prerequisite for a dynamical instability [117]. The Bogoliubov equation (2.20) is closely related to the Bogoliubov–de Gennes (BdG) equation describing the quasiparticles in fermionic superfluids [118]. However, the fermionic BdG equation does not have solutions with complex energies. The BG equation (2.20) is also sometimes referred to as the Bogoliubov–de Gennes equation [47] (see also Publication I).

The Bogoliubov equation (2.20) has two important symmetries that can be used to deduce the properties of the quasiparticle excitations. Let us define operators $\tau_1 = \sigma_1 \otimes \mathbb{1}$ and $\tau_3 = \sigma_3 \otimes \mathbb{1}$, where $\sigma_1, \sigma_2, \sigma_3$ are the spin-1/2 Pauli matrices and $\mathbb{1}$ is a 3×3 unit matrix. The BG equation has the following properties

$$\mathcal{D}^* = -\tau_1^\dagger \mathcal{D} \tau_1 \qquad \text{and} \qquad \mathcal{D}^\dagger = \tau_3^\dagger \mathcal{D} \tau_3. \tag{2.21}$$

The first relation implies that for a given eigenpair $(\hbar\omega_q, w_q)$, where $w_q = (u_q, v_q)$, there is a conjugate solution $(-\hbar\omega_q^*, \tau_1 w_q^*)$ which under the axial symmetry corresponds to a quasiparticle with an opposite angular momentum. The second identity in Eq. (2.21) shows that

$$\hbar(\omega_q^* - \omega_{q'}) \int \mathrm{d}\boldsymbol{r}\, w_q^\dagger(\boldsymbol{r}) \tau_3^\dagger w_{q'}(\boldsymbol{r}) = 0, \tag{2.22}$$

which implies that the quasiparticle amplitudes corresponding to real eigenvalues

can be normalised according to a pseudonorm[3]

$$\int \mathrm{d}\boldsymbol{r}\, w_q^\dagger(\boldsymbol{r})\tau_3^\dagger w_{q'}(\boldsymbol{r}) = \delta_{qq'}. \tag{2.23}$$

The correct normalisation of the eigenmodes with complex eigenvalues is somewhat complicated and it is discussed in Publication I. We also point out that the existence of complex eigenvalues in the BG equation indicates the failure of the usual Bogoliubov transformation [104] and special care must be taken to quantise the modes corresponding to the complex eigenvalues [119,120]. The methods of Refs. [119,120] can presumably be generalised to the spin-1 case considered here.

The BG equation (2.20) has a special zero energy solution $(u_q, v_q) = (\vec{\Psi}, -\vec{\Psi}^*)$ which corresponds to the Goldstone mode arising from the spontaneous breaking of the $U(1)$ symmetry [30, 47, 112, 121]. The effect of this mode is a phase diffusion which stems from the fact that the atom number of the condensate is fixed, implying that at $T = 0$ the phase of the condensate has to evolve slowly in time. At finite temperatures, atom number fluctuations are allowed and the phase diffusion is suppressed [121]. Moreover, the phase diffusion is a finite-size effect and it vanishes at the thermodynamical limit [121]. In spinor condensates, there are also other conserved quantities such as the magnetisation which gives rise to a spin diffusion that is coupled to the phase diffusion [122]. In this Thesis, we use the zero energy mode to check the numerical implementation of the Bogoliubov equation. In the absence of external magnetic fields, there are also dipole modes (Kohn modes) [123] for harmonically trapped systems. They correspond to the quasiparticle energies $\hbar\omega_a$ where $a = x, y, z$, and ω_a are the trap frequencies to the three spatial directions. The existence of the dipole modes for spin-1 BECs is shown in Publication I.

2.3 Hartree-Fock-Bogoliubov theory

To take into account the non-condensed atoms at $T \neq 0$ one may use the Hartree-Fock-Bogoliubov (HFB) approximation. Alternatively, the HFB theory gives rise to the Hartree-Fock-Popov (HFP) equations that are numerically more tractable than the HFB theory. The HFP equations have been utilised in Publication IX and they will be discussed further in Sections 2.3.1 and 7.3. For the weakly interacting single-component Bose gas, the HFB equations are derived in Ref. [124] and they can be straightforwardly generalised to the spinor case [125].

[3]The pseudonorm given by Eq. (2.23) is not a true norm since it is not positive definite. In principle, the left hand side of Eq. (2.23) can vanish for $q = q'$, but in practice this occurs only if the excitation is either the zero energy mode corresponding to the spontaneously broken $U(1)$ symmetry or a mode with a complex frequency ω_q [61]. The normalisation condition is discussed in detail in Ref. [119].

Let us assume for simplicity that there are no external magnetic fields. In this case $\hat{h}$ simplifies to $\hat{h}_{\alpha\beta} = \delta_{\alpha\beta}\,\mathcal{L}$, where $\mathcal{L} = -\frac{\hbar^2}{2m}\nabla^2 + V_{\rm tr}(\boldsymbol{r}) - \mu$ and we have assumed a grand canonical ensemble. Introducing a total density operator $\hat{n} = \hat{n}_+ + \hat{n}_0 + \hat{n}_-$ with $\hat{n}_\alpha = \hat{\Phi}_\alpha^\dagger \hat{\Phi}_\alpha$, the full Heisenberg equation of motion can be written as [125]

$$i\hbar\,\partial_t\,\hat{\Phi}_+ = \mathcal{L}\hat{\Phi}_+ + c_0\hat{n}\hat{\Phi}_+ + c_2(\hat{n}_+ + \hat{n}_0 - \hat{n}_-)\hat{\Phi}_+ + c_2\hat{\Phi}_-^\dagger\hat{\Phi}_0\hat{\Phi}_0, \tag{2.24a}$$

$$i\hbar\,\partial_t\,\hat{\Phi}_0 = \mathcal{L}\hat{\Phi}_0 + c_0\hat{n}\hat{\Phi}_0 + c_2(\hat{n}_+ + \hat{n}_-)\hat{\Phi}_0 + 2c_2\hat{\Phi}_0^\dagger\hat{\Phi}_+\hat{\Phi}_-, \tag{2.24b}$$

$$i\hbar\,\partial_t\,\hat{\Phi}_- = \mathcal{L}\hat{\Phi}_- + c_0\hat{n}\hat{\Phi}_- + c_2(\hat{n}_- + \hat{n}_0 - \hat{n}_+)\hat{\Phi}_- + c_2\hat{\Phi}_+^\dagger\hat{\Phi}_0\hat{\Phi}_0. \tag{2.24c}$$

Using the decomposition $\hat{\Phi}_\alpha(\boldsymbol{r},t) \approx \psi_\alpha(\boldsymbol{r},t) + \hat{\phi}_\alpha(\boldsymbol{r},t)$ and taking an expectation value from the both sides of Eq. (2.24), one obtains an equation of motion for the condensed component in the presence of a thermal component [125]. The equation of motion for the non-condensed part can be obtained by subtracting from Eq. (2.24) the equation of motion for the condensed component [124, 125]. This results in an exact equation of motion similar to the single-component case [124]. It can be simplified by treating the cubic terms with a self-consistent mean-field approximation such that

$$\begin{aligned}
&\hat{\phi}_\alpha^\dagger\hat{\phi}_\beta\hat{\phi}_\gamma \approx \langle\hat{\phi}_\alpha^\dagger\hat{\phi}_\beta\rangle\,\hat{\phi}_\gamma + \langle\hat{\phi}_\alpha^\dagger\hat{\phi}_\gamma\rangle\,\hat{\phi}_\beta + \langle\hat{\phi}_\beta\hat{\phi}_\gamma\rangle\,\hat{\phi}_\alpha^\dagger,\\
&\hat{\phi}_\alpha^\dagger\hat{\phi}_\beta \approx \langle\hat{\phi}_\alpha^\dagger\hat{\phi}_\beta\rangle,\\
&\hat{\phi}_\alpha\hat{\phi}_\beta \approx \langle\hat{\phi}_\alpha\hat{\phi}_\beta\rangle,\\
&\hat{\phi}_\alpha^\dagger\hat{\phi}_\beta^\dagger \approx \langle\hat{\phi}_\alpha^\dagger\hat{\phi}_\beta^\dagger\rangle.
\end{aligned}$$

The resulting HFB equations have been used to study the relation between magnetic ordering and Bose-Einstein condensation in spin-1 Bose gases [126].

2.3.1 Hartree-Fock-Popov approximation

The HFB theory can be further simplified by neglecting all terms of the form $\langle\hat{\phi}_\alpha\hat{\phi}_\beta\rangle$, $\langle\hat{\phi}_\alpha^\dagger\hat{\phi}_\beta^\dagger\rangle$, which generalises the Popov approximation [124, 127, 128] for the spinor condensates [125]. In the equation of motion for $\hat{\phi}_\alpha$, all off-diagonal terms such as $\langle\hat{\phi}_\alpha^\dagger\hat{\phi}_\beta\rangle$, $\alpha \neq \beta$, as well as all terms proportional to $\hat{\phi}_\beta^\dagger$ are neglected resulting in a set of equations

$$i\hbar\,\partial_t\,\hat{\phi}_+ = \mathcal{L}\,\hat{\phi}_+ + c_0(n + n_+)\hat{\phi}_+ + c_2(2n_+ + n_0 - n_-)\hat{\phi}_+, \tag{2.25a}$$

$$i\hbar\,\partial_t\,\hat{\phi}_0 = \mathcal{L}\,\hat{\phi}_0 + c_0(n + n_0)\hat{\phi}_0 + c_2(n_+ + n_-)\hat{\phi}_0, \tag{2.25b}$$

$$i\hbar\,\partial_t\,\hat{\phi}_- = \mathcal{L}\,\hat{\phi}_- + c_0(n + n_-)\hat{\phi}_- + c_2(2n_- + n_0 - n_+)\hat{\phi}_-, \tag{2.25c}$$

where $n_\alpha = \langle \hat{n}_\alpha \rangle = |\psi_\alpha|^2 + \langle \hat{\phi}_\alpha^\dagger \hat{\phi}_\alpha \rangle$ and $n = \langle \hat{n} \rangle = n_+ + n_0 + n_-$. Equations (2.25) are the HFP equations for the spin-1 case [125].

Further progress can be made using the semiclassical approximation in which $-i\hbar\nabla \to \hbar\boldsymbol{k}$. Using an ansatz $\hat{\phi}_\alpha(\boldsymbol{r}, t) = \exp[-i\varepsilon_\alpha(\boldsymbol{k}, \boldsymbol{r})t/\hbar]\phi_\alpha(\boldsymbol{r})$ which together with Eq. (2.25) yields the single particle spectrum

$$\varepsilon_+(\boldsymbol{k}, \boldsymbol{r}) = \frac{\hbar^2\boldsymbol{k}^2}{2m} + V_{\rm tr}(\boldsymbol{r}) - \mu + c_0(n + n_+) + c_2(2n_+ + n_0 - n_-), \tag{2.26a}$$

$$\varepsilon_0(\boldsymbol{k}, \boldsymbol{r}) = \frac{\hbar^2\boldsymbol{k}^2}{2m} + V_{\rm tr}(\boldsymbol{r}) - \mu + c_0(n + n_0) + c_2(n_+ + n_-), \tag{2.26b}$$

$$\varepsilon_-(\boldsymbol{k}, \boldsymbol{r}) = \frac{\hbar^2\boldsymbol{k}^2}{2m} + V_{\rm tr}(\boldsymbol{r}) - \mu + c_0(n + n_-) + c_2(2n_- + n_0 - n_+). \tag{2.26c}$$

The occupation numbers $n_\alpha^T = \langle \hat{\phi}_\alpha^\dagger \hat{\phi}_\alpha \rangle$ for the thermal (non-condensed) atoms can be computed using the Bose-Einstein distribution

$$n_\alpha^T(\boldsymbol{r}) = \int \frac{{\rm d}\boldsymbol{k}}{(2\pi)^3} \, \frac{1}{e^{\varepsilon_\alpha(\boldsymbol{k},\boldsymbol{r})/k_{\rm B}T} - 1}. \tag{2.27}$$

Equations (2.17), (2.26) and (2.27) form a closed set of equations that can be solved self-consistently to obtain the number of the thermal atoms[4].

In the single-component systems, the Popov approximation is expected to be reasonable at temperatures below the temperature $T_{\rm BEC}$, excluding the critical region near $T_{\rm BEC}$ [124,128,130,131]. The temperature $T_{\rm BEC}$ corresponds to the onset of BEC. Furthermore, the semiclassical approximation is valid when $\hbar\omega_a \ll k_{\rm B}T$, where ω_a, $a = x, y, z$, are the trap frequencies. The semiclassical HFP approximation has been found to agree with the experimental data reasonably well [132] and it is considered as a reasonable tool to investigate the thermodynamical properties of dilute trapped gases [133]. The semiclassical HFP approximation has also been used to investigate the finite temperature properties of spin-1 gases, yielding an agreement with the more rigorous HFB calculation [125, 126].

The semiclassical HFP method becomes unreliable in the critical region where strong fluctuations render the mean-field approximation invalid. In the next section, we discuss a method to cure this problem by assuming that the strongly fluctuating modes are restricted to the low-energy part of the spectrum which is treated non-perturbatively while the high-energy modes are taken into account using the semiclassical HFP scheme. This approach introduces a low-energy cutoff to the semiclassical integral in Eq. (2.27).

[4]The semiclassical approximation becomes actually inconsistent for the low-energy part of the spectrum and more accurate results are obtained if the integral in Eq. (2.27) has a low-energy cutoff [129] and the low-energy modes are treated using, e.g., the HFB theory.

3 Finite-temperature phase transitions – beyond the mean-field approximation

The ferromagnet–paramagnet transition and the superfluid–normal fluid transition are examples of phase transitions that are driven by thermal fluctuations. A common feature of these phase transitions is that the mean-field theories become unreliable below the upper critical dimension because the fluctuations neglected by the mean-field approach become important near the critical temperature. The critical dimension is typically four [105, 134], rendering the systems of practical interest outside the applicability of mean-field approaches.

Phase transitions take place in the thermodynamical limit at which both the volume and the number of particles tend to infinity while the density of the system remains constant [134]. In the trapped atomic gases, two complications arise. The number of atoms is far from the thermodynamical limit which changes the phase transitions to smooth crossovers. Furthermore, the external potential renders the density of the system inhomogeneous, which allows a co-existence of different phases in the trap. Unlike in the most solid state systems, these finite-size effects are not artefacts of the theoretical approaches and they give rise to new phenomena that are interesting in their own right. Despite the complications imposed by the inhomogeneity and the mesoscopic character of the system, recent experiments have succeeded in probing the critical properties of trapped Bose gases [135].

To interpret the experimental results near the critical regime, a theoretical formalism capable of taking into account the characteristics of the experimental systems is needed. While the traditional methods of many-body physics are more suited for uniform systems, there is a family of methods referred to as the c-field techniques [136] that take into account the various aspects of the external confinement. In this section, we generalise one of these methods, the projected Gross-Pitaevskii equation (PGPE), to the case of spin-1 bosons. The spin-1 version of the PGPE has been used in Publication IX to investigate finite-temperature phase transitions in antiferromagnetic spin-1 Bose gases.

3.1 Classical field methods and the projected Gross-Pitaevskii equation

The essential idea in the classical field (c-field) methods is the separation of the system into two regions: the c-field region which contains the degenerate modes with large occupation numbers and the incoherent region in which the sparsely occupied thermal modes reside [136]. In the approach based on the projected Gross-Pitaevskii equation, the low-energy c-field modes are described with classical fields

and they form a microcanonical system where the coupling to the incoherent modes is neglected. The c-field region and the incoherent region are assumed to be in a thermal and diffusive equilibrium such that once the temperature and the chemical potential of the c-field region are know, they can be used to calculate the properties of the incoherent region using, e.g., the HFP approximation discussed in the previous section. The essential features of the PGPE approach are summarised in Fig. 3.1 (see also [136]).

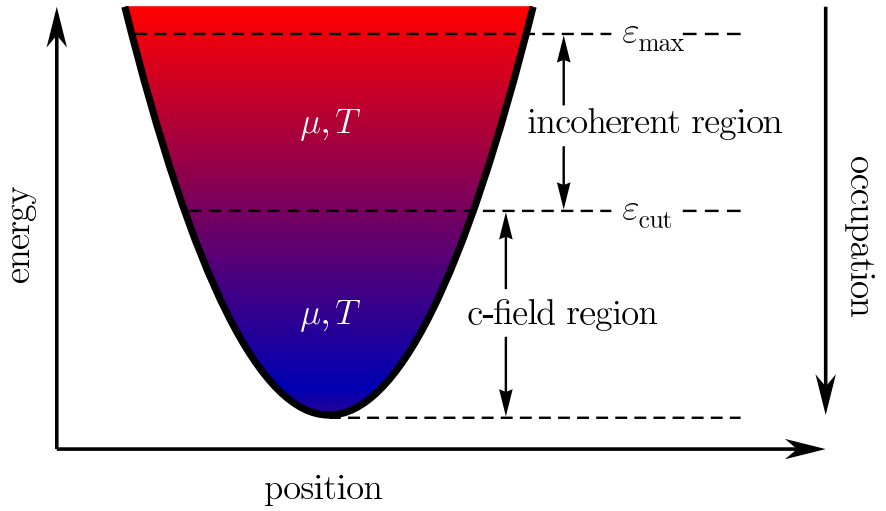

Figure 3.1: Illustration of the different energy scales in the PGPE approach. The modes below $\varepsilon_{\rm cut}$ form the c-field region. The incoherent modes between $\varepsilon_{\rm cut}$ and $\varepsilon_{\rm max}$ have small occupation and are taken into account using the HFP approximation. States above $\varepsilon_{\rm max}$ are in principle eliminated due to the use of the s-wave approximation for the two-particle scattering processes. The c-field region and the incoherent region are assumed to be in a thermal and diffusive equilibrium. The time evolution of the system is restricted to the c-field region by introducing an explicit projection operator to the equation of motion.

The PGPE approach can be motivated by the following observations. Let us assume that the system is confined into a harmonic potential in the absence of external magnetic fields. We expand the field operators $\hat{\Phi}_\alpha$ in terms of the eigenstates of the single particle operator $\hat{h}_0 = -\frac{\hbar^2}{2m}\nabla^2 + V_{\rm tr}$ such that

$$\hat{\Phi}_\alpha(\boldsymbol{r}) = \sum_{n\in\boldsymbol{C}} \hat{c}_{\alpha,n}\varphi_n(\boldsymbol{r}) + \sum_{n\in\boldsymbol{I}} \hat{a}_{\alpha,n}\varphi_n(\boldsymbol{r}) \approx \sum_{n\in\boldsymbol{C}} c_{\alpha,n}\varphi_n(\boldsymbol{r}) + \sum_{n\in\boldsymbol{I}} \hat{a}_{\alpha,n}\varphi_n(\boldsymbol{r}), \quad (3.1)$$

where we have replaced the $\hat{c}_{\alpha,n}$ operators in the $\boldsymbol{C}$ region with complex numbers (c-numbers) $c_{\alpha,n}$ in the spirit of the Bogoliubov substitution (2.8) used to describe

the highly occupied condensate mode at $T = 0$. The c-field region is defined as $\boldsymbol{C} = \{n \,|\, \varepsilon_n \leq \varepsilon_{\rm cut}\}$ and the incoherent region correspondingly $\boldsymbol{I} = \{n \,|\, \varepsilon_n > \varepsilon_{\rm cut}\}$. The energies ε_n are the eigenenergies of $\hat{h}_0$.

The c-number substitution [101] in single-component systems at $T = 0$ can be verified rigorously in the thermodynamical limit in the sense that it yields the correct values for the thermodynamical quantities. Moreover, the same proof extends to finite temperatures such that several other modes in addition to the lowest energy mode can be be treated as c-numbers [137,138]. This approximation is valid provided that the number of particles is much larger than the number of modes for which the c-number substitution is applied [137, 138]. This is similar to the condition that the occupation number of the c-field modes has to be large in the PGPE approach [136]. At the moment, there are no rigorous results to evaluate how large this occupation should be. In practice, the occupation of the c-field modes should be larger than n_{cut} where n_{cut} is from the range 1 to 10 [136]. The PGPE calculations model closely the experimental systems which typically are not in the thermodynamical limit, and therefore the rigorous results [137, 138] are not directly applicable to the PGPE approach.

In single-component systems, PGPE methods have been used to calculate the shift in the critical temperature of the condensation due to interactions [139, 140]. The PGPE results yield a good agreement with other numerical methods such as quantum Monte Carlo calculations, HFB, and HFP approximations as well as with experiments [136, 139, 140]. More recently, the c-field methods have been used to analyse the BKT transition in quasi-two-dimensional geometries [141–143] and a qualitative agreement with the c-field calculations and the experiments have been found [143, 144].

The heart of the PGPE method is a projection operator $\mathcal{P}_{\boldsymbol{C}}$ that restricts the time-evolution of the system to the low-energy region of the c-field modes in order to faithfully represent the dynamics of the relevant modes [136]. Using the basis defining the low-energy modes, the projection operator becomes

$$\mathcal{P}_{\boldsymbol{C}}[f(\boldsymbol{r})] = \sum_{n\in\boldsymbol{C}} \varphi_n(\boldsymbol{r}) \int \mathrm{d}\boldsymbol{r}'\, \varphi_n^*(\boldsymbol{r}') f(\boldsymbol{r}'), \tag{3.2}$$

where f is any function or operator. In the PGPE, the Hamiltonian (2.10) is restricted to the c-field region where

$$\psi_{\boldsymbol{C},\alpha}(\boldsymbol{r}) = \sum_{n\in\boldsymbol{C}} c_{\alpha,n}\varphi_n(\boldsymbol{r}). \tag{3.3}$$

The Poisson bracket for functionals F and G defined in the space of the c fields is

given by

$$\{F,G\} = \int \mathrm{d}\boldsymbol{r}\, \left[\frac{\delta F}{\delta \psi_{\boldsymbol{C},\alpha}(\boldsymbol{r})} \frac{\delta G}{\delta \psi^*_{\boldsymbol{C},\alpha}(\boldsymbol{r})} - \frac{\delta G}{\delta \psi_{\boldsymbol{C},\alpha}(\boldsymbol{r})} \frac{\delta F}{\delta \psi^*_{\boldsymbol{C},\alpha}(\boldsymbol{r})} \right], \tag{3.4}$$

where the functional derivatives are [136]

$$\frac{\delta}{\delta \psi_{\boldsymbol{C},\alpha}(\boldsymbol{r})} = \sum_{n\in\boldsymbol{C}} \varphi^*_n(\boldsymbol{r}) \frac{\partial}{\partial c_{\alpha,n}} \qquad \text{and} \qquad \frac{\delta}{\delta \psi^*_{\boldsymbol{C},\alpha}(\boldsymbol{r})} = \sum_{n\in\boldsymbol{C}} \varphi_n(\boldsymbol{r}) \frac{\partial}{\partial c^*_{\alpha,n}}. \tag{3.5}$$

The equation of motion for the c field is the Heisenberg equation of motion where the commutator is replaced by the Poisson bracket (3.4)

$$i\hbar\, \partial_t\, \psi_{\boldsymbol{C},\alpha} = \{\psi_{\boldsymbol{C},\alpha}, \mathcal{H}_{\boldsymbol{C}}\},$$

where $\mathcal{H}_{\boldsymbol{C}}$ is the Hamiltonian (2.10) restricted to the c-field region. This yields the projected Gross-Pitaevskii equation

$$i\hbar\, \partial_t \vec{\Psi}_{\boldsymbol{C}} = \hat{h}_0 \vec{\Psi}_{\boldsymbol{C}} + \mathcal{P}_{\boldsymbol{C}} \big\{ c_0 |\vec{\Psi}_{\boldsymbol{C}}|^2 \vec{\Psi}_{\boldsymbol{C}} + c_2 (\vec{\Psi}^\dagger_{\boldsymbol{C}} \boldsymbol{\mathcal{F}}\, \vec{\Psi}_{\boldsymbol{C}}) \cdot \boldsymbol{\mathcal{F}}\, \vec{\Psi}_{\boldsymbol{C}} \big\}. \tag{3.6}$$

An optical potential of the form $V_{\mathrm{tr}}(\boldsymbol{r}) = \frac{m}{2}(\omega_x^2 x^2 + \omega_y^2 y^2 + \omega_z^2 z^2)$ enables an efficient numerical implementation of the projection operator [136, 145].

The basic assumption of statistical mechanics is the equivalence of time averages and the corresponding equilibrium ensemble averages, which is known as the ergodic hypothesis [134]. In the context of the PGPE, invoking the ergodic hypothesis allows one to study the equilibrium properties of the gas by calculating the ensemble averages as the corresponding time averages. Typically, the calculations start from a randomised initial state which is allowed to thermalize to the equilibrium before the time averages are computed. For trapped Bose gases, the relaxation towards the equilibrium distribution is relatively fast [136]. This allows a computation of quantities such as the one-body density matrix (2.3) and gives rise to a dynamical calculation of the temperature and the chemical potential, which is discussed in the next section.

3.2 Thermodynamical quantities in the PGPE

The PGPE arises as an equation of motion for the Hamiltonian system determined by (2.10). This formulation provides a convenient method for calculating the temperature and the chemical potential using general results for the Hamiltonian systems [146, 147]. For single-component Bose gases, the Hamiltonian formulation provides an accurate method for determining the thermodynamical quantities [139, 148]

and it has become a standard method for computing the temperature and the chemical potential in the PGPE calculations [136]. Using Eq. (3.3), canonically conjugated coordinates for the Hamiltonian system (2.10) can be defined as (cf. [139, 148])

$$Q_{\alpha,n} = \frac{1}{\sqrt{2\varepsilon_n}}(c^*_{\alpha,n} + c_{\alpha,n}) \qquad \text{and} \qquad P_{\alpha,n} = i\sqrt{\frac{\varepsilon_n}{2}}(c^*_{\alpha,n} - c_{\alpha,n}). \tag{3.7}$$

The canonical coordinates are collectively denoted by $\mathbf{\Gamma} = \{Q_{\alpha,n}, P_{\alpha,n}\}$.

A general theorem [146] states that the temperature can be calculated as

$$\frac{1}{k_{\mathrm{B}}T} \equiv \left(\frac{\partial S}{\partial E}\right)_N = \langle \mathcal{D} \cdot \boldsymbol{X}_T(\mathbf{\Gamma})\rangle, \tag{3.8}$$

where the first identity is the standard definition of the temperature of a microcanonical system. The operator $\mathcal{D} = \{e_n \partial_{\Gamma_n}\}$ is determined by the real coefficients $\{e_n\}$ that can be chosen freely [148]. The vector field $\boldsymbol{X}_T$ is arbitrary as long as it satisfies the conditions

$$\mathcal{D}\mathcal{H}_C \cdot \boldsymbol{X}_T = 1 \qquad \text{and} \qquad \mathcal{D}\mathcal{N}_C \cdot \boldsymbol{X}_T = 0, \tag{3.9}$$

where $\mathcal{N}_C = \int \mathrm{d}\boldsymbol{r}\, |\vec{\Psi}_C|^2$ is the number of c-field atoms. The vector field $\boldsymbol{X}_T$ satisfying the above constraints can shown to be [139, 148]

$$\boldsymbol{X}_T = \frac{\mathcal{D}\mathcal{H}_C - \lambda_N \mathcal{D}\mathcal{N}_C}{|\mathcal{D}\mathcal{H}_C|^2 - \lambda_N(\mathcal{D}\mathcal{N}_C \cdot \mathcal{D}\mathcal{H}_C)}, \tag{3.10}$$

with $\lambda_N = (\mathcal{D}\mathcal{N}_C \cdot \mathcal{D}\mathcal{H}_C)/|\mathcal{D}\mathcal{N}_C|^2$. Computationally straightforward choices of the vector operator $\mathcal{D}$ are $\mathcal{D}_P = \{0, \partial_{P_n}\}$ and $\mathcal{D}_Q = \{\partial_{Q_n}, 0\}$ [148]. Since the temperature should be independent of the choice of the derivative $\mathcal{D}$, the two different choices serve also as a check for the numerical implementation. The average in Eq.(3.8) can be computed as a time-average.

The present formulation applies when the only conserving quantity is the particle number $\mathcal{N}_C$. In a cylindrically symmetric situation, also the angular momentum is conserved. Transforming to the coordinate system with a zero total angular momentum, this problem can be circumvented [147, 148]. In the spinor Bose gases, the conservation of the total magnetisation needs to be taken into account, but in the antiferromagnetic case where the magnetisation is zero, the conservation of the magnetisation can be neglected in the light of the previous argument. Using the definition $\mu/k_{\mathrm{B}}T = -(\partial S/\partial N)_E$, the chemical potential can be computed by interchanging $\mathcal{H}_C$ and $\mathcal{N}_C$.

4 Superfluidity and topological defects in spinor Bose gases

In spinor Bose gases, superfluidity and magnetic ordering are intertwined giving rise to multitudes of different topological defects. In order to understand the superfluidity, we first consider the possible topological defects that are manifested in the different phases of spinor Bose gases. An important differences to the single-component superfluids is that the superfluid circulation needs not to be quantised and the vorticity satisfies a condition relating the magnetic ordering to the superfluidity. This has a profound impact on the quantities such as the superfluid velocity which can be finite everywhere, allowing the existence of vortices without a singular core. Such vortices are referred to as coreless vortices and their properties will be discussed in detail in Section 5.

4.1 Classification of topological defects

Let us first consider the properties of the mean-field states that can arise in spinor Bose gases. To classify the possible mean-field states, we consider the spin-dependent part of the mean-field Hamiltonian (2.10). For the ferromagnetic phase corresponding to $c_2 < 0$, it is energetically favourable to maximise the local spin $\boldsymbol{\mathcal{S}} = \vec{\Psi}^\dagger \boldsymbol{\mathcal{F}} \vec{\Psi}$. For $c_2 > 0$, the local spin tends to vanish giving rise to the polar phase. The resulting mean-field states $\vec{\Psi} = \sqrt{\varrho}\,\vec{\zeta}$ are of the form [29]

$$\vec{\zeta}_F = e^{i(\theta-\tau)} \begin{pmatrix} e^{-i\alpha}\cos^2\frac{\beta}{2} \\ \sqrt{2}\sin\frac{\beta}{2}\cos\frac{\beta}{2} \\ e^{i\alpha}\sin^2\frac{\beta}{2} \end{pmatrix} \quad \text{and} \quad \vec{\zeta}_P = e^{i\theta} \begin{pmatrix} -\frac{1}{\sqrt{2}}e^{-i\alpha}\sin\beta \\ \cos\beta \\ \frac{1}{\sqrt{2}}e^{i\alpha}\sin\beta \end{pmatrix}, \tag{4.1}$$

for the ferromagnetic and the polar phases, respectively. The particle density is denoted by ϱ. The Euler angles parametrising the $SO(3)$ spin rotations $\mathcal{U}(\alpha,\beta,\tau) = e^{-i\alpha\mathcal{F}_z}\, e^{-i\beta\mathcal{F}_y}\, e^{-i\tau\mathcal{F}_z}$ are given by $\{\alpha,\beta,\tau\}$ and θ corresponds to the $U(1)$ phase. For the ferromagnetic phase, the local spin becomes

$$\boldsymbol{\mathcal{S}} = \vec{\zeta}_F^{\,\dagger} \boldsymbol{\mathcal{F}} \vec{\zeta}_F = \sin\beta\cos\alpha\hat{\boldsymbol{e}}_x + \sin\beta\sin\alpha\hat{\boldsymbol{e}}_y + \cos\beta\hat{\boldsymbol{e}}_z, \tag{4.2}$$

whereas in the polar phase, $\boldsymbol{\mathcal{S}}$ vanishes identically.

The mean-field states in Eq. (4.1) can be obtained by operating to a reference spinor[5] intrinsic to a given phase by the $SO(3)$ spin rotations and the $U(1)$ phase factor. The nontrivial operations on the reference spinors possess a group structure

[5] The reference spinors are for example $\vec{\zeta}_F = (1,0,0)$ and $\vec{\zeta}_P = (0,1,0)$.

corresponding to $\mathcal{G}_{\rm F} = SO(3)$ in the ferromagnetic phase and $\mathcal{G}_{\rm P} = [U(1) \times S^2]/\mathbb{Z}_2$ in the polar phase [29,90,149,150]. The group $\mathcal{G}$ is referred to as the order parameter space since the mean-field state (order parameter) can be locally identified with an element of $\mathcal{G}$.

According to the general principles [72,151], the existence of nontrivial topological defects is dictated by the topological properties of the order parameter space. In general, an m-dimensional defect in a d-dimensional space in characterised by the homotopy group $\pi_{d-m-1}(\mathcal{G})$ [72]. Zero-dimensional, i.e., point-like defects are called monopoles, one-dimensional defects are referred to as vortices and two-dimensional defects are coined as domain walls. This list does not exhaust all possible defects and there are important cases where the effective dimension of the defect coincides with the spatial dimension of the underlying space such that the defect still has properties similar to point-like defects. Such defects are commonly referred to as skyrmions mainly for historical reasons [105,152]. Another important class of defects is formed by structures characterised by the Hopf invariant [153,154]. The homotopy groups and the relevant defects for spin-1 Bose gases are listed in Table 4.1.

	$\mathcal{G} = [U(1) \times S^2]/\mathbb{Z}_2$	$\mathcal{G} = SO(3)$
$\pi_1(\mathcal{G})$	$\mathbb{Z}$ (vortices [29,90,149])	$\mathbb{Z}_2$ (vortices [29])
$\pi_2(\mathcal{G})$	$\mathbb{Z}$ (skyrmions [155], monopoles [73])	0 (Dirac monopoles [75])
$\pi_3(\mathcal{G})$	$\mathbb{Z}$ (Hopf textures [82])	$\mathbb{Z}$ (Hopf textures [81])

Table 4.1: List of the possible topological defects relevant to the spin-1 Bose gases. The polar phase corresponds to $\mathcal{G} = [U(1) \times S^2]/\mathbb{Z}_2$ and the ferromagnetic phase to $\mathcal{G} = SO(3)$. In the ferromagnetic case, isolated monopoles are not possible and there is a vortex (Dirac string) attached to the monopole.

4.1.1 Ferromagnetic phase

In the ferromagnetic phase, the topological defects are associated with the local spin $\boldsymbol{\mathcal{S}}$ and they are analogous to those found in ^{3}He-A which is a fermionic superfluid[6]. In particular, the ferromagnetic phase features only one type of nontrivial vortices referred to as disgyrations in the context of ^{3}He-A [28,156]. The possible configurations of $\boldsymbol{\mathcal{S}}$ are depicted in Fig. 4.1 and they correspond to $\theta = \tau = 0$ and $\alpha = \pm\varphi$ in Eq. (4.1). The disgyrations are singular defects for which the particle density vanishes at the centre of the vortex. In spin-1 BECs such defects are energetically

[6] In the superfluid ^{3}He-A, the quantity corresponding to the local spin $\boldsymbol{\mathcal{S}}$ is the angular momentum vector $\vec{\ell}$ associated with the Cooper pairs.

unfavourable compared to defects which have the disgyration structure of Fig. 4.1 outside of the core but exhibit a vanishing spin and a finite particle density at the vortex core. These vortices are referred to as the polar-core vortices [157] and they present an interesting example of the co-existence of competing magnetic phases in spinor condensates. The properties of the polar-core vortices in spinor BECs have been considered in Refs. [110,111,157–160] as well as in Publication IV in which the quasiparticle spectrum in the presence of an external magnetic field was calculated. We discuss the results of Publication IV in more detail in Section 5.5.

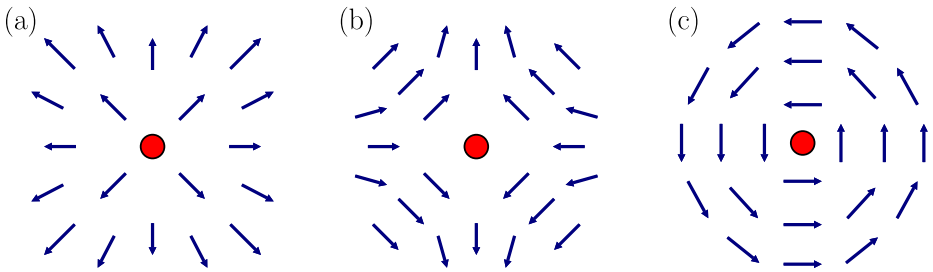

Figure 4.1: Different disgyration textures that can take place in the ferromagnetic phase. The illustrated configurations correspond to the local spin $\boldsymbol{\mathcal{S}}$ which for simplicity is restricted to 2D plane. The disgyration has a singular core with vanishing particle density. In spinor BECs, it is energetically more favourable to form vortices with a soft core where the local spin $\boldsymbol{\mathcal{S}}$ vanishes. The textures in (a) and (c) are equivalent in the sense that they can be converted to each other by local spin rotation, see Ref. [151] and Publication VI. On the other hand, the texture in (b) is distinct from (a) and (c) since it has an opposite winding number in the 2D plane [151].

Continuing the analogy to the superfluid ^{3}He-A, there are also vortex configurations that can be continuously changed into a uniform texture. Such vortices are referred to as continuous vortices [88, 89] or coreless vortices [58, 161] and they correspond to $\theta - \tau = \pm\alpha$ and $\alpha = \pm\varphi$ in Eq. (4.1). Some of the possible textures are presented in Fig. 4.2. Equations (4.1) and (4.2) imply that the behaviour of $\beta(\boldsymbol{r})$ at the boundary of the condensate ($|\boldsymbol{r}_\perp| = R$) determines the type of the spin texture. The textures in Fig. 4.2 (a) and (c) correspond to the Mermin-Ho (MH) and the Anderson-Toulouse (AT) vortices, respectively. The MH vortex has $\beta(R) = \pi/2$ and the AT vortex yields $\beta(R) = \pi$. They were originally introduced in the context of ^{3}He-A [63, 162].

In the ^{3}He experiments, the boundary of the vessel in which the liquid is enclosed sets a natural boundary condition that favours the MH vortex [87]. In gaseous spin-1 BECs, there are no rigid boundaries and in principle, the spin texture can take any

form between a uniform texture and the AT texture in Fig. 4.2 (c) (see Fig. 4.2). The coreless vortices in spin-1 BECs are energetically unstable in the absence of external rotation or magnetic fields and they can also exhibit dynamical instabilities. The energetic and dynamical instabilities associated with coreless vortices were investigated in Publications I and IV and the results are reviewed in Sections 5.1 and 5.5. In the presence of external rotation, one can select either the MH or the AT vortex by changing the magnetisation of the condensate [111, 157, 159]. An interesting feature of spinor Bose gases is the generation of superfluid flow by the application of an external magnetic field [160]. This can be shown to stabilise the coreless vortices and it also plays an important role in the generation of vortices carrying multiple quanta of angular momentum. These aspects are considered in Publications II, III, IV, V, and Section 5.

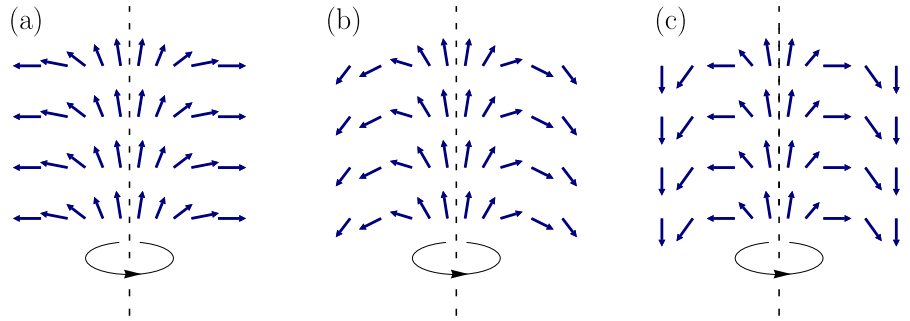

Figure 4.2: Possible configurations of coreless vortices. The figure illustrates the condensate spin $\boldsymbol{\mathcal{S}}$ such that the spin texture extends only to the boundary of the condensate ($|\boldsymbol{r}_\perp| = R$). The Mermin-Ho (MH) vortex is shown in (a) and the Anderson-Toulouse (AT) vortex in (c). In trapped gases, $\boldsymbol{\mathcal{S}}$ can in principle take any value at the boundary of the condensate and the texture in (b) is one of the other possible textures that interpolate between the MH and the AT vortices. The textures are symmetric with respect to rotations about the core of the vortex denoted by the dashed line. At the core of the defect, the spin $\boldsymbol{\mathcal{S}}$ is continuous and the particle density ϱ is non-vanishing.

Coreless vortices do not have quantised circulation in the same sense as singular vortices in the single-component condensates. However, when the system is effectively two-dimensional and the direction of $\boldsymbol{\mathcal{S}}$ is asymptotically fixed by a strong enough magnetic field or due to the existence of a periodic vortex lattice in rotated condensates, the spin texture gives rise to a mapping $\hat{\boldsymbol{s}} : S^2 \mapsto S^2$ where $\hat{\boldsymbol{s}} = \boldsymbol{\mathcal{S}}/|\boldsymbol{\mathcal{S}}|$. The coreless vortex can be characterised by a number that indicates how many times the spin texture covers the unit sphere. Formally, this is expressed as a topological

charge [88]

$$\mathcal{Q}_{2D} = \frac{1}{4\pi} \int \mathrm{d}x\, \mathrm{d}y \;\; \varepsilon_{abc}\, \hat{\boldsymbol{s}}_a\, \partial_x \hat{\boldsymbol{s}}_b\, \partial_y \hat{\boldsymbol{s}}_c, \tag{4.3}$$

where the Levi-Civita symbol is denoted by ε_{abc} and the integral is taken over the x-y plane. The existence of a nontrivial topological charge does not contradict the previous result (see Table 4.1) of the ferromagnetic order parameter space having a trivial second homotopy group since external fields or rotation are required to fix $\boldsymbol{\mathcal{S}}$ asymptotically. The coreless vortices characterised by the topological charge (4.3) are an example of skyrmions which have been widely studied in the context of dense nuclear matter [163], quantum-Hall ferromagnets [164, 165], and frustrated magnets [166, 167].

Due to the trivial second homotopy group, there are no isolated monopoles in the ferromagnetic phase. This does not completely exclude the existence of monopoles and, in fact, they can take place as the endpoints of vortex lines. Originally several variations of this idea were introduced in the studies of superfluid ^{3}He [64, 65, 88, 89, 168], and the same concept was subsequently discovered in the context of spinor BECs [75]. The monopole defects in the ferromagnetic phase have the interesting feature that the associated vorticity is analogous to the magnetic field of a magnetic monopole [75]. Furthermore, the vortex filament extending outwards from the monopole is a physical realisation of the Dirac string that is essential in the construction of magnetic point charges in terms of the conventional electromagnetism [169, 170]. Since magnetic monopoles have never been observed in real electromagnetic fields, there has been interest in realising analogs of magnetic monopoles in condensed matter systems [171–175]. In Publication VI, a method to create Dirac monopoles in spinor BECs was introduced and it is discussed in detail in Section 6.2.

Some of the possible monopole configurations are illustrated in Fig. 4.3 and they can be characterised by the charge

$$\mathcal{Q}_{3D} = \frac{1}{8\pi} \int_{\Sigma} \mathrm{d}^2\sigma_i \;\; \varepsilon_{ijk}\varepsilon_{abc}\, \hat{s}_a\, \partial_j \hat{s}_b\, \partial_k \hat{s}_c, \tag{4.4}$$

where the integral is taken over a surface Σ enclosing the defect. Unlike $\mathcal{Q}_{2D}$, the charge $\mathcal{Q}_{3D}$ is not a topological invariant in the case of the Dirac monopole since $\hat{\boldsymbol{s}}$ is not well-defined along the Dirac string [75]. The charge of the texture has an interesting connection to the superfluid flow and it will be elaborated in Section 4.2.

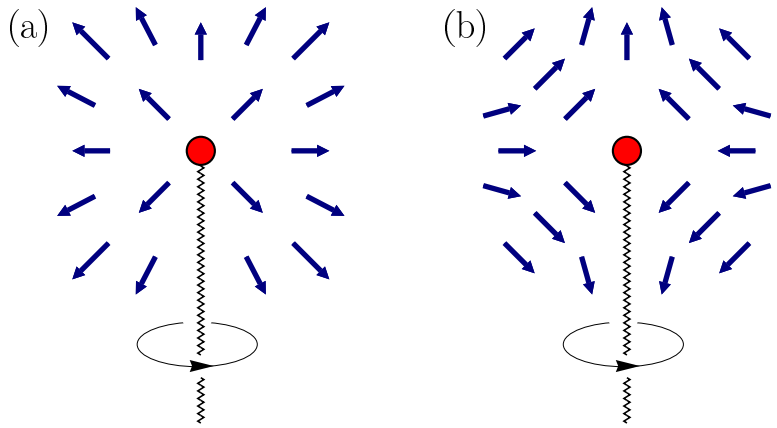

Figure 4.3: Schematic illustrations of the condensate spin $\boldsymbol{\mathcal{S}}$ corresponding to the possible Dirac monopoles. Both configurations are characterised by the charge $\mathcal{Q}_{3D} = 1$ and they give rise to identical superfluid flows. A monopole with $\mathcal{Q}_{3D} = -1$ is obtained by inverting the arrows. Only the defect in panel (b) can be created using the methods of Publication VI. The Dirac string is located at the negative z axis and denoted by the zigzag line. The configurations are symmetric with respect to rotations about the z axis.

The ferromagnetic phase can also feature defects that are characterised by the third homotopy group π_3. The spin texture of these defects takes a uniform asymptotic form as $|\boldsymbol{r}| \to \infty$ but has otherwise a non-trivial structure. According to Table 4.1, a plethora of such configurations is allowed in the ferromagnetic phase. Analogous configurations are expected to exist also in ^{3}He-A [176] and they are referred to as the Shankar monopoles even though they are non-singular configurations [72, 176]. The simplest structures have been theoretically constructed in the case of spin-1 BECs some years a ago [177], but to date an experimental realisation of these states is still lacking.

4.1.2 Polar phase

The polar phase of spin-1 Bose gases has an equally rich variety of possible topological defects including vortices [29], skyrmions [155], monopoles [73] and textures characterised by the Hopf invariant [82]. We consider here only vortices and skyrmions since they are the relevant defects for our discussion of the BKT transition in spin-1 Bose gases in Section 7. Similarly to the ferromagnetic phase with polar-core vortices, the polar phase has vortices where the core region is ferromagnetic. These vortices are an interesting example of fractionalised vortices where the superfluid flow carries only a half of the angular momentum quantum. This half-quantum vortex (HQV) consists of a phase defect bound to a spin defect [83, 86, 90, 178] and

its detailed structure will be discussed later in this section. Due to the existence of vortices with ferromagnetic cores, we will from now on refer to the Bose gases with $c_2 > 0$ as antiferromagnetic and use the term polar to refer to the phase where the local spin vanishes identically.

The Hamiltonian in Eq. (2.10) is written in the basis consisting of the Zeeman substates $|1, \beta\rangle$, $\beta = +, 0, -$ and it is thus important to note that the explicit expressions in Eq. (4.1) are specific to this particular basis. Although this basis has the advantage that the different components can be readily accessed using the Stern-Gerlach separation with external magnetic fields [58], the properties of the system are sometimes more transparent in the basis where the order parameter transforms as a Cartesian vector under the spin rotations [28, 96]. The change of basis is given by [66, 96]

$$\psi_x = \frac{1}{\sqrt{2}}(\psi_+ - \psi_-), \tag{4.5a}$$

$$\psi_y = \frac{i}{\sqrt{2}}(\psi_+ + \psi_-), \tag{4.5b}$$

$$\psi_z = \psi_0, \tag{4.5c}$$

and we use the Greek indices $\alpha, \beta, ...$ to refer to the Zeeman basis and the Roman indices $a, b, ...$ to indicate the Cartesian basis given by Eq. (4.5). It is important to ensure that the physical predictions are independent of the choice of the basis and, for example, one observes that the number of the condensate atoms given by Eq. (2.4) is indeed the same in all bases.

Although the local spin vanishes identically in the polar phase, there is still magnetic ordering which can be probed using the magnetic quadrupole moment Q_{ab} which in the Cartesian basis is defined as [66]

$$Q_{ab} = \frac{\psi_a^* \psi_b + \psi_b^* \psi_a}{2|\vec{\Psi}|^2}. \tag{4.6}$$

There are also several other definitions in the context of cold atoms [179–181], depending on which type of fluctuations are included. The common feature of the different definitions is that in the absence of ferromagnetic order, Q_{ab} is characterised by only a single real unit vector $\hat{\boldsymbol{n}}$ corresponding to the largest eigenvalue of Q_{ab}. Such ordering was first investigated in the context of liquid crystals and it is dubbed as nematic ordering [182–184]. The same concept arises also in certain frustrated magnets [185, 186] where it describes the staggered magnetisation of the antiferromagnetic state. In this Thesis, we refer to $\hat{\boldsymbol{n}}$ as the local magnetic axis [90] and use the term nematic order to indicate the order characterised by Q_{ab}.

Using the Cartesian basis, the order parameter in the polar phase can be written as [66]

$$\vec{\Psi} = \sqrt{\varrho} e^{i\theta} \hat{\boldsymbol{n}}. \tag{4.7}$$

This gives rise to a local $\mathbb{Z}_2$ gauge invariance corresponding to $(\theta, \hat{\boldsymbol{n}}) \to (\theta + \pi, -\hat{\boldsymbol{n}})$. This gauge invariance was originally omitted [29] and the correct order parameter space was discovered somewhat later [90,149,150,187]. The $\mathbb{Z}_2$ gauge invariance has profound consequences to the properties of possible topological defects. Topological defects can take place in the texture determined by the local magnetic axis $\hat{\boldsymbol{n}}$ and most of them are equivalent to those associated with the local spin $\boldsymbol{\mathcal{S}}$. Unlike the ferromagnetic phase, the polar phase can feature skyrmions and isolated monopoles but due to the $\mathbb{Z}_2$ gauge invariance, textures characterised by a topological charge $\mathcal{Q}_0$ are homotopically equivalent to those with the charge $-\mathcal{Q}_0$ [187]. For this reason, the local magnetic axis is typically depicted as a headless vector [66].

In general, the magnetic quadrupole moment Q_{ab} has three distinct nonzero eigenvalues and the local magnetic axis is identified as the eigenvector corresponding to the largest eigenvalue [66]. This, in particular, preserves the local $\mathbb{Z}_2$ gauge invariance. Apart from defects that are solely associated with the spin sector, antiferromagnetic condensates can exhibit composite vortices where a $U(1)$ phase vortex and a spin vortex occur simultaneously. An important example is the half-quantum vortex [83, 86, 90, 178] which in the two-dimensional geometry has an asymptotic expression [178]

$$\lim_{|\boldsymbol{r}|\to\infty} \theta(\boldsymbol{r}) = \varphi/2 \quad \text{and} \quad \lim_{|\boldsymbol{r}|\to\infty} \hat{\boldsymbol{n}}(\boldsymbol{r}) = (\cos\varphi/2, \pm\sin\varphi/2, 0), \tag{4.8}$$

where φ is the azimuthal angle of the cylindrical coordinates. At the core of the defect, the decomposition (4.7) does not hold and the core becomes ferromagnetic [66, 178]. In general, $\hat{\boldsymbol{n}}$ is not restricted to a plane and two-dimensional (2D) systems can also feature skyrmions. The possible HQV textures are illustrated in Fig. 4.4 and in the literature they are sometimes referred to as π disclinations [66, 184].

The half-quantum vortices also play an important role in the BKT transition of the antiferromagnetic spin-1 Bose gases [90]. In Publication IX, the BKT transition in trapped quasi-2D gases was considered and we summarise the results in Section 7. In addition to HQVs, skyrmions also have an important role in the BKT transition. The gauge invariance dictates the equivalence between skyrmions with $\mathcal{Q}_{2D}$ and $-\mathcal{Q}_{2D}$ [187] where in Eq. (4.3) the unit spin $\hat{\boldsymbol{s}}$ is replaced by the local magnetic axis $\hat{\boldsymbol{n}}$. The HQVs can be characterised using the polarisation of the vortex core [178].

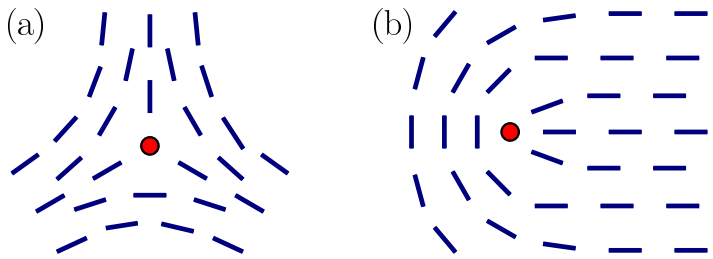

Figure 4.4: The basic types of half-quantum vortices. The local magnetic axis $\hat{\boldsymbol{n}}$ is here restricted to a plane for simplicity. Due to the local $\mathbb{Z}_2$ gauge invariance, $\hat{\boldsymbol{n}}$ and $-\hat{\boldsymbol{n}}$ are equivalent and vectors $\hat{\boldsymbol{n}}$ are drawn without the arrowhead.

4.2 Superfluid velocity and vorticity

The difference between the ferromagnetic and the polar phase becomes evident in the superfluid velocity associated with the topological defects discussed in Section 4.1. In general, the superfluid velocity can be defined as [29, 75, 188]

$$\boldsymbol{v}_s = -\frac{i\hbar}{m}\vec{\zeta}^{\,\dagger}\nabla\vec{\zeta}, \tag{4.9}$$

and the associated vorticity, describing the motion of the system associated with a rigid-body rotation [189], is given by

$$\boldsymbol{\Omega}_s = \nabla \times \boldsymbol{v}_s. \tag{4.10}$$

In the polar phase, $\boldsymbol{\Omega}_s = 0$ corresponding to an irrotational flow [190] whereas in the ferromagnetic phase[7], the superfluid velocity satisfies the Mermin-Ho relation [63, 188, 191]

$$\boldsymbol{\Omega}_s = \frac{\hbar}{2m}\,\varepsilon_{abc}\,\hat{s}_a\nabla\hat{s}_b \times \nabla\hat{s}_c. \tag{4.11}$$

This is tantamount to the existence of the coreless vortices with a non-divergent superfluid velocity at the vortex core. An important consequence of the Mermin-Ho relation is that spatially varying ferromagnetic order can give rise to a component rotating like a rigid body. Although the polar phase features in principle only singular vortices similar to the single-component superfluids, the half-quantum vortex discussed in the previous section is an example of a non-singular vortex with a finite particle density at the core. Thus the HQV can also be regarded as a coreless vortex.

In the single-component Bose systems, the circulation Γ associated with a given vortex is always quantised in the units of h/m [30, 112]. For spinor condensates, the

[7] In both cases, the contribution arising from the cores of the possible singular vortices is left out.

circulation can be defined in an analogous way such that

$$\Gamma = \oint_\gamma \mathrm{d}\boldsymbol{\ell} \cdot \boldsymbol{v}_s, \tag{4.12}$$

where $\boldsymbol{v}_s$ is the superfluid velocity given by Eq. (4.9) and γ is a path encircling the vortex core. For spinor condensates, however, the circulation is not typically quantised but it is possible to write the total circulation Γ as a sum of the circulation $\Gamma_{U(1)}$ that stems from the $U(1)$ phase and the circulation Γ_S associated with the spin sector of the order parameter. The HQV with the asymptotic expression (4.8) and the decomposition (4.7) yields $\Gamma = \Gamma_{U(1)} = h/2m$.

In the ferromagnetic phase, the Mermin-Ho relation gives an interesting connection between the vorticity and the topological charges $\mathcal{Q}_{2D}$ and $\mathcal{Q}_{3D}$ in Eqs. (4.3) and (4.4). In the two-dimensional case, the vorticity is perpendicular to the 2D plane and it is effectively a scalar function ($\boldsymbol{\Omega}_s = \Omega_s\, \hat{\boldsymbol{e}}_z$). Integrating the scalar vorticity Ω_s over the 2D plane, one obtains the total vorticity that is equal $\frac{h}{m}\mathcal{Q}_{2D}$. In the 3D case, the total flux of $\boldsymbol{\Omega}_s$ through a surface Σ enclosing the defect equals to $2\frac{h}{m}\mathcal{Q}_{3D}$. Hence, also other topological defects in addition to the usual singular vortices can carry quantised vorticity in spinor Bose gases.

In the presence of external magnetic fields, the condensate spin tends to align (or anti-align) with the external field and instead of using the basis consisting of the Zeeman substates, it is more convenient to use an adiabatic basis corresponding to the local eigenstates of the linear Zeeman operator $g_{\mathrm{F}}\mu_{\mathrm{B}}\boldsymbol{\mathcal{F}} \cdot \boldsymbol{B}(\boldsymbol{r})$. In this basis, assuming that the external magnetic field completely determines the spin sector of the order parameter (adiabatic limit), the equation of motion for the condensate reduces to an equation of motion of charged particles in an electromagnetic field. The vector potential of the electromagnetic field corresponds to the superfluid velocity of the condensate [188].

In the adiabatic limit, spinor condensates form an ideal platform to study certain exotic objects that have not been observed in the usual electromagnetism. The Dirac monopole discussed earlier is a particularly interesting example and the superfluid velocity corresponding to the textures in Fig. 4.3 (a) and (b) takes the form

$$\boldsymbol{v}_s = -\frac{\hbar}{m}\,\frac{1+\cos\vartheta}{r\sin\vartheta}\,\hat{\boldsymbol{e}}_\varphi, \tag{4.13}$$

where (r, ϑ, φ) denote the spherical coordinates[8]. The fact that both textures yield the same superfluid velocity is evident from the general expression of the superfluid

[8]There are different conventions to designate the spherical coordinates. We use here the standard notation (ISO 31-11) where r denotes the radial distance, ϑ the inclination with respect to the positive z axis, and φ is the azimuthal angle in the x-y plane.

velocity for the ferromagnetic phase [29]. The superfluid velocity (4.13) is equivalent to the vector potential of a Dirac monopole [75, 169] with a Dirac string at the negative z axis. The corresponding vorticity is given by

$$\mathbf{\Omega}_s = \frac{\hbar}{m}\frac{1}{r^2}\,\hat{\boldsymbol{e}}_r, \tag{4.14}$$

and it is equivalent to the magnetic field of a magnetic point charge. In Eq. (4.14), the contribution that stems from the Dirac string is omitted. In Publication VI, we showed that the texture in Fig. 4.3 (b) can be imprinted to a condensate, enabling a robust creation of the Dirac monopole. This topic is discussed in detail in Section 6.2.

5 Topological vortex creation and coreless vortices

Nucleation of quantised vortices in a response to external rotation is one of the hallmarks of superfluidity[9]. In the superfluid Helium, vortices have been created simply by rotating the container where the liquid is placed [192]. For trapped atomic gases, the situation is more complicated since the system does not have a clear boundary. Nevertheless, the same ideology has been utilised in experiments with atomic gases where quantised vortices have been produced by stirring the condensate with a laser beam [54] or rotating the condensate with an asymmetric trapping potential [193].

Atomic gases also offer more sophisticated routes to produce vortices. For example, coherent transitions between two hyperfine spin states have been put to use to generate vortices [52, 53], and recently a coherent transfer of the angular momentum of photons to the condensate has been demonstrated [194]. The spin degree of freedom offers another elegant way of generating vortices by utilising a coupling of the condensate spin to a spatially dependent external magnetic field [67, 68]. This method is referred to as topological vortex creation since it can be interpreted in terms of geometric phases. It provides a robust method that is insensitive to the details of the external fields. The topological vortex creation was reviewed in Publication II and in this section, we present the aspects that are most relevant for this Thesis. We also discuss the different applications and extensions of this method following Publications III, IV, and V. We start by discussing the properties of coreless vortices in the absence of external fields.

5.1 Properties of coreless vortices in spinor condensates

Coreless vortices in the absence of external fields or rotation exhibit energetic instabilities in the sense that the quasiparticle spectrum has modes with negative energy. Let us consider a cylindrically symmetric coreless vortices of the form [195]

$$\psi_\alpha(r,\varphi,z) = \psi_\alpha(r,z)\,\exp[i(\gamma_\alpha + \kappa_\alpha\varphi)]. \tag{5.1}$$

The winding numbers in the different hyperfine spin states are denoted by $\langle\kappa_1,\kappa_0,\kappa_{-1}\rangle$ and the stationary configurations satisfy the condition $2\kappa_0 = \kappa_1 + \kappa_{-1}$ [195]. We consider a vortex of the form $\langle 0,1,2\rangle$ which in the ferromagnetic phase gives rise to the vortices depicted in Fig. 4.2. The combination $\langle -1,0,1\rangle$ in the ferromagnetic

[9] On the other hand, activation of vortices due to thermal fluctuations indicates the loss of superfluidity and only at sufficiently low temperatures the appearance of vortices indicates conclusively superfluidity.

phase corresponds to the polar core vortex and it will be discussed in Section 5.5. In the absence of external magnetic fields, all combinations obtained through the transformations $\kappa_\alpha \to -\kappa_\alpha$ and $\kappa_\alpha \to \kappa_{-\alpha}$ are equivalent in the sense that they have the same stability properties. Furthermore, all other combinations yield singular vortices or coreless vortices that are multiples of the two basic configurations. Singular vortices cannot usually be stabilised using external magnetic fields.

The population of the sublevels $\alpha = \pm 1$ can be controlled using an external bias field $\boldsymbol{B} = B\hat{\boldsymbol{e}}_z$, giving rise to the relative magnetisation

$$M = \frac{1}{N}\int \mathrm{d}\boldsymbol{r}\,\left[|\psi_+|^2 - |\psi_-|^2\right], \tag{5.2}$$

where N is the total particle number. Since M is freely adjustable, the $\langle 0, 1, 2\rangle$ vortex interpolates between two extreme cases corresponding to a single-component condensate without a vortex ($M = 1$) and a single-component condensate with a two-quantum vortex ($M = -1$). Since vortices with a winding number $|\kappa| > 1$ are usually unstable in the single-component systems [59, 116, 117, 196–198], one expects that the $\langle 0, 1, 2\rangle$ vortex also becomes dynamically unstable as M decreases. The instabilities of coreless vortices have been investigated in Publication I for both ferromagnetic and antiferromagnetic interactions and in this section we summarise these findings.

An important property regarding the quasiparticle excitations is the appearance of the complex eigenmodes as pairs $(\hbar\omega_q, w_q)$ and $(\hbar\omega_q^*, \bar{w}_q)$ where $\bar{w}_q$ is obtained by a unitary transformation from w_q^*. Due to the symmetries of the Bogoliubov equation in Eq. (2.21), there are also excitations corresponding to $(-\hbar\omega_q^*, \tau_1 w_q^*)$ and $(-\hbar\omega_q, \tau_1 \bar{w}_q^*)$. This enables the decay of a dynamically unstable state in the absence of dissipation since exciting both $(\hbar\omega_q, w_q)$ and $(-\hbar\omega_q^*, \tau_1 w_q^*)$ modes conserves the energy and the angular momentum. Let us assume that the system is rotated externally about the z axis with angular velocity Ω small enough such that vortex lattices do not form and the ansatz of Eq. (5.1) remains valid. In the GP equation (2.17), the rotation term $-\boldsymbol{\Omega}\cdot(-i\hbar\boldsymbol{r}\times\nabla)$ for the coreless $\langle 0, 1, 2\rangle$ vortex can be absorbed in the chemical potential and external magnetic field. In the BG equation, the quasiparticle energies change as $\hbar\omega_q \to \hbar\omega_q - \hbar\Omega\kappa_q$ where κ_q is the angular momentum quantum number. Without losing any generality, we may therefore take $\Omega = 0$ in the presence of conserved magnetisation.

The existence of dynamical instabilities was investigated using the Bogoliubov equation (2.20) for a fixed magnetisation ranging from -1 to 1 such that the GP equation was solved using the ansatz (5.1) and assuming a uniform system system in the z direction. The excitations are labelled by $\alpha = 0, \pm 1$ indicating that

the component α has the largest amplitude in the particular excitation. In the limit $M = -1$, modes $\alpha = 1, 0, -1$ can be characterised as longitudinal spin fluctuations, transverse spin fluctuations, and density fluctuations. In the general case, such simple classification is not possible. Two different types of dynamical instabilities were found: (I) a dynamical instability leading to splitting of the two-quantum vortex in the $\alpha = -1$ component, and (II) a dynamical instability leading to "phase separation" in which the condensate tends to break into separate domains containing only $\alpha = 0$ component or both of the $\alpha = \pm 1$ components. Type I instabilities occurred for $\kappa_q = \pm 2$ and type II instabilities for $\kappa_q = \pm 1$.

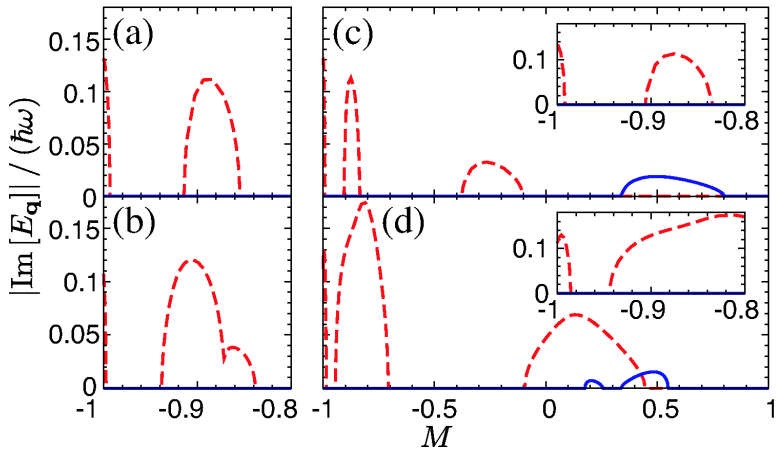

Figure 5.1: Existence of dynamical instabilities as a function of the relative magnetisation M. The dimensionless coupling constant $\tilde{c}_2$ is -0.001 (a), -0.01 (b), 0.001 (c), and 0.01 (d). The type I instability is denoted by the dashed line and the type II instability by the solid line.

The existence of the dynamical instabilities was investigated for different values of the dimensionless interaction strength $\tilde{c}_2 = c_2/(\hbar\omega_\perp d^3)$, where $\omega_\perp$ is the trapping frequency perpendicular to the z axis and $d = \sqrt{\hbar/m\omega_\perp}$ is the corresponding harmonic oscillator length. The value of $\tilde{c}_2$ can be tuned, for example, by changing the trapping frequency $\omega_\perp$. The type I instability appears for both ferromagnetic and antiferromagnetic interactions and it is consistent with the dynamical instability of the two-quantum vortex in the single-component condensates [116, 117, 196–198]. The existence of this mode near $M = -1$ is clear since the population of the $\alpha = -1$ component is large and the system resembles a single-component condensate. The existence of the type I instability for a wider range of magnetisation in the antiferromagnetic case is due to the energetically unfavourable spin polarised core of the

vortex. This gives rise to core localised modes that are responsible for the third peak in Fig. 5.1 (c) and (d).

The type II instability is intrinsic to antiferromagnetic interactions and it takes place for positive values of the magnetisation. This mode carries an angular momentum quantum number $\kappa_q = \pm 1$ and therefore it does not initiate the splitting of the two-quantum vortex in $\alpha = -1$ component. This mode reflects the intrinsic instability of the spin texture related to the coreless vortex in the presence of antiferromagnetic interactions and it tends to break the texture without affecting the two-quantum vortex in $\alpha = -1$ component.

5.2 Phase imprinting in the Ioffe-Pritchard trap

The first dilute Bose-Einstein condensates were confined in magnetic traps such as the Ioffe-Pritchard (IP) trap [199, 200] which is formed by four Ioffe bars proving confinement in the x-y plane and two closed current loops generating confinement in the z direction. For our purposes, it is sufficient to neglect the quadratic terms of the IP field [201,202] as they are relevant only for the confinement in the z direction. In this case, the IP field can be written as

$$\boldsymbol{B}(\boldsymbol{r}, t) = \boldsymbol{B}_{\perp}(\boldsymbol{r}) + \boldsymbol{B}_{z}(t) = B' x \hat{\boldsymbol{e}}_x - B' y \hat{\boldsymbol{e}}_y + B_z(t) \hat{\boldsymbol{e}}_z, \tag{5.3}$$

where B' in a radial magnetic field gradient generated by the Ioffe bars and $B_z(t)$ is a homogeneous bias field. The IP field gives rise to a magnetic field equivalent to the spin texture in Fig. 4.1 (b). The magnetic confinement in spin-F Bose gases is provided only for the so-called weak-field seeking states (WFSSs) which correspond to the eigenvalues $m_{\rm F} g_{\rm F} \mu_{\rm B} |\boldsymbol{B}(\boldsymbol{r})|$, $m_{\rm F} = 1, ..., F$, of the linear Zeeman Hamiltonian $\mathcal{H}_{Z} = g_{\rm F} \mu_{\rm B} \boldsymbol{B}(\boldsymbol{r}) \cdot \boldsymbol{\mathcal{J}}$, where $\boldsymbol{\mathcal{J}}$ is a vector of the dimensionless spin-F operators. Here we assume that $g_{\rm F} > 0$.

Let us assume that the bias field $B_z(t)$ is initially strong enough to render the system spin polarised corresponding to one of the eigenstates of $\mathcal{J}_z$. If the bias field is reversed adiabatically, the system remains in the instantaneous eigenstate of $\mathcal{H}_{Z}$. The unit vector corresponding to the external field $\boldsymbol{B}$ is denoted by $\hat{\boldsymbol{b}} = (\sin\beta\cos\alpha, \sin\beta\sin\alpha, \cos\beta)$, where $\alpha = -\varphi$ and $\beta = \tan^{-1}(|\boldsymbol{B}_{\perp}|/B_z(t))$ for the IP field. The instantaneous eigenstate of $\mathcal{H}_{Z}$ can be written as $|\Psi(\alpha,\beta)\rangle = \mathcal{U}^{\dagger}(\alpha,\beta)|F, m_{\rm F}\rangle$, where $\mathcal{U}(\alpha,\beta) = e^{i\beta\hat{\boldsymbol{n}}(\alpha)\cdot\boldsymbol{\mathcal{J}}}$ and $\hat{\boldsymbol{n}}(\alpha) = (-\sin\alpha, \cos\alpha, 0)$ is a unit vector orthogonal to $\hat{\boldsymbol{b}}$. Physically $\mathcal{U}^{\dagger}$ corresponds to a rotation of the local spin by an angle β with respect to the axis given by $\hat{\boldsymbol{n}}$. Since both α and β have spatial dependence, the local spin rotates differently in different spatial locations. If $B_z(0) = -B_z(T) \gg B'R$, where R is the spatial extent of the condensate, the local

spin is effectively rotated by π with respect to $\hat{\boldsymbol{n}}$ and the final state becomes

$$|\Psi(\alpha,\pi)\rangle = (-1)^{F+m_{\rm F}} e^{2im_{\rm F}\alpha}|F,-m_{\rm F}\rangle. \tag{5.4}$$

Since $\alpha = -\varphi$, the final state has a phase winding of $2m_{\rm F}$, corresponding to a vortex with $2m_{\rm F}$ quanta of angular momentum. This scheme was originally proposed in Refs. [67–69] and subsequently realised in the experiments to create two- and four-quantum vortices in single-component condensates [57–59, 70].

5.3 Geometric phases and topological vortex creation

The phase imprinting in the IP trap can be interpreted geometrically [57, 69] by studying the motion of individual spins in the phase space. In the spin polarised initial state, all spins correspond to the north pole of a unit sphere. During the adiabatic inversion of the bias field, the spins trace different great circles from the north pole to the south pole, see Fig. 5.2. Identifying a relative phase of a given spin $\boldsymbol{\mathcal{S}}_2$ with respect to a fixed reference spin $\boldsymbol{\mathcal{S}}_1$ as the geometric phase associated with the adiabatic transport of spin $\boldsymbol{\mathcal{S}}_2$ along the loop indicated in Fig. 5.2, gives a relative phase $\gamma = -m_{\rm F}\Omega(\theta) = -2m_{\rm F}\theta$ [57, 203].

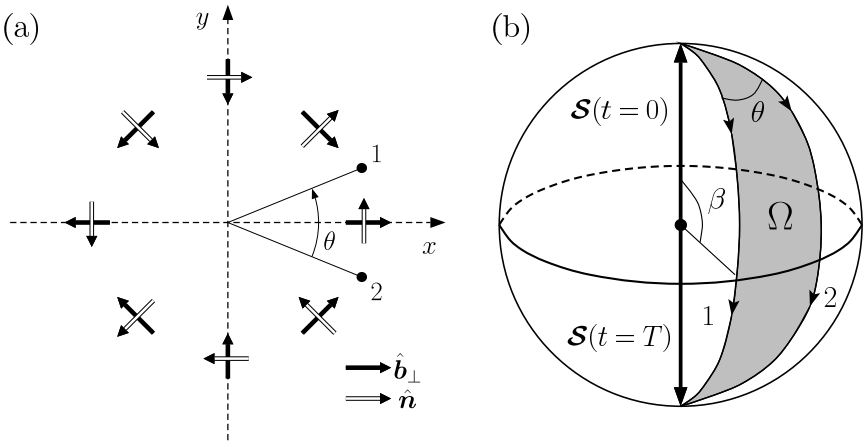

Figure 5.2: (a) Rotation of the spin in the x-y plane. The spins are rotated about the unit vector $\hat{\boldsymbol{n}}$ and the vector $\hat{\boldsymbol{b}}_\perp$ indicates the direction of the quadrupole field $\boldsymbol{B}_\perp$. The spins discussed in the text are denoted by 1 and 2. (b) In the adiabatic inversion, the local spins 1 and 2 follow distinct great circles from the north pole to the south pole acquiring a relative phase that is proportional to the solid angle Ω. Figure is adapted from Ref. [57].

The main difficulty in creating multi-quantum vortices with the phase imprinting method is the requirement of atoms with large total hyperfine spin F. Although the

scheme is realisable, e.g., for $F = 1, 2, 3$, it eventually becomes impractical. Since the topological phase imprinting process is reversible, inverting the bias field back to its initial value will take away the $2m_{\mathrm{F}}$ quanta of angular momentum and no net vorticity is gained. Using the hexapole field

$$\boldsymbol{B}_h = B_h' r[\cos(2\varphi)\hat{\boldsymbol{e}}_x - \sin(2\varphi)\hat{\boldsymbol{e}}_y] + B_z(t)\hat{\boldsymbol{e}}_z \tag{5.5}$$

instead of the quadrupole field $\boldsymbol{B}_\perp$, the bias field inversion results in the state $|\Psi\rangle = (-1)^{F+m_{\mathrm{F}}}\, e^{-4im_{\mathrm{F}}\varphi}|F, -m_{\mathrm{F}}\rangle$. If the hexapole field is replaced by the quadrupole field and the bias field is inverted back to its initial value, the final state is $|\Psi'\rangle = e^{-2im_{\mathrm{F}}\varphi}|F, m_{\mathrm{F}}\rangle$ and the local phase factor indicates the appearance of a $2m_{\mathrm{F}}$-quantum vortex. As discussed in Publication II, the resulting process corresponds to a cyclic adiabatic evolution for which the resulting local phase factor corresponds to the accumulated Berry phase. The idea of using a combination of the quadrupole and the hexapole fields to cyclically pump vorticity into the condensate was introduced in Publication III and it is discussed in more detail in the next section.

5.4 Vortex pump: accumulation of angular momentum

The concept of a vortex pump based on the adiabatic evolution of the condensate spin in the presence of quadrupole and hexapole fields was discussed in Section 5.3. However, under realistic experimental conditions, the interactions between particles and the finite timescales limit the adiabaticity. In Publication IV, an optically trapped spin-1 BEC was considered as a proof-of-concept system. The optical potential was augmented with an optical plug to prevent the Landau-Zener transitions and to stabilise the multi-quantum vortices against splitting. The simulation was performed using the zero-temperature GP equation (2.17) for the parameters of ^{87}Rb such that the switch between the hexapole and the quadrupole fields was done by ramping the fields up and down linearly in time. The accumulation of the angular momentum is shown in Fig. 5.3 (a). The deviation of the angular momentum from the integer values after each half-cycle is due to the slight splitting of the multi-quantum vortices, which in this case was mainly caused by numerical noise. Use of a stronger optical plug would decrease this effect.

The vortex pumping is also possible in the absence of optical fields, and the original experiments utilising the topological phase imprinting were conducted such that the confinement was provided by the IP field only [57, 58]. This requires a careful design of the axial trap to keep the condensate confined after the bias field inversion. This has been realised in the studies of the dynamical instabilities of the imprinted two-quantum vortices [59]. In Publication IV, the vortex pump was

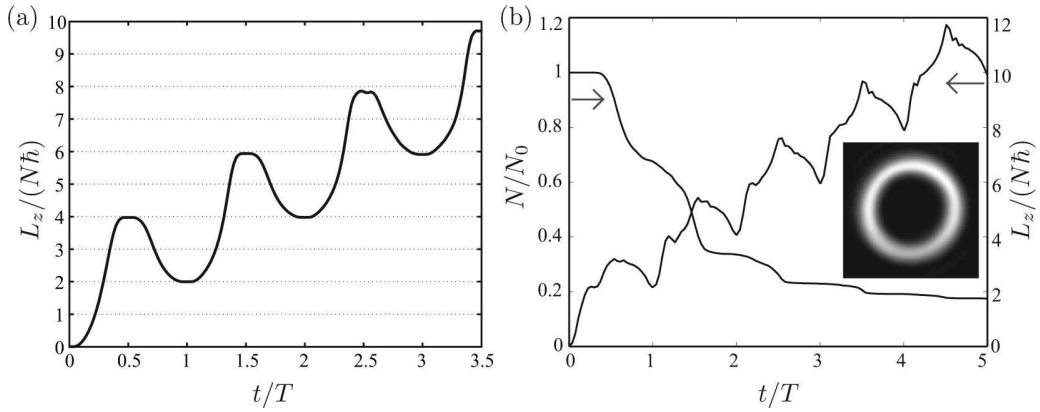

Figure 5.3: (a) Accumulation of the angular momentum for an optically trapped condensate during the adiabatic pumping. (b) Angular momentum (right axis) and the total particle number (left axis) during the partially non-adiabatic pumping without optical fields.

also modelled in a pancake-shaped geometry such that particles were allowed to escape from the trap. The switch between the hexapole and the quadrupole fields was instantaneous in this case. Computational resources limited the simulations to a rather fast pumping frequency which had the advantage that the created multi-quantum vortices had less time available for splitting. The loss of particles is due to the spin flips that transfer particles from the WFSS to the untrapped states. Since these transitions take place at the centre of the trap, the appearance of the multi-quantum vortex tends to decrease the particle loss since the vortex core is effectively void of particles, see Fig. 5.3.

5.5 Coreless vortices and multi-quantum vortices in the topological phase imprinting

The topological phase imprinting enables the creation of both multi-quantum vortices and coreless vortices. In this section, we discuss the results of Publications IV and V in the context of the topological phase imprinting. In Section 5.1, the properties of coreless vortices were already discussed in the absence of external fields. In Publication IV, the stability of coreless vortices of the form $\langle 2, 1, 0\rangle$ and $\langle 1, 0, -1\rangle$ was investigated in the presence of the IP field given in Eq. (5.3). The bias field B_z was assumed to be a time-independent constant as the emphasis was on the stationary properties of the coreless vortices. The interactions were taken to be ferromagnetic.

The external field tends to stabilise the coreless vortices such that they can

become either the ground state of the system or energetically stable states corresponding to local minima of the mean-field energy [160]. A large transverse part $\boldsymbol{B}_\perp$ of the IP field favours the polar core vortex $\langle 1, 0, -1\rangle$ while for large $|B_z|$ either $\langle 2, 1, 0\rangle$ or $\langle 0, -1, -2\rangle$ vortex is more favourable. If the winding numbers in the different components satisfy the condition $\kappa_0 = \kappa_1 - 1 = \kappa_{-1} + 1$, the contribution of $\mu_{\mathrm{B}} g_{\mathrm{F}} \boldsymbol{B}(\boldsymbol{r}) \cdot \boldsymbol{\mathcal{S}}(\boldsymbol{r})$ to the mean-field energy becomes axisymmetric and the quasiparticle amplitudes can be taken to be of the form

$$u_{q,\alpha}(\boldsymbol{r}) = u_{q,\alpha}(r, z) \exp[i(\kappa_q + \kappa_\alpha)\varphi], \tag{5.6a}$$

$$v_{q,\alpha}(\boldsymbol{r}) = v_{q,\alpha}(r, z) \exp[i(\kappa_q - \kappa_\alpha)\varphi]. \tag{5.6b}$$

This decomposition enables an efficient numerical solution of the Bogoliubov equation in cylindrical coordinates.

The quasiparticle energies computed from the Bogoliubov equation showed that the coreless vortex $\langle 2, 1, 0\rangle$ evolves from the global minimum to an energetically stable local minimum of the mean-field energy with increasing B_z. Subsequently, $\langle 2, 1, 0\rangle$ vortex becomes first energetically unstable and finally upon increasing B_z further, it starts to exhibit dynamical instability. This is again intuitively clear for large B_z since the $\alpha = 1$ component with the two-quantum vortex has a large population and the dynamical instability is associated with the splitting of the vortex. Similarly to Publication I, the dynamical instability carries the quantum number $\kappa_q = \pm 2$. The effect of the instability mode was investigated by considering configurations of the form $\tilde{\Psi}(\boldsymbol{r}) = \Psi(\boldsymbol{r}) + \eta[u_q(\boldsymbol{r}) + v_q^*(\boldsymbol{r})]$ which corresponds to the simultaneous excitation of the mode (u_q, v_q) and its conjugate (v_q^*, u_q^*). The parameter η describes the population of the excitation. An example of the resulting configurations is shown in Fig. 5.4.

In the case $B_z = 0$, the $\langle 2, 1, 0\rangle$ vortex corresponds to the AT vortex in Fig. 4.2 (a) and for large B_z, the vortex is the MH texture in Fig. 4.2 (c). The different configurations of the $\langle 2, 1, 0\rangle$ vortex can be created with the topological phase imprinting method when the bias field is ramped down to some small intermediate value. The $\langle 2, 1, 0\rangle$ and $\langle 1, 0, -1\rangle$ vortices represent the two topologically distinct classes discussed in Section 4.1 with the polar core defect being the nontrivial one. Hence, the transition between the two vortices as the ground state configuration is a topological phase transition driven by the quantum fluctuations corresponding to the Bogoliubov quasiparticles. Unlike the $\langle 2, 1, 0\rangle$ vortex, the polar core vortex $\langle 1, 0, -1\rangle$ does not become dynamically unstable as $|B_z|$ increases. The polar core vortex can be crated using the phase imprinting method with the initial state $|F, m_{\mathrm{F}} = 0\rangle$ [204]. The required initial state can be achieved using rf pulses and magnetic field gradients

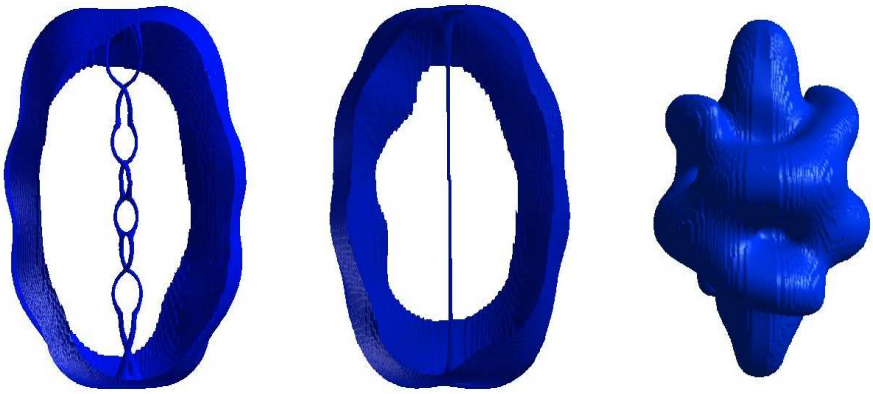

Figure 5.4: Isosurfaces of particle densities in the different hyperfine spin states corresponding to the $\langle 2, 1, 0\rangle$ vortex in an elongated condensate and a slight excitation of the dynamical instability mode. Parameters are as in Publication IV.

to adjust the population of the different Zeeman substates [204, 205].

The topological phase imprinting method has enabled an experimental investigation of the dynamical instability of two-quantum vortices in the single-component condensates [59]. The splitting of the two-quantum vortex was indeed observed but the ultimate mechanism for the observed splitting came under debate after the suggestion that the thermal component of the gas was an essential ingredient in the observed splitting [206, 207]. In Publication V, the experiment of Ref. [59] was simulated and the gravitational sag was found to give a sufficient impetus for the splitting process. This is in agreement with Ref. [59] which stated that the splitting process was not driven by the effects of dissipation.

In Publication V, the properties of the splitting process were found to depend on the parameter $an_z = a\int |\psi(x, y, z)|^2 \mathrm{d}x\mathrm{d}y$ describing the strength of interactions at a point z. For small $an_{z=0}$, the splitting initiates along the whole length of the vortex line whereas for large $an_{z=0}$ the splitting starts from the both ends of the vortex line and the resulting two vortices tend to intertwine similarly to the spinor case shown in Fig. 5.4. The intertwining was argued to impede the identification of the vortex splitting in the experiment of Ref [59] since the experimental method relied on the tomographic imaging technique that corresponds to integrating the density profile along the z direction.

The simulation in Publication V neglected the multi-component nature of the condensate. In the topological phase imprinting process, a singular two-quantum vortex is the final state but all the intermediate states are analogous to the coreless

vortex $\langle 2, 1, 0 \rangle$ considered in Publication IV. The results of Publication IV augment the simulation of Publication V by showing that at some point of the bias field inversion, the intermediate state becomes dynamically unstable.

6 Monopoles and gauge invariance in spinor Bose gases

The Bose gases considered in this Thesis consist of neutral atoms and they possess global symmetries associated with conserved quantities such as the total particle number or the magnetisation of the condensate. On the other hand, there are also more general symmetries corresponding to the invariance under local transformations of the underlying fields. This is referred to as the local gauge invariance[10] and in its contemporary form it was first recognised in the context of charged particles in electromagnetic fields [209] and somewhat later in a more general setting of non-commuting gauge fields [210]. Theories based on gauge symmetries are now the cornerstone of the description of interactions between the elementary particles [211].

The local gauge invariance can also arise in atomic systems in the case of effective theories describing systems for which the dynamics is restricted by different adiabatic approximations. In this section, we discuss two separate cases: the adiabatic motion of multilevel atoms in spatially varying laser fields and the adiabatic spin states in external magnetic fields. The latter finalises the concept of the superfluid analog to the magnetic point charge discussed in Sections 4.1 and 4.2 while the former scheme gives rise to more complicated non-Abelian monopole configurations that are akin to the 't Hooft–Polyakov monopoles [212, 213] in unified gauge theories. The creation of the Dirac monopole is discussed in detail in Section 6.2 and the properties of the non-Abelian monopoles are addressed in Section 6.3.

6.1 Local gauge invariance

In the presence of external magnetic fields, the use of the adiabatic spin states (see Section 5.2) as the basis for the condensate order parameter simplifies the equations of motion with the cost of introducing a local $U(1)$ symmetry. As discussed in Section 4.2, the equation of motion for a system constricted to a single adiabatic state corresponds to the motion of charged scalar particles in an electromagnetic field [188]. We assume the local spin to be either aligned or anti-aligned with the magnetic field $\boldsymbol{B}$, rendering a local spin rotation $\mathcal{U}(\boldsymbol{r}) = \exp[i\chi(\boldsymbol{r})\,\hat{\boldsymbol{b}}\cdot\boldsymbol{\mathcal{J}}]$ physically redundant. However, this spin rotation changes the superfluid velocity such that $\boldsymbol{v}_s \to \boldsymbol{v}_s + \frac{\hbar F}{m}\nabla\chi(\boldsymbol{r})$ and it must be accompanied by the local $U(1)$ gauge transformation $\psi(\boldsymbol{r}) \to \psi(\boldsymbol{r})\exp[iF\chi(\boldsymbol{r})]$ of the scalar order parameter [188]. Hence, the spinor BECs in external magnetic fields provide, within the adiabatic approximation, a complete analog to the systems of charged particles interacting with electromagnetic fields.

[10] The term gauge invariance arose originally in the context of Einstein's general theory of relativity in which the gauge invariance denoted the scale invariance of the space-time [208].

A more general non-Abelian local gauge invariance can arise in the adiabatic dynamics of systems with several degenerate internal states [214]. Let us consider a particular example in which three degenerate atomic states $\{|1\rangle, |2\rangle, |3\rangle\}$ are excited to a common virtual state $|0\rangle$ using external laser fields represented by the Rabi frequencies $\{\Omega_1, \Omega_2, \Omega_3\}$, see Fig. 6.1. This tripod scheme was originally investigated in the context of quantum optics [215–217] and later on, as a possible platform for quantum computing and quantum memories [218–220]. The Hamiltonian describing the tripod system in the rotating wave approximation (RWA) is given by

$$\hat{H}_{\rm rwa} = -\hbar\big(\Omega_1|0\rangle\langle 1| + \Omega_2|0\rangle\langle 2| + \Omega_3|0\rangle\langle 3|\big) \;+\; \text{h.c.}, \tag{6.1}$$

and it neglects processes in which atoms are either de-excited while absorbing a photon or excited while emitting a photon. This approximation is valid near the resonances of the atomic transitions [221]. The Hamiltonian (6.1) corresponds to the interaction picture and the electromagnetic fields are treated classically.

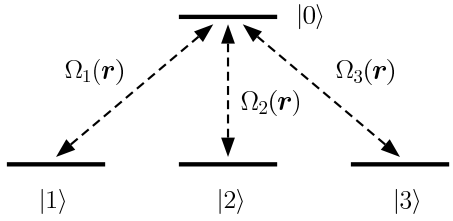

Figure 6.1: The tripod scheme in which degenerate atomic states $\{|1\rangle, |2\rangle, |3\rangle\}$ are excited to a common excited state $|0\rangle$ using external laser fields. The lasers give rise to the Rabi frequencies Ω_1, Ω_2, and Ω_3.

The Hamiltonian (6.1) has two zero energy eigenstates $|D_1\rangle$ and $|D_2\rangle$ as well as eigenstates $|B_1\rangle$ and $|B_2\rangle$ corresponding to energies $\pm\hbar\Omega$, where $\Omega = \sqrt{\sum_{k=1}^{3}|\Omega_k|^2}$. States $|D_1\rangle$ and $|D_2\rangle$ have a vanishing projection to the excited state $|0\rangle$ and they are referred to as the dark states [216, 217] since they do not couple to the laser fields. By the same token, states $|B_1\rangle$ and $|B_2\rangle$ are coined as bright states. If $\hbar\Omega$ is large enough compared to the other energy scales of the system, one may evoke the adiabatic approximation, in which the coupling between the dark and the bright states is negligible. Taking into account the spatial dependence of the external laser fields, the single-particle Hamiltonian corresponding to the equation of motion is [76]

$$\hat{H}_{\rm sp} = \int \mathrm{d}\boldsymbol{r}\, \left[\frac{\hbar^2}{2m}(D_\mu\hat{\boldsymbol{\psi}})^\dagger(D_\mu\hat{\boldsymbol{\psi}}) + \hat{\boldsymbol{\psi}}^\dagger(V_{\rm tr}+\Phi)\hat{\boldsymbol{\psi}}\right], \tag{6.2}$$

where $D_\mu = \partial_\mu - iA_\mu$ and $\hat{\boldsymbol{\psi}} = (\hat{\psi}_1, \hat{\psi}_2)$ is a field operator corresponding to the dark states $|D_1\rangle$ and $|D_2\rangle$. The matrix-valued Berry connection A_μ and the scalar potential Φ are given by [76]

$$(A_\mu)_{nm} = i\langle D_n|\partial_\mu D_m\rangle, \tag{6.3}$$

$$\Phi_{nm} = \frac{\hbar^2}{2m}\left(\langle\nabla D_n|\nabla D_m\rangle + \sum_{k=1}^{2}\langle D_n|\nabla D_k\rangle\langle D_k|\nabla D_m\rangle\right). \tag{6.4}$$

We use a notation convention in which $A_\mu = A_\mu^0\sigma^0 + A_\mu^a\sigma^a$, indices $a \in \{x, y, z\}$ denote the three components of the pseudospin determined by the spin-1/2 Pauli matrices $\boldsymbol{\sigma} = (\sigma^x, \sigma^y, \sigma^z)$, and the 2×2 identity matrix is denoted by σ^0.

Since the dark states are degenerate, any basis generated from the dark states $|D_1\rangle$ and $|D_2\rangle$ by a local unitary transformation $U(\boldsymbol{r})$ is equivalent. Therefore $\boldsymbol{A} = A_\mu\hat{\boldsymbol{e}}_\mu$ and Φ transform as $\boldsymbol{A} \to U\boldsymbol{A}U^\dagger - i(\nabla U)U^\dagger$ and $\Phi \to U\Phi U^\dagger$ under a local change of basis $\hat{\boldsymbol{\psi}} \to U\hat{\boldsymbol{\psi}}$. As discussed in Publication VII, the interaction part of the Hamiltonian for the dark states at the mean-field level ($\hat{\psi}_\alpha \to \langle\hat{\psi}_\alpha\rangle = \psi_\alpha$) becomes

$$\hat{H}_{\text{int}} = \frac{c_0}{2}\int \mathrm{d}\boldsymbol{r}\,(\psi_\alpha^\dagger\psi_\alpha)^2, \tag{6.5}$$

if the spin-dependent interaction in Eq. (2.5) can be neglected[11] and the population of the bright states is vanishingly small. Hence, the system described by Eqs. (6.2) and (6.5) has a local $U(2)$ gauge invariance at the mean-field level, providing a generalisation of the local $U(1)$ gauge invariance associated with the adiabatic motion of atoms in external magnetic fields.

Studies of the light-induced gauge potentials have become a burgeoning field and several seminal works investigating relativistic effects in the Dirac-like Hamiltonians arising from the tripod configuration [222, 223], different analogs to the spin-Hall effect and spintronics [224,225], and effects of the emergent spin-orbit coupling [226, 227] have recently emerged. There is also an alternative scheme to generate artificial gauge potentials based on the modulation of an optical lattice [228].

6.2 Creation of the Dirac monopole

Let us assume that the texture in Fig. 4.3 (b) can be created with an external magnetic field. Sections 4.1, 4.2, and 6.1 imply that in the adiabatic limit, this system becomes an exact analog to a system of charged particles in the electromagnetic field of a magnetic point charge. The external field that gives rise to the texture in Fig. 4.3 (b) is a generalisation of the IP field in Eq. (5.3); it is a combination of two

[11] This is a valid approximation for systems consisting of, e.g., ^{87}Rb atoms.

quadrupole fields and a bias field

$$\boldsymbol{B}(\boldsymbol{r},t) = B_1'(x\hat{\boldsymbol{e}}_x + y\hat{\boldsymbol{e}}_y) + B_2' z\,\hat{\boldsymbol{e}}_z + B_0(t)\,\hat{\boldsymbol{b}}_0, \tag{6.6}$$

where the usual Maxwell's equations impose the condition $2B_1' + B_2' = 0$ and the bias field direction is determined by a unit vector $\hat{\boldsymbol{b}}_0$. The magnetic field in Eq. (6.6) can be generated using two Helmholz coils and it was the first experimental realisation of a magnetic trap for neutral atoms [202,229]. The Dirac monopole is located at the point where the magnetic field vanishes. The location of this point is determined by the value of the bias field $B_0(t)$ and the monopole can be moved from the outskirts of the condensate to the centre of the trap by ramping down the bias field.

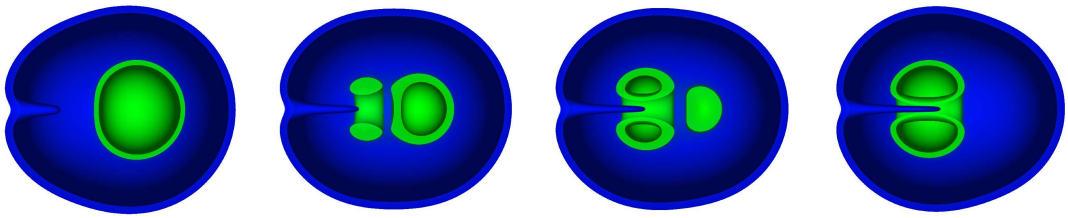

Figure 6.2: Particle density at different stages of the creation of the Dirac monopole. The green (light) colour denotes a large particle density and the blue (dark) colour indicates a low particle density. The Dirac string corresponds to the density depletion propagating through the condensate. Time is given in the units of $1/\omega_r$ corresponding to a spherically symmetric 3D trap $V_{\rm tr}(\boldsymbol{r}) = \frac{1}{2}m\omega_r r^2$.

In Publication VI, a full simulation of the monopole creation including all non-adiabatic effects was performed using the time-dependent GP equation (2.17) for an optically trapped spin-1 BEC. The creation of the Dirac string can be observed as a density depletion in Fig. 6.2. The Dirac string carries two quanta of angular momentum (see Section 4.2 and Publication VI) and it tends to split into two strings carrying a single-quantum of angular momentum under perturbations that break the rotational symmetry. This becomes evident when the bias field is chosen such that $\hat{\boldsymbol{b}}_0 \times \hat{\boldsymbol{z}} \neq 0$. The resulting vorticity $\boldsymbol{\Omega}_s$ is shown in Fig. 6.3 together with the vorticity corresponding to the axisymmetric situation. If the external field pinning the monopole is removed, the monopole drifts outside of the condensate such that the final state is a closed vortex ring in the spin texture. The Dirac string extending from the monopole core represents an interesting example of a vortex which is neither a coreless vortex nor a usual singular vortex. The winding numbers are given by $\langle 0,1,2\rangle$ but the particle density is fully depleted along the vortex line.

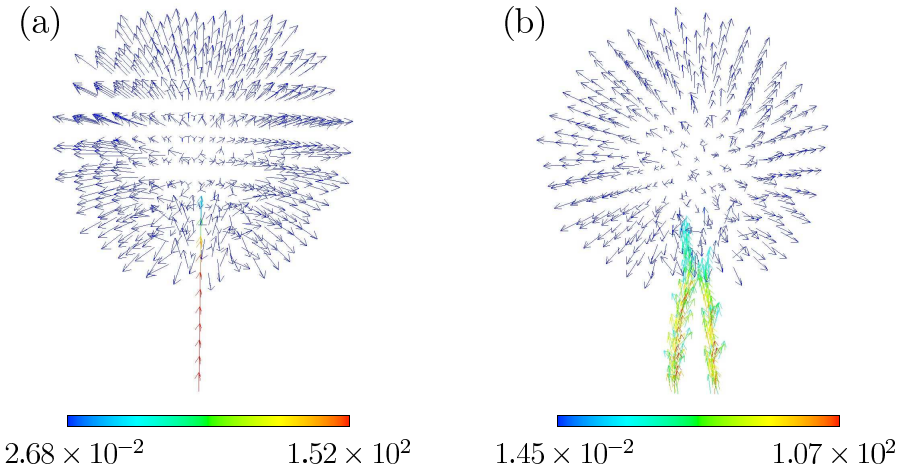

Figure 6.3: Vorticity $\boldsymbol{\Omega}_s$ after the Dirac monopole has been created at the centre of the trap. (a) The bias field is parallel to the z axis and the Dirac string carries two quanta of angular momentum. (b) The bias field forms a 21° angle with respect to the z axis and breaks the rotation symmetry of the system. This perturbation sets off the splitting of the Dirac string. For clarity, only the relevant parts of the vector field are shown.

6.3 Non-Abelian magnetic monopole

The non-Abelian magnetic monopole arises when the external laser fields [see Eq. (6.1)] carry angular momentum corresponding to the Rabi frequencies $\Omega_{1,2}(\boldsymbol{r}) = \Omega_0(\rho/\sqrt{2}R) \times e^{i(kz\mp\varphi)}$ and $\Omega_3(\boldsymbol{r}) = \Omega_0(z/R)e^{ik'x}$ with $\rho = \sqrt{x^2+y^2}$ [76]. The vector potential in the reduced Hamiltonian (6.2) is of the form

$$\boldsymbol{A} = -\frac{\cos\vartheta}{r\sin\vartheta}\,\hat{\boldsymbol{e}}_\varphi\,\sigma^x \;+\; \text{other terms}, \tag{6.7}$$

for which the corresponding (pseudo) magnetic field becomes

$$\boldsymbol{B} = \frac{1}{r^2}\,\hat{\boldsymbol{e}}_\varphi\,\sigma^x + \cdots . \tag{6.8}$$

Unlike the Dirac monopole in the Abelian case, the non-Abelian monopole can be removed by a gauge transformation $U_0(\boldsymbol{r}) = e^{i\varphi\sigma^x}e^{-i\vartheta\sigma^y/2}$. This yields a new vector potential $\boldsymbol{A}'$ that no longer diverges at the z axis, see Publication VII. The vector potential $\boldsymbol{A}'$ remains ill-defined at the z axis, but the spinor part of the order parameter can cancel the problematic terms. A simple example is $\boldsymbol{\psi} = \phi(\boldsymbol{r})\boldsymbol{\zeta}_\pm$, where $\boldsymbol{\zeta}_\pm = (1, \pm 1)/\sqrt{2}$ gives rise to a well-defined variational problem for the scalar part $\phi(\boldsymbol{r})$.

A gauge invariant formulation of the magnetic charge was constructed in Publication VII utilising the pseudospin and its covariant derivative

$$s^a = \boldsymbol{\psi}^\dagger \sigma^a \boldsymbol{\psi}, \tag{6.9}$$

$$\mathcal{D}_\mu s^a = \boldsymbol{\psi}^\dagger \sigma^a D_\mu \boldsymbol{\psi} + c.c. = \partial_\mu s^a + 2\varepsilon^{abc} A^b_\mu s^c, \tag{6.10}$$

with $a, b, c \in \{x, y, x\}$. The total charge of the system can be written as an integral of the charge density $j = \varepsilon_{\mu\nu\lambda}\partial_\mu G_{\nu\lambda}$, corresponding to the gauge invariant tensor

$$G_{\mu\nu} = \frac{1}{|s|} F^a_{\mu\nu} s^a - \frac{1}{2|s|^3} \varepsilon^{abc} s^a \, \mathcal{D}_\mu s^b \, \mathcal{D}_\nu s^c, \tag{6.11}$$

where $F^a_{\mu\nu} = \partial_\mu A^a_\nu - \partial_\mu A^a_\mu + 2\varepsilon^{abc} A^b_\mu A^c_\nu$ is the non-Abelian magnetic field strength tensor. The tensor $G_{\mu\nu}$ is formally the same as the one introduced in the studies of unified gauge theories in high-energy physics [212], but in the present case s^a is defined by Eq. (6.9) which changes radically the properties of the monopole solutions.

The total charge $\mathcal{Q}$ can be expressed as a difference of charges $\mathcal{Q}_S$ and $\mathcal{Q}_M$ where $\mathcal{Q}_S$ depends only on the topology of the pseudospin texture and the magnetic part $\mathcal{Q}_M$ combines the pseudospin and the matrix-valued vector potential to a scalar-valued magnetic field [230]. Furthermore, the charge $\mathcal{Q}_S$ is proportional to the topological charge $\mathcal{Q}_{3D}$ in Eq. (4.4). The s field depends on $\boldsymbol{\psi} = (\psi_1, \psi_2)$ and corresponds to the order parameter space $U(2)$. Hence, globally defined states with $\mathcal{Q}_S \neq 0$ are not allowed since the second homotopy group of $U(2)$ is trivial (cf. Section 4.1). Due to the local gauge invariance, it could be possible to construct locally defined states with $\mathcal{Q}_S \neq 0$ analogously to the Wu–Yang monopole [231–233].

In Publication VII, the charges $\mathcal{Q}_S$ and $\mathcal{Q}_M$ were used to classify the different low-energy states of the mean-field Hamiltonian with the non-singular vector potential $\boldsymbol{A}'$. Assuming $k = k'$ and a spherically symmetric trap with frequency ω_r, the different mean-field states were analysed as a function of the parameter ka_{ho} where $a_{\mathrm{ho}} = \sqrt{\hbar/m\omega_r}$. Apart from the values $ka_{\mathrm{ho}} < 0.1$, the ground state was found to be non-degenerate. The ground state configuration had two coreless vortices which for large enough ka_{ho} eventually merge to form a singular vortex. For $ka_{\mathrm{ho}} \gtrsim 2$ there is a pair of solutions which are degenerate within the numerical accuracy and can be differentiated by the behaviour of the charges $\mathcal{Q}_S$ and $\mathcal{Q}_M$ under gauge transformations, see Publication VII.

The possibility of a fragmented condensate in the context of light-induced gauge potentials has been investigated for Bose gases with a spin-orbit coupling generated by external laser fields [227]. In this case, the fragmentation stems from degeneracies in the single-particle spectrum. For the non-Abelian monopole, the single-particle

Hamiltonian (6.2) has a two-fold symmetry which was shown to explain the existence of degenerate mean-field solutions. It remains to be seen if the same symmetry also leads to a fragmented condensate.

7 Phase transitions in Bose gases

The formation of a Bose-Einstein condensate represents the most obvious phase transition in dilute Bose gases, but the internal degrees of freedom can also give rise to other phase transitions. For the spinor Bose gases, the formation of a ferromagnetic or antiferromagnetic order is an example of a phase transition which shares an important common feature with the onset of a BEC—a broken symmetry. Low-dimensional systems can also feature phase transitions that do not involve any broken symmetry. The BKT transition is perhaps the most notable example of such transitions[12] and it is analysed in this section. As a related subject, the existence of clusters composed of vortices and antivortices is discussed.

Uniform Bose gases in one and two spatial dimensions are intriguing since the they do not support a coherent BEC in the thermodynamical limit at finite temperatures due to thermal fluctuations that destroy the long-range order associated with the true condensate. The superfluid phase of two-dimensional Bose gases can be viewed as a quasi-condensate where the $U(1)$ phase can fluctuate while the density fluctuations are suppressed [94, 95]. The external confinement changes the situation such that the different phase transitions become smooth crossovers and a coherent BEC is expected at extremely low temperatures for 2D gases [46]. In external traps, these systems are quasi-2D in the sense that the scattering is typically 3D while otherwise the systems are effectively 2D [46]. In this section, we discuss the existence and the nature of a condensed component as well as the BKT transition in the context of trapped quasi-2D spin-1 Bose gases.

7.1 Berezinskii-Kosterlitz-Thouless transition

The transition from the superfluid phase to the normal fluid phase in two-dimensions is associated with the unbinding of pairs composed of vortices and antivortices. This phase transition is the Berezinskii-Kosterlitz-Thouless transition [48–51]. At temperatures much below the BKT transition temperature, the phase fluctuations in the quasi-condensate are dominated by the phonons. With increasing temperature, fluctuations due to the creation of bound vortex pairs start to dominate and eventually at high enough temperatures, the vortex pairs break into free vortices resulting in a non-superfluid state. The loss of phase coherence due to the proliferation of free vortices is shown schematically in Fig. 7.1 for a single-component Bose gas.

Recent experiments for single-component Bose systems [144] suggest that the quasi-condensate component can persist somewhat above the BKT transition tem-

[12] Other examples include, e.g., the formation of the fractional quantum Hall liquid in two-dimensional electron gases [208] and the topological insulators in three spatial dimensions [234].

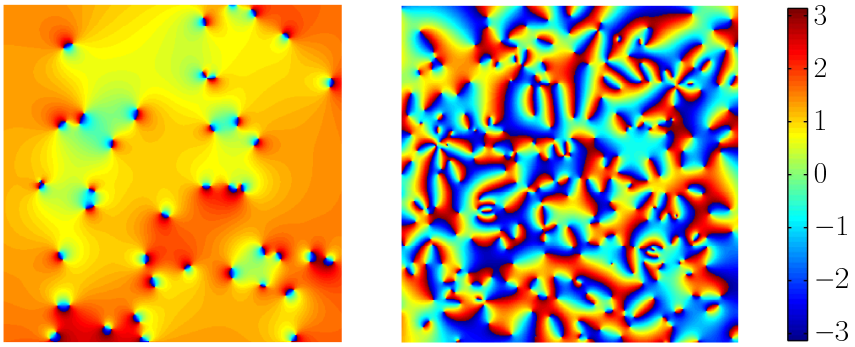

Figure 7.1: Schematic illustration of the $U(1)$ phase corresponding to a single component Bose gas. Left panel: locally phase coherent Bose gas in the superfluid phase below T_{BKT}. Right panel: non-superfluid Bose gas at a high temperature. The phase coherence is lost due to the unbinding of the initially tightly bound vortex–antivortex pairs.

perature T_{BKT}. At high temperatures, the quasi-long-range order characterised by algebraically decaying correlations is completely destroyed by the thermal fluctuations. This picture is supported by numerical calculations using the PGPE formalism which predict the existence of another temperature $T_c > T_{\mathrm{BKT}}$ corresponding to the onset of a condensed component in the sense of Eq. (2.4). The situation in antiferromagnetic spin-1 Bose gases was discussed in Publication IX and the results are reviewed in Section 7.3. Next, we discuss a related effect for the low-temperature condensate phase—stationary configurations composed of vortices and antivortices.

7.2 Vortex clusters in single-component systems

Since pairs composed of vortices and antivortices play a central role in the BKT transition, it is natural to ask whether they can exist in the quasi-2D limit in the presence of a coherent condensate. The dynamics of the vortex-antivortex pairs (VAPs) in the single-component condensates has turned out to be rich [235–237] and the existence of clusters formed by vortices and antivortices as stationary solutions of the Gross-Pitaevskii equation has been intensively studied in non-rotated condensates [238–242]. However, the results of Refs. [239, 240, 242] are to some extent contradictory and in Publication VIII, a systematic stability analysis of a vortex dipole (VD), a vortex tripole (VT), and a vortex quadrupole (VQ) in pancake-shaped single-component condensates was undertaken. The density profiles corresponding to the stationary VD, VT, and VQ are shown in Fig. 7.2.

The existence and the stability of the vortex clusters was investigated as a func-

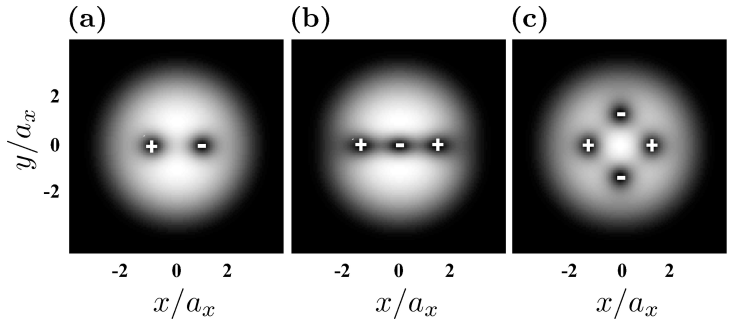

Figure 7.2: Density profiles for a stationary vortex dipole (a), tripole (b), and quadrupole (c). The charge of the vortex is denoted by + or −. The dimensionless interaction strength is $\tilde{g} = 170$ and the harmonic oscillator length in the x direction is denoted by a_x, see Publication VIII.

tion of the dimensionless interaction strength $\tilde{g} = 4\sqrt{2\pi}Na/a_z$, where a_z is the harmonic oscillator length in the tightly trapped direction and a is the s-wave scattering length. The VQ was found to exist for all $\tilde{g}$ while VD and VT existed for $\tilde{g} \gtrsim 42$ and $\tilde{g} \gtrsim 108$, respectively. All states are energetically unstable since the energy can be lowered either by the annihilation vortices with opposite topological charges or by the expulsion of vortices from the condensate. However, the energy of a VD can be lower than the energy of an isolated vortex in non-rotated condensates, which can facilitate the experimental realisation of the VD. All vortex clusters were found to have dynamical instabilities since the quasiparticle spectrum computed from the single-component Bogoliubov equation [112] contained excitations with complex energies.

The dynamical instabilities were found to fall into two different categories: instabilities that rotate the vortex cluster rigidly but do not break the structure (rotational mode) and instabilities that destroy the cluster due to an annihilation or expulsion of vortices (decay mode), see Fig. 7.3. The rotational mode was found to exist for all stationary configurations and it vanished upon adding a small amount of anisotropy to the trap. It was interpreted in Publication VIII as the Goldstone mode corresponding to the broken rotational symmetry. The decay mode is more interesting since it persists also in the non-symmetric traps. For VD and VQ, the decay mode vanishes for certain values of $\tilde{g}$, indicating that VD and VQ can be long-lived if the dissipation is weak enough. Although the VT has the dynamical instability giving rise to the expulsion of one of the outermost vortices for all $\tilde{g}$, the configuration has nevertheless been observed in a recent experiment where vortices were generated using oscillating magnetic quadrupole fields [243].

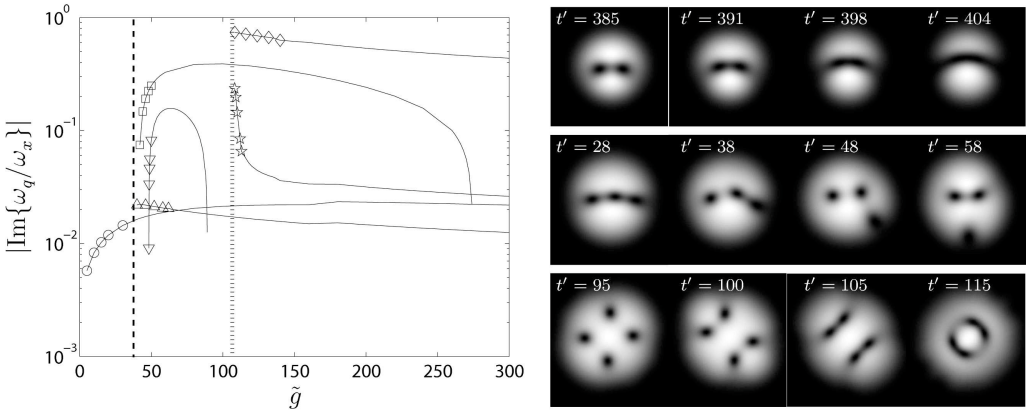

Figure 7.3: Left panel: The dynamical instability modes as a function of the interaction strength $\tilde{g}$ for VD, VT, and VQ in a rotationally symmetric trap. Instability modes corresponding to the VD are marked with $\triangledown$ (decay mode) and $\triangle$ (rotational mode), to the VT with $\diamondsuit$ (decay mode) and $\star$ (rotational mode), and to the VQ with $\square$ (decay mode) and $\bigcirc$ (rotational mode). The dashed and dotted lines indicate the critical value of $\tilde{g}$ below which VD and VT cease to exist, respectively. Right panel: The decay of VD (top), VT (middle), and VQ (bottom) when the initial state is slightly perturbed using the decay mode. Time is given in the units of $1/\omega_x$ where ω_x is the trap frequency to the x direction.

7.3 Finite-temperature phase transitions in spinor Bose gases

Bose gases with the spin degree of freedom offer an interesting platform to study the BKT transition since they combine magnetic ordering and superfluidity, both of which are susceptible to the enhanced thermal fluctuations in 2D geometries. The basic theory for the BKT transition in antiferromagnetic spin-1 Bose gases [90] predicts that the transition is mediated by the HQVs and the superfluid density changes non-continuously by $\Delta\rho_s = 8m^2 k_{\mathrm{B}} T_{\mathrm{BKT}}/(\pi\hbar^2)$, where T_{BKT} is the transition temperature. Also the ferromagnetic phase can undergo a BKT-type of transition which is mediated by either the coreless or the polar core vortices discussed in Section 4.1. Both types of defects have an infinite energy in uniform systems such that paired configurations are finite energy excitations and the unbinding of such pairs can set off a transition analogous to the BKT transition in single-component systems. Furthermore, an antiferromagnetic Heisenberg model in a triangular lattice corresponds to the same order parameter space as the ferromagnetic spin-1 Bose gas and a BKT-type of transition has been predicted [244, 245].

In Publication IX, the BKT transition and the existence of a condensate in the trapped quasi-2D antiferromagnetic Bose gases were investigated using the PGPE

formalism. All ensemble averages were computed using the corresponding time averages. The temperature and the chemical potential were determined dynamically using the approach of Section 3.2. The number of atoms in the incoherent region was calculated using the HFP approximation presented in Eqs. (2.26) and (2.27). The trap aspect ratio was chosen such that only the lowest axial mode in the c-field region became populated. The HQVs were identified as the π disclinations in the texture given by the local magnetic axis $\hat{\boldsymbol{n}}$. The different HQVs are illustrated in Eq. (4.8) and in Fig. 4.4.

Assuming a quadratic Zeeman shift $\mathcal{H}_{qZ} = qB_z^2\mathcal{F}_z^2$, where q is negative[13] and $|q|B_z^2$ much larger than $k_{\mathrm{B}}T$, the nematic order is restricted to the x-y plane since the $\alpha = 0$ component is effectively eliminated from the problem. In Publication IX, this phase is referred to as the "in-plane" nematic in a contrast to the general nematic phase where the local magnetic axis has three degrees of freedom and was coined as the "out-of-plane" nematic. The condensate fraction is defined as N_0/N_{tot}, where N_0 is given by Eq. (2.4). The quasi-condensate density is of the form

$$n_{qc}(\boldsymbol{r}) = \sqrt{2\langle|\vec{\Psi}_{\boldsymbol{C}}(\boldsymbol{r})|^2\rangle^2 - \langle|\vec{\Psi}_{\boldsymbol{C}}(\boldsymbol{r})|^4\rangle}, \tag{7.1}$$

which generalises the definition of the quasi-condensate from the single-component case [94,95] and explicitly excludes the incoherent region atoms, see Publication IX.

In the calculation presented in Publication IX, the cutoff energy $\varepsilon_{\mathrm{cut}}$ is fixed, which causes the total particle number N_{tot} to increase with the increasing temperature T. To make the different data points comparable, all quantities are presented as a function of the reduced temperature $T' = T/T_0$, where T_0 is the critical temperature of a quasi-2D ideal Bose gas corresponding to a given N_{tot}. The condensate and the quasi-condensate fractions are shown in Fig. 7.4 as functions of T'. The onset temperatures $T' = 0.97 \pm 0.02$ and $T' = 1.16 \pm 0.04$ for the condensate and the quasi-condensate are equal for both nematic phases within the numerical accuracy.

The crossover from the BKT superfluid to a normal fluid was probed in Publication IX using the radial probability distribution $P_r(r)$ [142] for the excitation of different topological defects. An estimate for the crossover temperature was obtained as the temperature at which $P_r(r)$ becomes nonzero at the centre of the trap. This resulted in $T'_{\mathrm{BKT}} = 0.82 \pm 0.05$ and $T'_{\mathrm{BKT}} = 0.89 \pm 0.04$ for the in-plane and the out-of-plane nematic phases, respectively. The difference in the crossover temperatures was attributed to the thermally activated skyrmions (see Section 4.1) which are allowed in the out-of-plane phase and reduce the entropy change associated with the creation

[13] The negative quadratic Zeeman shift can be induced by a polarised light detuned slightly from the hyperfine level splitting, see Ref. [246] and references therein.

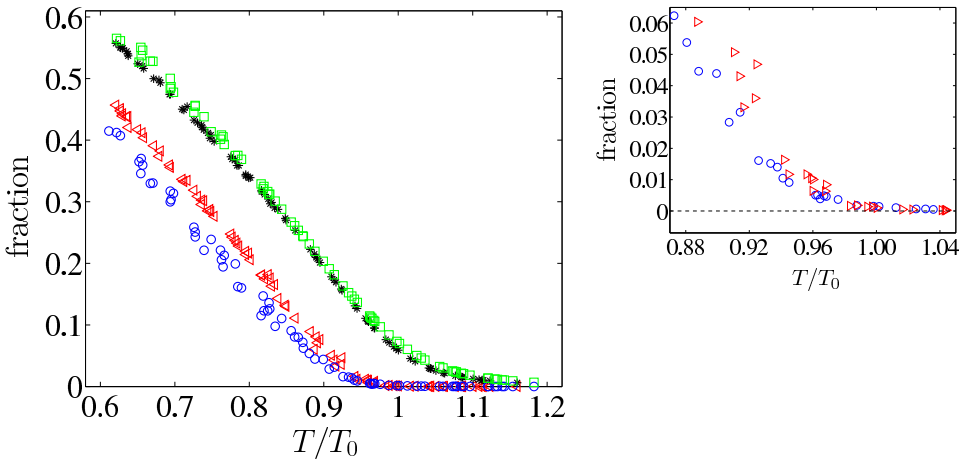

Figure 7.4: Left panel: condensate fraction for the in-plane nematic (circles) and the out-of-plane nematic (triangles) phases as functions of the reduced temperature. The quasi-condensate fraction for the in-plane nematic (squares) and out-of-plane nematic (asterisks) phases almost coincide. Right panel: the condensate fraction near the temperature corresponding to the onset of the condensate. The dashed line is a guide for the eye.

of the HQV pairs and free HQVs, resulting in a higher crossover temperature.

The hypothesis of the different crossover temperatures was supported by the inspection of the phase-space density $\bar{n}_c^{(2D)}\lambda^2$, where $\bar{n}_c^{(2D)}$ is the average 2D density of the c-field atoms at at the centre of the trap and $\lambda = \sqrt{2\pi\hbar^2/mk_BT}$ is the thermal wavelength. For the single-component case, the phase-space density at the critical temperature satisfies the condition $\bar{n}_{\rm crit}^{(2D)}\lambda^2 = \ln(C/\bar{g})$, where $\bar{g} = \sqrt{8\pi}a/a_z$ and $C \simeq 380$ [95]. Calculation of the phase-space density indicated that the existence of a universal critical phase-space density for the crossover, irrespective of the nematic phase, yields a higher crossover temperature for the out-of-plane nematic if the crossover takes place below the condensation temperature. The preceding estimates for the $T'_{\rm BKT}$ yield a critical phase space density $\bar{n}_c^{(2D)}\lambda^2 \simeq 25$ for both nematic phases. At the crossover temperature, the predicted superfluid density is smaller than the average density of the c-field atoms at the centre of the trap, $\rho_s/\bar{n}_c^{(2D)} = 0.64$, and the condition $\bar{n}_c^{(2D)}\lambda^2 = 25$ is consistent with the expected jump $\Delta\rho_s$ in the superfluid density.

The recent advances in the trapping of neutral atoms in oblate optical traps [144], in the evaporative cooling of optically trapped atoms [247], and in the imaging of the different components of the spin quadrupole operator [248, 249] suggest that experimental investigations of superfluidity and condensation in quasi-2D spinor Bose gases can become reality in the foreseeable future.

8 Summary and discussion

The central topic in this Thesis has been superfluidity and its different manifestations in Bose gases with the hyperfine spin degree of freedom. In particular, the properties and creation of different vortices in spinor Bose-Einstein condensates were investigated. In Publications I and IV, the stability of coreless vortices was analysed and coreless vortices with a winding number two in one of the hyperfine spin states were found to have regions of dynamical instability, rendering the vortex susceptible to decay even in the absence of dissipation. Publications II and III demonstrated a generalisation of the topological phase imprinting method to increase cyclically the angular momentum of the condensate, enabling a robust creation of vortices with multiple quanta of angular momentum. This method can possibly be used to create condensates with large vortex densities for exploring some aspects of the quantum Hall fluids.

The topological phase imprinting method reviewed in Publication II has enabled the creation of two- and four-quantum vortices that usually are dynamically unstable. In Publication V, the first experiment [59] probing the dynamical instability of the two-quantum vortex was simulated and the gravitational sag breaking the rotation symmetry was found to be sufficient impetus for the splitting observed in the experiment. Publication IV augmented this analysis by taking into account the spin degree of freedom neglected in Publication V and showed that the splitting of the two-quantum vortex likely initiates already at the creation process.

The spin degree of freedom enables the existence and creation of pointlike defects that are absent in the single-component Bose gases. In Publication VI, an experimentally straightforward method for creating the Dirac monopole was constructed. The method was found to be robust against the typical perturbations present in the experiments and it should enable creation of the Dirac monopole with the present experimental capabilities. The Dirac string associated with the monopole was found to carry two quanta of angular momentum and it presents an interesting example of a dynamically unstable two-quantum vortex which does not correspond to any of the vortices discussed in Publications I, IV, and V. Another type of monopole arising from the adiabatic motion of multilevel atoms in external laser fields was investigated in Publication VII. A gauge invariant formulation of the total charge of the system was devised and used to resolve the degeneracy of the mean-field states. The ground state of the system was found to be non-degenerate and support singular vortices for a certain range of parameters.

Different aspects of low-dimensional Bose systems were explored in Publications VIII and IX. Publication VIII features a comprehensive study of the stability

properties of vortex clusters consisting of vortices and antivortices, indicating that structures with zero total vorticity can be made dynamically stable wheres the linear structure consisting of two vortices and one antivortex is always dynamically unstable. Vortex clusters with zero total vorticity were found to revive after the initial collapse of the cluster under the excitation of the instability modes. In Publication IX, finite-temperature phase transitions in trapped quasi-2D spin-1 Bose gases were analysed and a hierarchy of crossover temperatures corresponding the onset of quasi-condensate, condensate, and superfluid with decreasing temperature were found. In addition, a condition for the critical phase-space density at the BKT crossover temperature was presented and the dependence of the BKT crossover temperature from the type of nematic ordering was discussed.

Superfluidity in low-dimensional spinor Bose gases seems to be a fairly unexplored subject and some of the basic questions concerning the characteristics of the BKT transition remain open even in the simplest spin-1 case. As discussed in Publication IX, the characterisation of the superfluid component in trapped systems is challenging and further theoretical work is needed. Furthermore, the ferromagnetic spin-1 Bose gas is also expected to have a BKT-type of phase transition and this could be explored in the future. Bose gases with the total hyperfine spin $F = 2$ and $F = 3$ could feature interesting superfluid transitions in 2D geometries due to the non-Abelian statistics of the vortices in certain magnetic phases [250]. The research in the field of cold atomic gases continues at a breathtaking pace, suggesting that also the experimental studies of the different phase transitions in spinor Bose gases could take place in the near future.

An important issue ignored in this Thesis is the long-range magnetic dipole-dipole interaction [251]. Recent experiments indicate that the dipole-dipole interaction can be important for ^{87}Rb in the absence of external magnetic fields [205, 252]. In the situations considered in this Thesis, however, the effects arising from the dipole-dipole interactions are expected to be unimportant. On the other hand, inclusion of the dipole-dipole interactions is likely to give rise to new interesting phases in low-dimensional systems and there is a clear incentive for the studies of phase transitions in spinor Bose gases with dipole-dipole interactions.

References

[1] S. N. Bose, Z. Phys **26**, 178 (1924).

[2] A. Einstein, Sitzber. Kgl. Preuss. Akad. Wiss. **1924**, 261 (1924).

[3] A. Einstein, Sitzber. Kgl. Preuss. Akad. Wiss. **1925**, 3 (1925).

[4] P. Kapitza, Nature **141**, 74 (1938).

[5] J. F. Allen and A. D. Misener, Nature **141**, 75 (1938).

[6] F. London, Nature **141**, 643 (1938).

[7] P. Sokol, in *Bose-Einstein Condensation*, edited by A. Griffin, D. W. Snoke, and S. Stringari (Cambridge University Press, Cambridge, 1995), Chap. 4, pp. 51–85.

[8] D. M. Ceperley, Rev. Mod. Phys. **67**, 279 (1995).

[9] S. Stenholm, Rev. Mod. Phys. **58**, 699 (1986).

[10] S. Chu, Rev. Mod. Phys. **70**, 685 (1998).

[11] C. N. Cohen-Tannoudji, Rev. Mod. Phys. **70**, 707 (1998).

[12] W. D. Phillips, Rev. Mod. Phys. **70**, 721 (1998).

[13] M. H. Anderson, J. R. Ensher, M. R. Matthews, C. E. Wieman, and E. A. Cornell, Science **269**, 198 (1995).

[14] C. C. Bradley, C. A. Sackett, J. J. Tollett, and R. G. Hulet, Phys. Rev. Lett. **75**, 1687 (1995), erratum: Phys. Rev. Lett. **79**, 1170 (1997).

[15] K. B. Davis, M.-O. Mewes, M. R. Andrews, N. J. van Druten, D. S. Durfee, D. M. Kurn, and W. Ketterle, Phys. Rev. Lett. **75**, 3969 (1995).

[16] B. DeMarco and D. D. Jin, Science **285**, 1703 (1999).

[17] F. Schreck, L. Khaykovich, K. L. Corwin, G. Ferrari, T. Bourdel, J. Cubizolles, and C. Salomon, Phys. Rev. Lett. **87**, 080403 (2001).

[18] A. G. Truscott, K. E. Strecker, W. I. McAlexander, G. B. Partridge, and R. G. Hulet, Science **291**, 2570 (2001).

[19] D. M. Stamper-Kurn, M. R. Andrews, A. P. Chikkatur, S. Inouye, H.-J. Miesner, J. Stenger, and W. Ketterle, Phys. Rev. Lett. **80**, 2027 (1998).

[20] M. D. Barrett, J. A. Sauer, and M. S. Chapman, Phys. Rev. Lett. **87**, 010404 (2001).

[21] J. Stenger, S. Inouye, D. M. Stamper-Kurn, H.-J. Miesner, A. P. Chikkatur, and W. Ketterle, Nature **396**, 345 (1998).

[22] T. Loftus, C. A. Regal, C. Ticknor, J. L. Bohn, and D. S. Jin, Phys. Rev. Lett. **88**, 173201 (2002).

[23] E. Tiesinga, B. J. Verhaar, and H. T. C. Stoof, Phys. Rev. A **47**, 4114 (1993).

[24] S. Inouye, M. R. Andrews, J. Stenger, H.-J. Miesner, D. M. Stamper-Kurn, and W. Ketterle, Nature **392**, 151 (1998).

[25] D. M. Eagles, Phys. Rev. **186**, 456 (1969).

[26] A. J. Leggett, in *Modern Trends in the Theory of Condensed Matter*, edited by A. Pekalski and J. A. Przystawa (Springer, Heidelberg, 1980), p. 13.

[27] M. W. Zwierlein, J. R. Abo-Shaeer, A. Schirotzek, C. H. Schunck, and W. Ketterle, Nature **435**, 1047 (2005).

[28] T. Ohmi and K. Machida, J. Phys. Soc. Jpn. **67**, 1822 (1998).

[29] T.-L. Ho, Phys. Rev. Lett. **81**, 742 (1998).

[30] C. J. Pethick and H. Smith, *Bose-Einstein Condensation Dilute Gases*, 2$^{\text{nd}}$ ed. (Cambridge University Press, Cambridge, 2008).

[31] D. G. Fried, T. C. Killian, L. Willmann, D. Landhuis, S. C. Moss, D. Kleppner, and T. J. Greytak, Phys. Rev. Lett. **81**, 3811 (1998).

[32] S. L. Cornish, N. R. Claussen, J. L. Roberts, E. A. Cornell, and C. E. Wieman, Phys. Rev. Lett. **85**, 1795 (2000).

[33] A. Robert, O. Sirjean, A. Browaeys, J. Poupard, S. Nowak, D. Boiron, C. I. Westbrook, and A. Aspect, Science **292**, 461 (2001).

[34] F. P. D. Santos, J. Léonard, J. Wang, C. J. Barrelet, F. Perales, E. Rasel, C. S. Unnikrishnan, M. Leduc, and C. Cohen-Tannoudji, Phys. Rev. Lett. **86**, 3459 (2001).

[35] G. Modugno, G. Ferrari, G. Roati, R. J. Brecha, A. Simoni, , and M. Inguscio, Science **294**, 1320 (2001).

[36] T. Weber, J. Herbig, M. Mark, H.-C. Nägerl, and R. Grimm, Science **299**, 232 (2003).

[37] Y. Takasu, K. Maki, K. Komori, T. Takano, K. Honda, M. Kumakura, T. Yabuzaki, and Y. Takahashi, Phys. Rev. Lett. **91**, 040404 (2003).

[38] G. Roati, M. Zaccanti, C. D'Errico, J. Catani, M. Modugno, A. Simoni, M. Inguscio, and G. Modugno, Phys. Rev. Lett. **99**, 010403 (2007).

[39] A. Griesmaier, J. Werner, S. Hensler, J. Stuhler, and T. Pfau, Phys. Rev. Lett. **94**, 160401 (2005).

[40] F. V. S. Kraft, O. Appel, F. Riehle, and U. Sterr, Phys. Rev. Lett. **103**, 130401 (2009).

[41] S. Stellmer, M. K. Tey, B. Huang, R. Grimm, and F. Schreck, Phys. Rev. Lett. **103**, 200401 (2009).

[42] Y. N. de Escobar, P. G. Mickelson, M. Yan, B. J. DeSalvo, S. B. Nagel, and T. C. Killian, Phys. Rev. Lett. **103**, 200402 (2009).

[43] S. Jochim, M. Bartenstein, A. Altmeyer, G. Hendl, S. Riedl, C. Chin, J. H. Denschlag, and R. Grimm, Science **302**, 2101 (2003).

[44] M. Greiner, C. A. Regal, and D. S. Jin, Nature **426**, 537 (2003).

[45] Q. Beaufils, R. Chicireanu, T. Zanon, B. Laburthe-Tolra, E. Maréchal, L. Vernac, J.-C. Keller, and O. Gorceix, Phys. Rev. A **77**, 061601(R) (2008).

[46] I. Bloch, J. Dalibard, and W. Zwerger, Rev. Mod. Phys. **80**, 855 (2008).

[47] H. T. C. Stoof, K. B. Gubbels, and D. B. M. Dickerscheid, *Ultracold Quantum Fields* (Springer, Dordrecht, 2009).

[48] V. L. Berezinskii, Sov. Phys. JETP **32**, 493 (1971).

[49] V. L. Berezinskii, Sov. Phys. JETP **34**, 610 (1972).

[50] J. M. Kosterlitz and D. J. Thouless, J. Phys. C **5**, 124 (1972).

[51] J. M. Kosterlitz and D. J. Thouless, J. Phys. C **6**, 1181 (1973).

[52] J. E. Williams and M. J. Holland, Nature **401**, 568 (1999).

[53] M. R. Matthews, B. P. Anderson, P. C. Haljan, D. S. Hall, C. E. Wieman, and E. A. Cornell, Phys. Rev. Lett. **83**, 2498 (1999).

[54] K. W. Madison, F. Chevy, W. Wohlleben, and J. Dalibard, Phys. Rev. Lett. **84**, 806 (2000).

[55] J. R. Abo-Shaeer, C. Raman, J. M. Vogels, and W. Ketterle, Science **292**, 476 (2001).

[56] A. L. Fetter and A. A. Svidzinsky, J. Phys.: Condens. Matter **13**, R135 (2001).

[57] A. E. Leanhardt, A. Görlitz, A. P. Chikkatur, D. Kielpinski, Y. Shin, D. E. Pritchard, and W. Ketterle, Phys. Rev. Lett. **89**, 190403 (2002).

[58] A. E. Leanhardt, Y. Shin, D. Kielpinski, D. E. Pritchard, and W. Ketterle, Phys. Rev. Lett. **90**, 140403 (2003).

[59] Y. Shin, M. Saba, M. Vengalattore, T. A. Pasquini, C. Sanner, A. E. Leanhardt, M. Prentiss, D. E. Pritchard, and W. Ketterle, Phys. Rev. Lett. **93**, 160406 (2004).

[60] K. Kasamatsu, Int. J. Mod. Phys. B **19**, 1835 (2005).

[61] A. L. Fetter, Rev. Mod. Phys. **81**, 647 (2009).

[62] D. M. Stamper-Kurn and W. Ketterle, in *Coherent atomic matter waves – Ondes de matière cohérentes*, *Les Houches, Session LXXII*, edited by R. Kaiser, C. Westbrook, and F. David (Springer, Heidelberg, 2001), pp. 137–217.

[63] N. D. Mermin and T.-L. Ho, Phys. Rev. Lett. **36**, 594 (1976).

[64] S. Blaha, Phys. Rev. Lett. **36**, 874 (1976).

[65] G. E. Volovik and V. P. Mineev, JETP. Lett. **23**, 593 (1976).

[66] E. J. Mueller, Phys. Rev. A **69**, 033606 (2004).

[67] M. Nakahara, T. Isoshima, K. Machida, S.-I. Ogawa, and T. Ohmi, Physica B **284–288**, 17 (2000).

[68] T. Isoshima, M. Nakahara, T. Ohmi, and K. Machida, Phys. Rev. A **61**, 063610 (2000).

[69] S.-I. Ogawa, M. Möttönen, M. Nakahara, T. Ohmi, and H. Shimada, Phys. Rev. A **66**, 013617 (2002).

[70] T. Isoshima, M. Okano, H. Yasuda, K. Kasa, J. A. M. Huhtamäki, M. Kumakura, and Y. Takahashi, Phys. Rev. Lett. **99**, 200403 (2007).

[71] A. Vilenkin and E. P. S. Shellard, *Cosmic Strings and Other Topological Defects* (Cambridge University Press, Cambridge, 1994).

[72] M. Nakahara, *Geometry, Topology and Physics* (IOP Publishing Ltd, Bristol, 1990).

[73] H. T. C. Stoof, E. Vliegen, and U. Al Khawaja, Phys. Rev. Lett. **87**, 120407 (2001).

[74] J. P. Martikainen, A. Collin, and K.-A. Suominen, Phys. Rev. Lett. **88**, 090404 (2002).

[75] C. M. Savage and J. Ruostekoski, Phys. Rev. A **68**, 043604 (2003).

[76] J. Ruseckas, G. Juzeliūnas, P. Öhberg, and M. Fleischhauer, Phys. Rev. Lett. **95**, 010404 (2005).

[77] U. Al Khawaja and H. Stoof, Nature **411**, 918 (2001).

[78] J. Ruostekoski and J. R. Anglin, Phys. Rev. Lett. **86**, 3934 (2001).

[79] R. A. Battye, N. R. Cooper, and P. M. Sutcliffe, Phys. Rev. Lett. **88**, 080401 (2002).

[80] C. M. Savage and J. Ruostekoski, Phys. Rev. Lett. **91**, 010403 (2003).

[81] E. Babaev, Phys. Rev. Lett. **88**, 177002 (2002).

[82] Y. Kawaguchi, M. Nitta, and M. Ueda, Phys. Rev. Lett. **100**, 180403 (2008).

[83] U. Leonhardt and G. E. Volovik, JETP. Lett. **72**, 66 (2000).

[84] E. Demler and F. Zhou, Phys. Rev. Lett. **88**, 163001 (2002).

[85] G. W. Semenoff and F. Zhou, Phys. Rev. Lett. **98**, 100401 (2007).

[86] M. M. Salomaa and G. E. Volovik, Rev. Mod. Phys. **59**, 533 (1988).

[87] D. Vollhardt and P. Wölfle, *The Superfluid Phases of Helium* 3 (Taylor & Francis, London, 1990).

[88] G. E. Volovik, *Exotic Properties of Superfluid* ^{3}*He* (World Scientific, Singapore, 1992).

[89] G. E. Volovik, *The Universe in a Helium Droplet* (Oxford University Press, Oxford, 2003).

[90] S. Mukerjee, C. Xu, and J. E. Moore, Phys. Rev. Lett. **97**, 120406 (2006).

[91] V. L. Ginzburg and L. D. Landau, Zh. Eksp. Teor. Fiz. **20**, 1064 (1950).

[92] O. Penrose, Phil. Mag. **42**, 1373 (1951).

[93] O. Penrose and L. Onsager, Phys. Rev. **104**, 576 (1956).

[94] Y. Kagan, B. V. Svistunov, and G. V. Shlyapnikov, Sov. Phys. JETP **66**, 314 (1987).

[95] N. Prokof'ev, O. Ruebenacker, and B. V. Svistunov, Phys. Rev. Lett. **87**, 270402 (2001).

[96] E. J. Mueller, T. L. Ho, M. Ueda, and G. Baym, Phys. Rev. A **74**, 033612 (2006).

[97] C. K. Law, H. Pu, and N. P. Bigelow, Phys. Rev. Lett **81**, 5257 (1998).

[98] T.-L. Ho and S. K. Yip, Phys. Rev. Lett. **84**, 4031 (2000).

[99] P. Nozières and D. S. James, J. Physique **43**, 1133 (1982).

[100] J. W. Kane and L. P. Kadanoff, Phys. Rev. **155**, 80 (1967).

[101] N. N. Bogoliubov, J. Phys. USSR **11**, 23 (1947).

[102] S. T. Beliaev, Sov. Phys. JETP **7**, 289 (1958).

[103] S. T. Beliaev, Sov. Phys. JETP **7**, 299 (1958).

[104] A. L. Fetter, Ann. Phys. **70**, 67 (1972).

[105] A. Altland and B. Simons, *Condensed Matter Field Theory* (Cambridge University Press, Cambridge, 2006).

[106] C. W. Gardiner, Phys. Rev. A **56**, 1414 (1997).

[107] M. Girardeau and A. Arnowitt, Phys. Rev **113**, 755 (1959).

[108] M. Girardeau, Phys. Rev. A **58**, 775 (1998).

[109] Y. Castin and R. Dum, Phys. Rev. A **57**, 3008 (1998).

[110] T. Isoshima, K. Machida, and T. Ohmi, J. Phys. Soc. Jon. **70**, 1604 (2001).

[111] T. Mizushima, K. Machida, and T. Kita, Phys. Rev. Lett. **89**, 030401 (2002).

[112] L. Pitaevskii and S. Stringari, *Bose-Einstein Condensation* (Oxford University Press, Oxford, 2003).

[113] Y. Castin and R. Dum, Eur. J. Phys. D **7**, 399 (1999).

[114] R. J. Dodd, K. Burnett, M. Edwards, and C. W. Clark, Phys. Rev. A **56**, 587 (1997).

[115] T. Isoshima and K. Machida, J. Phys. Soc. Jpn. **66**, 3502 (1997).

[116] H. Pu, C. K. Law, J. H. Eberly, and N. P. Bigelow, Phys. Rev. A **59**, 1533 (1999).

[117] E. Lundh and H. M. Nilsen, Phys. Rev. A. **74**, 063620 (2006).

[118] P. G. de Gennes, *Superconductivity in Metals and Alloys* (W. A. Benjamin, New York, 1966).

[119] M. Mine, M. Okamura, T. Sunaga, and Y. Yamanaka, Ann. Phys. (N.Y.) **322**, 2327 (2007).

[120] L. J. Garay, J. R. Anglin, J. I. Cirac, and P. Zoller, Phys. Rev. Lett **85**, 4643 (2000).

[121] M. Lewenstein and L. You, Phys. Rev. Lett. **77**, 3489 (1996).

[122] S. Yi, O. E. Müstecaplioğlu, and L. You, Phys. Rev. Lett. **90**, 140404 (2003).

[123] W. Kohn, Phys. Rev. **123**, 1242 (1961).

[124] A. Griffin, Phys. Rev. B **53**, 9341 (1996).

[125] W. Zhang, S. Yi, and L. You, Phys. Rev. A **70**, 043611 (2004).

[126] T. Isoshima, T. Ohmi, and K. Machida, J. Phys. Soc. Jpn. **69**, 3864 (2000).

[127] V. N. Popov, *Functional Integrals and Collective Excitations* (Cambridge University Press, Cambridge, 1987).

[128] H. Shi and A. Griffin, Phys. Rep. **304**, 1 (1998).

[129] J. Reidl, A. Csordás, R. Graham, and P. Szépfalusy, Phys. Rev. A **59**, 3816 (1999).

[130] S. Giorgini, L. P. Pitaevskii, and S. Stringari, Phys. Rev. A **54**, R4633 (1996).

[131] R. J. Dodd, M. Edwards, C. W. Clark, and K. Burnett, Phys. Rev. A **57**, R32 (1998).

[132] A. Minguzzi, S. Conti, and M. P. Tosi, J. Phys.: Condens. Matter **9**, L33 (1997).

[133] F. Dalfovo, S. Giorgini, L. P. Pitaevskii, and S. Stringari, Rev. Mod. Phys **71**, 463 (1999).

[134] N. Goldenfeld, *Lectures on Phase Transitions and the Renormalization Group* (Westview Press, New York, 1992).

[135] T. Donner, S. Ritter, T. Bourdel, A. Öttl, M. Köhl, and T. Esslinger, Science **315**, 1556 (2007).

[136] P. B. Blakie, A. S. Bradley, M. J. Davis, R. J. Ballagh, and C. W. Gardiner, Adv. Phys. **57**, 363 (2008).

[137] E. H. Lieb, R. Seiringer, and J. Yngvason, Phys. Rev. Lett. **94**, 080401 (2005).

[138] E. H. Lieb, R. Seiringer, J. P. Solovej, and J. Yngvason, *The Mathematics of the Bose Gas and its Condensation* (Birkhäuser, Basel, 2005).

[139] M. J. Davis and S. A. Morgan, Phys. Rev. A **68**, 053615 (2003).

[140] M. J. Davis and P. B. Blakie, Phys. Rev. Lett. **96**, 060404 (2006).

[141] T. P. Simula and P. B. Blakie, Phys. Rev. Lett. **96**, 020404 (2006).

[142] T. P. Simula, M. J. Davis, and P. B. Blakie, Phys. Rev. A **77**, 023618 (2008).

[143] R. N. Bisset, M. J. Davis, T. P. Simula, and P. B. Blakie, Phys. Rev. A **79**, 033626 (2009).

[144] P. Cladé, C. Ryu, A. Ramanathan, K. Helmerson, and W. D. Phillips, Phys. Rev. Lett. **102**, 170401 (2009).

[145] P. B. Blakie, Phys. Rev. E **78**, 026704 (2008).

[146] H. H. Rugh, Phys. Rev. Lett. **78**, 772 (1997).

[147] H. H. Rugh, Phys. Rev. E **64**, 055101(R) (2001).

[148] M. J. Davis and P. B. Blakie, J. Phys. A: Math. Gen. **38**, 10259 (2005).

[149] F. Zhou, Phys. Rev. Lett. **87**, 080401 (2001).

[150] H. Mäkelä, Y. Zhang, and K.-A. Suominen, J. Phys. A **36**, 8555 (2003).

[151] N. D. Mermin, Rev. Mod. Phys. **51**, 591 (1979).

[152] T. H. R. Skyrme, Proc. R. Soc. Lond. A **260**, 127 (1961).

[153] G. E. Volovik and V. P. Mineev, Sov. Phys. JETP **46**, 401 (1977).

[154] L. D. Faddeev and A. J. Niemi, Nature **387**, 58 (1997).

[155] H. Zhai, W. Q. Chen, Z. Xu, and L. Chang, Phys. Rev. A **68**, 043602 (2003).

[156] K. Maki and T. Tsuneto, J. Low Temp. Phys. **27**, 635 (1977).

[157] T. Mizushima, N. Kobayashi, and K. Machida, Phys. Rev. A **70**, 043613 (2004).

[158] J.-P. Martikainen, A. Collin, and K.-A. Suominen, Phys. Rev. A **66**, 053604 (2002).

[159] T. Mizushima, K. Machida, and T. Kita, Phys. Rev. A **66**, 053610 (2002).

[160] E. N. Bulgakov and A. F. Sadreev, Phys. Rev. Lett. **90**, 200401 (2003).

[161] T.-L. Ho, Phys. Rev. B **18**, 1144 (1978).

[162] P. W. Anderson and G. Toulouse, Phys. Rev. Lett. **38**, 508 (1977).

[163] I. Klebanov, Nucl. Phys. B **262**, 133 (1985).

[164] D. H. Lee and C. L. Kane, Phys. Rev. Lett. **64**, 1313 (1990).

[165] A. G. Green, I. I. Kogan, and A. M. Tsvelik, Phys. Rev. B **54**, 16838 (1996).

[166] T. Senthil, A. Vishwanath, L. Balents, S. Sachdev, and M. P. A. Fisher, Science **303**, 1490 (2004).

[167] I. Herbut, *A Modern Approach to Critical Phenomena* (Cambridge University Press, Cambridge, 2007).

[168] M. M. Salomaa, Nature **326**, 367 (1987).

[169] P. A. M. Dirac, Proc. Roy. Soc. Lond. **A 133**, 60 (1931).

[170] P. A. M. Dirac, Phys. Rev. **74**, 817 (1948).

[171] I. Chuang, R. Durrer, N. Turok, and B. Yurke, Science **251**, 1336 (1991).

[172] Z. Fang, N. Nagaosa, K. S. Takahashi, A. Asamitsu, R. Mathieu, T. Ogasawara, H. Yamada, M. Kawasaki, Y. Tokura, and K. Terakura, Science **302**, 92 (2003).

[173] C. Castelnovo, R. Moessner, and S. L. Sondhi, Nature **451**, 42 (2008).

[174] L. D. C. Jaubert and P. C. W. Holdsworth, Nature Phys. **5**, 258 (2009).

[175] X.-L. Qi, R. Li, J. Zang, and S.-C. Zhang, Science **323**, 1184 (2009).

[176] R. Shankar, J. Physique **38**, 1405 (1977).

[177] U. Al Khawaja and H. T. C. Stoof, Phys. Rev. A **64**, 043612 (2001).

[178] A.-C. Ji, W. M. Liu, J. L. Song, and F. Zhou, Phys. Rev. Lett. **101**, 010402 (2008).

[179] A. Imambekov, M. Lukin, and E. Demler, Phys. Rev. A **68**, 063602 (2003).

[180] M. Snoek and F. Zhou, Phys. Rev. B **69**, 094410 (2004).

[181] S. Powell and S. Sachdev, Phys. Rev. A **76**, 033612 (2007).

[182] C. W. Oseen, Trans. Faraday Soc. **29**, 883 (1933).

[183] F. C. Frank, Disc. Faraday Soc. **25**, 19 (1958).

[184] P. M. Chaikin and T. C. Lubensky, *Principles of condensed matter physics* (Cambridge University Press, Cambridge, 2000).

[185] H. H. Chen and P. M. Levy, Phys. Rev. Lett. **27**, 1383 (1971).

[186] A. F. Andreev and A. Grishchuk, Sov. Phys. JETP **60**, 267 (1984).

[187] F. Zhou, Int. J. Mod. Phys. **B17**, 2643 (2003).

[188] T. L. Ho and V. B. Shenoy, Phys. Rev. Lett. **77**, 2595 (1996).

[189] P. G. Saffman, *Vortex Dyamics* (Cambridge University Press, Cambridge, 1992).

[190] L. D. Landau and E. M. Lifshitz, *Fluid Mechanics* (Pergamon Press, Oxford, 1982).

[191] A. Lamacraft, Phys. Rev. A **77**, 063622 (2008).

[192] R. J. Donnelly, *Quantised Vortices in Helium II* (Cambridge University Press, Cambridge, 1991).

[193] E. Hodby, G. Heckenblaikner, S. A. Hopkins, O. M. Maragó, and C. J. Foot, Phys. Rev. Lett. **88**, 010405 (2002).

[194] M. F. Andersen, C. Ryu, P. Cladé, V. Natarajan, A. Vaziri, K. Helmerson, and W. D. Phillips, Phys. Rev. Lett. **97**, 170406 (2006).

[195] T. Isoshima and K. Machida, Phys. Rev. A **66**, 023602 (2002).

[196] M. Möttönen, T. Mizushima, T. Isoshima, M. M. Salomaa, and K. Machida, Phys. Rev. A **68**, 023611 (2003).

[197] Y. Kawaguchi and T. Ohmi, Phys. Rev. A **70**, 043610 (2004).

[198] J. A. M. Huhtamäki, M. Möttönen, and S. M. M. Virtanen, Phys. Rev. A **74**, 063619 (2006).

[199] Y. V. Gott, M. S. Ioffe, and V. G. Tel'kovskii, Nucl. Fusion Suppl. **3**, 1045 (1962).

[200] D. E. Pritchard, Phys. Rev. Lett. **51**, 1336 (1983).

[201] T. Bergeman, G. Erez, and H. J. Metcalf, Phys. Rev. A **35**, 1535 (1987).

[202] *Bose-Einstein Condensation in Atomic Gases*, edited by M. Inguscio, S. Stringari, and C. E. Wieman (IOS Press, Amsterdam, 1999).

[203] M. V. Berry, Proc. R. Soc. Lond. A **392**, 45 (1984).

[204] H. Pu, S. Raghavan, and N. P. Bigelow, Phys. Rev. A **63**, 063603 (2001).

[205] M. Vengalattore, J. Guzman, S. Leslie, F. Serwane, and D. M. Stamper-Kurn, arXiv:0901.3800 (unpublished).

[206] K. Gawryluk, M. Brewczyk, and K. Rzążewski, J. Phys. B **39**, L225 (2006).

[207] K. Gawryluk, T. Karpiuk, M. Brewczyk, and K. Rzążewski, Phys. Rev. A **78**, 025603 (2008).

[208] X.-G. Wen, *Quantum Field Theory of Many-Body Systems* (Oxford University Press, Oxford, 2007).

[209] H. Weyl, Z. Phys. **56**, 330 (1929).

[210] C. N. Yang and R. Mills, Phys. Rev. **96**, 191 (1954).

[211] C. Quigg, *Gauge Theories Of Strong, Weak, And Electromagnetic Interactions* (Westview Press, New York, 1997).

[212] G. 't Hooft, Nucl. Phys. B **79**, 276 (1974).

[213] A. M. Polyakov, JETP Lett. **20**, 276 (1974).

[214] F. Wilczek and A. Zee, Phys. Rev. Lett. **52**, 2111 (1984).

[215] G. W. Coulston and K. Bergmann, J. Chem. Phys. **96**, 3467 (1992).

[216] R. Unanyan, M. Fleischhauer, B. W. Shore, and K. Bergmann, Opt. Commun. **155**, 144 (1998).

[217] R. G. Unanyan, B. W. Shore, and K. Bergmann, Phys. Rev. A **59**, 2910 (1999).

[218] L.-M. Duan, J. I. Cirac, and P. Zoller, Science **292**, 1695 (2001).

[219] Y. Li, P. Zhang, P. Zanardi, and C. P. Sun, Phys. Rev. A **70**, 032330 (2004).

[220] R. G. Unanyan and M. Fleischhauer, Phys. Rev. A **69**, 050302 (2004).

[221] C. Cohen-Tannoudji, J. Dupont-Roc, and G. Grynberg, *Atom-Photon Interactions* (John Wiley & Sons, Inc., New York, 1992).

[222] J. Y. Vaishnav and C. W. Clark, Phys. Rev. Lett. **100**, 153002 (2008).

[223] G. Juzeliūnas, J. Ruseckas, M. Lindberg, L. Santos, and P. Öhberg, Phys. Rev. A **77**, 011802(R) (2008).

[224] X.-J. Liu, X. Liu, L. C. Kwek, and C. H. Oh, Phys. Rev. Lett **98**, 026602 (2007).

[225] J. Y. Vaishnav, J. Ruseckas, C. W. Clark, and G. Juzeliūnas, Phys. Rev. Lett. **101**, 256002 (2008).

[226] T. D. Stanescu, C. Zhang, and V. Galitski, Phys. Rev. Lett. **99**, 110403 (2007).

[227] T. D. Stanescu, B. Anderson, and V. Galitski, Phys. Rev. A **78**, 023616 (2008).

[228] K. Osterloh, M. Baig, L. Santos, P. Zoller, and M. Lewenstein, Phys. Rev. Lett. **95**, 010403 (2005).

[229] A. L. Migdall, J. V. Prodan, W. D. Phillips, T. H. Bergeman, and H. J. Metcalf, Phys. Rev. Lett. **54**, 2596 (1985).

[230] J. Arafune, P. G. O. Freund, and C. J. Goebel, J. Math. Phys. **16**, 433 (1975).

[231] T. T. Wu and C. N. Yang, Phys. Rev. D **12**, 3845 (1975).

[232] M. Minami, Prog. Theor. Phys. **62**, 1128 (1979).

[233] L. H. Ryder, J. Phys. A: Math. Gen. **13**, 437 (1980).

[234] L. Fu, C. L. Kane, and E. J. Mele, Phys. Rev. Lett. **98**, 106803 (2007).

[235] J.-P. Martikainen, K.-A. Suominen, L. Santos, T. Schulte, and A. Sanpera, Phys. Rev. A **64**, 063602 (2001).

[236] G. Molina-Terriza, L. Torner, E. M. Wright, J. J. García-Ripoll, and V. M. Pérez-García, Opt. Lett. **26**, 1601 (2001).

[237] W. Li, M. Haque, and S. Komineas, Phys. Rev. A **77**, 053610 (2008).

[238] J. J. García-Ripoll, G. Molina-Terriza, V. M. Pérez-García, and L. Torner, Phys. Rev. Lett. **87**, 140403 (2001).

[239] L. C. Crasovan, G. Molina-Terriza, J. P. Torres, L. Torner, V. M. Pérez-García, and D. Mihalache, Phys. Rev. E **66**, 036612 (2002).

[240] L. C. Crasovan, V. Vekslerchik, V. M. Pérez-García, J. P. Torres, D. Mihalache, and L. Torner, Phys. Rev. A **68**, 063609 (2003).

[241] Q. Zhou and H. Zhai, Phys. Rev. A **70**, 043619 (2004).

[242] M. Möttönen, S. M. M. Virtanen, T. Isoshima, and M. M. Salomaa, Phys. Rev. A **71**, 033626 (2005).

[243] J. A. Seman, E. A. L. Henn, M. Haque, R. F. Shiozaki, E. R. F. Ramos, M. Caracanhas, C. C. Branco, G. Roati, K. M. F. Magalhães, and V. S. Bagnato, arXiv:0907.1584v2 (unpublished).

[244] H. Kawamura and S. Miyashita, J. Phys. Soc. Jpn. **53**, 4138 (1984).

[245] B. W. Southern and A. P. Young, Phys. Rev. B **48**, 13170 (1993).

[246] D. Podolsky, S. Chandrasekharan, and A. Vishwanath, Phys. Rev. B **80**, 214513 (2009).

[247] C.-L. Hung, X. Zhang, N. Gemelke, and C. Chin, Phys. Rev. A **78**, 011604(R) (2008).

[248] I. Carusotto and E. J. Mueller, J. Phys. B.: At. Mol. Opt. Phys. **37**, S115 (2004).

[249] J. M. Higbie, L. E. Sadler, S. Inouye, A. P. Chikkatur, S. R. Leslie, K. L. Moore, V. Savalli, and D. M. Stamper-Kurn, Phys. Rev. Lett. **95**, 050401 (2005).

[250] M. Kobayashi, Y. Kawaguchi, M. Nitta, and M. Ueda, Phys. Rev. Lett. **103**, 115301 (2009).

[251] T. Lahaye, C. Menotti, L. Santos, M. Lewenstein, and T. Pfau, Rep. Prog. Phys. **72**, 126401 (2009).

[252] M. Vengalattore, S. R. Leslie, J. Guzman, and D. M. Stamper-Kurn, Phys. Rev. Lett. **100**, 170403 (2008).

[253] A. L. Fetter and J. D. Walecka, *Quantum Theory of Many-Particle Systems* (Dover Publication Inc., Mineola, 2003).

[254] J. W. Negele and H. Orland, *Quantum Many-Particle Systems* (Addison–Wesley, Redwood City, 1988).

Appendix A Finite-temperature approach to the Bogoliubov equation

The quasiparticle spectrum for a stationary state satisfying the GP equation (2.17) was resolved using the Bogoliubov transformation (2.19). Excitations carrying a given spin index α_0 are of the form $u_{q,\alpha} = \delta_{\alpha,\alpha_0} u_q$ and $v_{q,\alpha} = \delta_{\alpha,\alpha_0} v_q$. Hence, the assumption that only the quasiparticle amplitudes carry a spin index does not restrict the generality of the Bogoliubov transformation (2.19).

The quasiparticle spectrum can also be resolved without invoking any explicit Bogoliubov transformation by generalising the derivation of the Bogoliubov equation in the single-component case [47]. Let us consider a finite temperature system in the grand canonical ensemble described by the Hamiltonian $\hat{H} - \mu\hat{N}$ where $\hat{N}$ is the total particle number operator. The Bogoliubov shift takes the form $\hat{\Phi}_\alpha(\boldsymbol{r},\tau) \approx \psi_\alpha(\boldsymbol{r}) + \hat{\phi}_\alpha(\boldsymbol{r},\tau)$ where τ is defined in the interval $[0, \hbar/k_\mathrm{B}T]$ and the bosonic fields $\hat{\phi}_\alpha(\boldsymbol{r},\tau)$ are periodic in τ. The grand canonical Hamiltonian can be decomposed analogously to the decomposition (2.9). The zeroth-order term is $1/k_\mathrm{B}T$ times $\hat{H}_0$ in Eq. (2.10), the first order term vanishes if $\psi_\alpha(\boldsymbol{r})$ is the stationary solution of the GP equation (2.17), and the second order term is given by

$$\hat{H}_2' = -\frac{1}{2}\int_0^{\hbar/k_\mathrm{B}T} \mathrm{d}\tau\,\mathrm{d}\tau' \int \mathrm{d}\boldsymbol{r}\,\mathrm{d}\boldsymbol{r}' \;:\left(\hat{\phi}_\alpha^\dagger(\boldsymbol{r},\tau)\;\; \hat{\phi}_\alpha(\boldsymbol{r},\tau)\right) \mathcal{G}^{-1}_{\alpha\beta}(\boldsymbol{r}\tau;\boldsymbol{r}'\tau') \begin{pmatrix} \hat{\phi}_\beta(\boldsymbol{r}',\tau') \\ \hat{\phi}_\beta^\dagger(\boldsymbol{r}',\tau') \end{pmatrix} :, \tag{A.1}$$

where the inverse Green's function $\mathcal{G}^{-1}_{\alpha\beta}$ in the Bogoliubov approximation corresponds to

$$\mathcal{G}^{-1}_{\alpha\beta}(\boldsymbol{r}\tau;\boldsymbol{r}'\tau') = \begin{pmatrix} G^{-1}_{\alpha\beta}(\boldsymbol{r}\tau;\boldsymbol{r}'\tau') & 0 \\ 0 & G^{-1}_{\beta\alpha}(\boldsymbol{r}'\tau';\boldsymbol{r}\tau) \end{pmatrix} - \frac{1}{\hbar}\begin{pmatrix} \Sigma_{\alpha\beta} & \Delta_{\alpha\beta} \\ \Delta^*_{\alpha\beta} & \Sigma_{\beta\alpha} \end{pmatrix} \delta(\boldsymbol{r}-\boldsymbol{r}')\delta(\tau-\tau'). \tag{A.2}$$

Using the standard techniques [47, 105, 253], the non-interacting part $G^{-1}_{\alpha\beta}$ can be written in the Fourier transformed form

$$\hbar\, G^{-1}_{\alpha\beta}(\boldsymbol{r},\boldsymbol{r}';i\omega_n) = -(-i\hbar\omega_n\delta_{\alpha\beta} + \hat{h}_{\alpha\beta} - \mu\delta_{\alpha\beta})\delta(\boldsymbol{r}-\boldsymbol{r}'), \tag{A.3}$$

where ω_n are the bosonic Matsubara frequencies.

According to the usual nomenclature, the quasiparticle energies are the poles of the full Green's function [47, 202, 254]. The poles can be found from the zeros of

$\mathrm{Det}[\mathcal{G}^{-1}]$ which satisfy the equation [47]

$$\int \mathrm{d}\boldsymbol{r}'\, \mathcal{G}^{-1}_{\alpha\beta}(\boldsymbol{r},\boldsymbol{r}';\omega) \begin{pmatrix} \tilde{u}_\beta(\boldsymbol{r}') \\ \tilde{v}_\beta(\boldsymbol{r}') \end{pmatrix} = 0, \tag{A.4}$$

and give rise to the Bogoliubov equation

$$\widetilde{\mathcal{D}}_{\alpha\beta} \begin{pmatrix} \tilde{u}_{\beta,q} \\ \tilde{v}_{\beta,q} \end{pmatrix} \equiv \begin{pmatrix} \mathcal{A}_{\alpha\beta} & \mathcal{B}_{\alpha\beta} \\ -\mathcal{B}^*_{\alpha\beta} & -\mathcal{A}^*_{\alpha\beta} \end{pmatrix} \begin{pmatrix} \tilde{u}_{\beta,q} \\ \tilde{v}_{\beta,q} \end{pmatrix} = \hbar\omega_q \begin{pmatrix} \tilde{u}_{\alpha,q} \\ \tilde{v}_{\alpha,q} \end{pmatrix}. \tag{A.5}$$

Equation (A.5) is equivalent to the original Bogoliubov equation (2.20) since it can be obtained from Eq. (2.20) using a unitary transformation, $\widetilde{\mathcal{D}} = \tau_3^\dagger \mathcal{D} \tau_3$, where $\tau_3 = \sigma_3 \otimes \mathbb{1}$. In particular, the quasiparticle energies are not changed in this transformation.